ABSTRACT

Title of Dissertation:	MOLECULAR ROUTES TO SORTING CARBON NANOTUBES
	Brendan Meany, Doctor of Philosophy, 2017
Dissertation directed by:	Professor Y.H. Wang, Department of Chemistry and Biochemistry

Carbon nanotubes are molecular cylinders of graphene that are synthesized as heterogeneous mixtures consisting of an assortment of structures. Because the optical and electronic properties of nanotubes are strongly dependent on their atomic structure and bundling states, effectively dispersing and separating the nanotubes by the different structures is of great importance for their applications ranging from personal electronics and sensors to bioimaging and drug delivery systems.

In this thesis, we describe new molecular approaches to address the challenge of dispersing and sorting carbon nanotubes. First, an open-ring molecular container, acyclic cucurbit[n]uril, clips onto small diameter nanotubes stabilizing them in water leaving the remaining larger diameter nanotubes to agglomerate. At a concentration 1000 times lower than typically required for surfactants, these C-shaped molecules complex with carbon nanotubes creating large exposed surface areas along the tube outerwall. Simple addition of

surfactant, sodium dodecylbenzene sulfonate, patches the exposed areas creating a nanotube fluorescent turn-on effect. A second approach to dispersing carbon nanotubes uses ammonium laurate, a previously unused surfactant though similar in structure to the popular sodium dodecylsulfate. When compared to sodium dodecylsulfate, we observe selectivity towards small diameter nanotubes and cleaner substrate deposition which is important for future applications. Lastly, a gel chromatography method is designed utilizing diazonium chemistry to improve the selectivity allowing nearly identical structures to be sorted in high purity. The surface chemistry disrupts the typical interaction between surfactant dispersed nanotubes and gel resin leading to differences in flow rates based on nanotube structure and therefore significantly improve the capability to sort nanotubes. Finally, we show that optical excitation of individual single-walled carbon nanotubes in the semi-dilute concentration regime is capable of melting double-stranded DNA on the excited nanotubes. These molecular approaches open new opportunities to dispersing and sorting carbon nanotubes in cleaner and highly selective manners.

MOLECULAR ROUTES TO SORTING CARBON NANOTUBES

by

Brendan Meany

Dissertation submitted to the Faculty of the Graduate School of the
University of Maryland, College Park, in partial fulfillment
of the requirements for the degree of
Doctor of Philosophy
2017

Advisory Committee:
Professor YuHuang Wang, Chair
Professor John T. Fourkas
Professor Zhihong Nie
Professor Garegin A. Papoian
Dean's Representative: Professor Min Ouyang

Dedication

To my family.

Acknowledgements

This work would not have been possible without the support of numerous people. First and foremost, my advisor Professor YuHuang Wang has been instrumental to the success of these projects. He inspires us to be creative in our approach to science. Second I would like to thank the many colleagues I have had the pleasure of collaborating with, they have each taught me invaluable lessons. I would like to thank Dr. Earl Stone for his trust in me as a TA. And I would like to thank my committee members for their support and guidance. Lastly, my family and friends who have been with me through it all, their encouragement kept me going.

I would like to thank the following financial support. This research was supported in part by the Office of Naval Research (N000141110465), the National Science Foundation (CAREER CHE-1055514), the NIH/NIGMS through grant number R01GM114167, and the University of Maryland.

Table of Contents

List of Tables

List of Figures

List of Abbreviations

(n,m): index for a specific nanotube structure

6-FAM: 6-carboxyfluorescein

AFM: atomic force microscopy

AL: Ammonium Laurate

APTES: (3-aminopropyl)triethoxysilane

ATPE: aqueous two phase extraction

C: carbon

Ch: chiral vector

CB: acyclic cucurbit[n]uril

CMC: critical micelle concentraion

CNT: Carbon Nanotube

CW: continuous wave

DGU: density gradient ultracentrifugation

DNA: deoxyribonucleic acid

DOS: Density of States

dsDNA: double stranded DNA

DX: dextran

Dz: diazonium

E_{11}: CNT energy transition from first valence band to first conduction band

E_{11}^{-}: defect induced intra-bandgap energy transition

Elu: elution (from a column)

FT: flowthrough (from a column)

HiPco: High Pressure Carbon Monoxide

MWCNT: Multi-walled carbon nanotube

NP: nanoparticle

PEG: polyethylene glycol

PL: photoluminescence

SC: sodium cholate

SDBS: sodium dodecylbenezene sulfonate

SDS: sodium dodecyl sulfate

ssDNA: single stranded DNA

SWCNT: single-walled carbon nanotube

TEM: transmission electron microscopy

UV-vis-NIR: ultraviolet-visible-near infared

Chapter 1: Introduction

With the discovery of carbon nanotubes (CNTs) in 1991 by Iijima a new field of study in nanomaterials is developed.[1-3] Due to their variety of exceptional properties, CNTs continue to be at the forefront of both fundamental research and novel application design. Even after 25 years of intensive effort studying these unique nanostructures, research into CNTs endures. The advancement of CNTs has developed a greater understanding of nanomaterials and their applications.

The objective of this thesis is to address central issues concerning dispersion and sorting of CNTs in order to advance fundamental research and develop novel applications. To date these nanostructures are mass produced with a broad distribution of metallic and semiconducting nanotubes strongly bundled by van der Waals attractive forces. This heterogeneous mixture leads to a diverse set of properties which hinders CNTs incorporation into novel applications. In order for CNTs to demonstrate their full potential they must be sorted by structure to capture their intrinsic optical and electronic properties. Here, we develop chemical methods to sort carbon nanotubes in aqueous solution through selective dispersion or physical separation. Furthermore, sorted CNTs are then implemented into a potential drug delivery system.

1.1 Background

CNTs are structurally unique nanomaterials consisting of sp^2 hybridized carbon, and are modeled as graphene rolled into a tube. Single-walled carbon nanotubes (SWCNTs) are conceptualized as a rolled, single sheet of graphene,

while multi-walled carbon nanotubes (MWCNTs) consist of several concentric, nested SWCNTs. The CNTs properties are determined by its structure which is defined by a unique chiral vector (C_h) and the equation $C_h = na_1 + ma_2$ where *n* and *m* are integers and a_1 and a_2 are lattice vectors (Figure 1-1a,b).[4] This chiral vector determines the nanotube's chirality, or how the graphitic lattice is oriented relative to the nanotube's lengthwise axis. Chirality is classified by the above indices as *(n,m)* and unequivocally describes a specific nanotube's molecular structure. Both the chiral angle θ (the angle between C_h and a_2) and the nanotube diameter d_t are calculated using *(n,m)* by the following equations

$$dt = \frac{a}{\pi}\sqrt{n^2 + nm + m^2} \quad (1)$$

$$\theta = \tan^{-1}\frac{\sqrt{3}m}{2n+m} \quad (2)$$

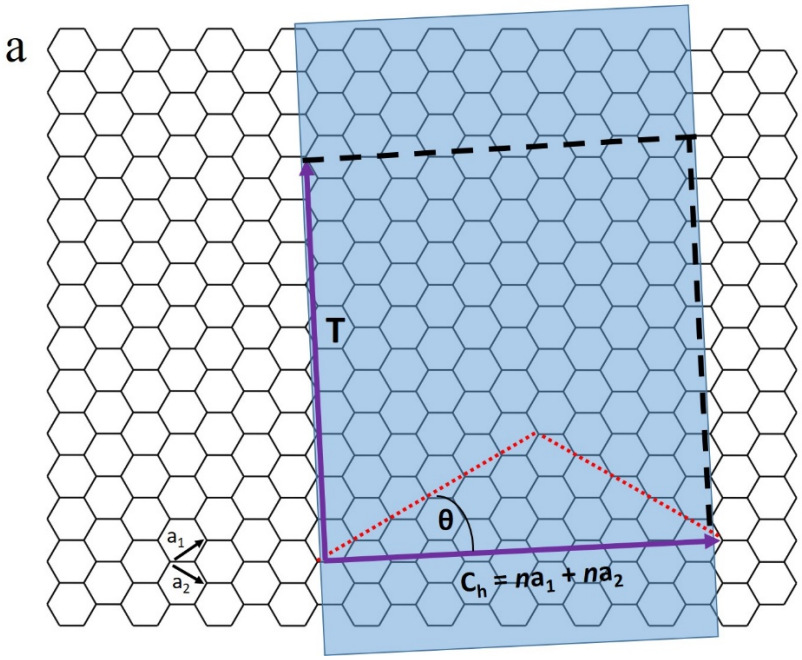

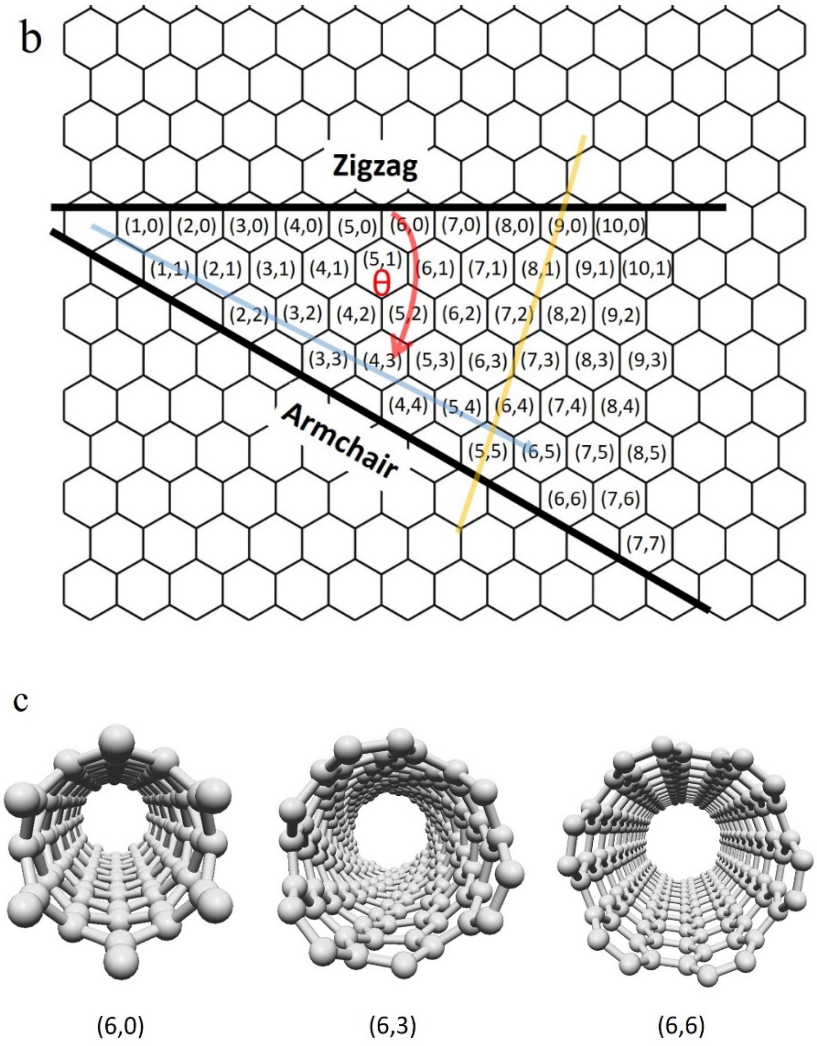

Figure 1-1. (a) Diagram conceptualizing a (6,5)-single-walled carbon nanotube as a rolled-up strip of graphene. The chiral vector, C_h, joins the graphitic lattice points upon rolling and determines the circumference of the nanotube. The angle between C_h and the zig-zag line or (*n*,0) is the chiral angle, θ. Each CNT are defined by the chiral angle and chiral vector while T, the unit vector, establishes the CNT unit cell and the longitudinal axis. (b) The periodic table of CNTs depicts only a few of the potential nanotube structures possible based upon the indices (*n*,*m)*. Between the Zigzag (*n*,0) and the armchair (*n*,*n*) CNTs are the multiple chiral structures (*n*,*m*) determined by the chiral angle (red arrow) and the chiral vector (blue arrow). The yellow line represents the CNT axis. Zig-zag nanotubes are those species with a chiral angle of 0, while armchair species have a chiral angle of 30. All other nanotubes in the periodic table of CNTs are named chiral with varying chiral angles $0 < \theta < 30$. (c) Representative single-walled carbon nanotubes show the molecular arrangement of carbon atoms from the symmetric zig-zag (6,0) and armchair (6,6) to the twisting chiral nanotubes (6,3*)*.

The chirality is important as it establishes whether a CNT is metallic or semiconducting. The electronic energy bands of CNTs are calculated from the graphene electronic structure under boundary conditions, known as zone-folding.[5] In this method, cutting lines are placed through the energy dispersion diagram of graphene (Figure 1-2). The cutting line is based on the translational and chiral vector. If the line crosses the *K* or *K´* points then the energy band is zero band gap or metallic. If on the other hand the line does not fall on either points the CNT has a band gap and is semiconducting. Due to zone folding approximation the electronic property of a CNT chirality can be easily ascertained with the (*n,m)* indices, if the calculation *n-m* gives a multiple of three it is metallic otherwise it is semiconducting. Consequently, mass produced SWCNTs are more likely to be semiconducting by approximately 2:1.[5]

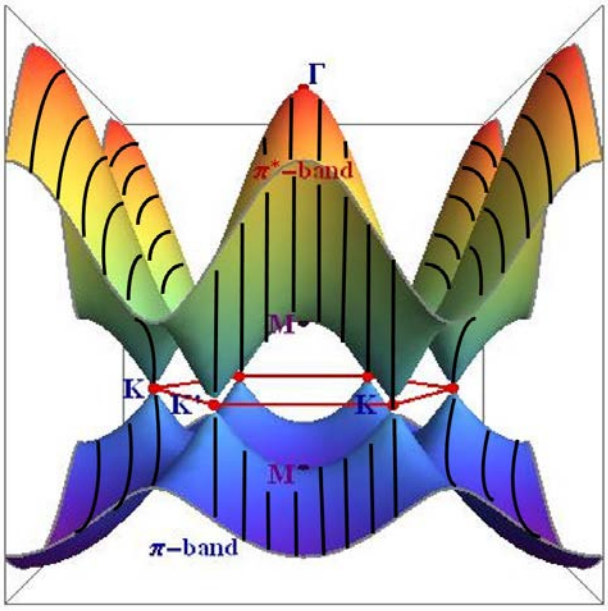

Figure 1-2. The graphene Brillouin zone (with periodic zone folding cutting lines in black) showing the electronic band structure with intersecting K points as the degeneracies of π and π* or valence and conduction bands, respectively. *Image augmented from Wolfram Demonstrations Project.*[6]

CNTs are exceptional materials due to their high aspect ratio. With an ~1 nm diameter but over 200 nm length, these structures are essentially one-dimensional. This gives rise to unique optical and electrical properties from their singular electronic density of states (DOS) or van Hove singularities. Each chirality of CNT has unique van Hove singularities which control the specific and discreet energy transitions. This limits the absorption and photoluminescence (for semiconducting species) to distinct energies ranging within the ultraviolet to the near-infrared. Throughout the spectrum each CNT chirality has a unique optical fingerprint based on these singularities.

To understand these energy transitions and the optical properties of CNTs, DOS diagrams depict both the van Hove singularities and the respective transitions (Figure 1-3). For metallic carbon nanotubes there is a seamless continuum from valence to conduction bands. These gapless nanostructures absorb discreet photons relative to their van Hove singularities. However, they cannot emit light or photoluminesce because of nonradiative quenching from the multiple continuum states surrounding the Fermi energy level. Conversely, semiconducting nanotubes do photoluminesce. Their DOS have a bandgap with multiple, widening energy transitions S_{11}, S_{22}, S_{33}. Photoluminescence begins with the excitation of an electron to the larger (higher energy) transition (S_{22} or S_{33}) followed by vibrational relaxation to the S_{11} state. From the conduction S_{11} state, the electron crosses the bandgap in radiative relaxation through the emission of a photon of lesser energy.

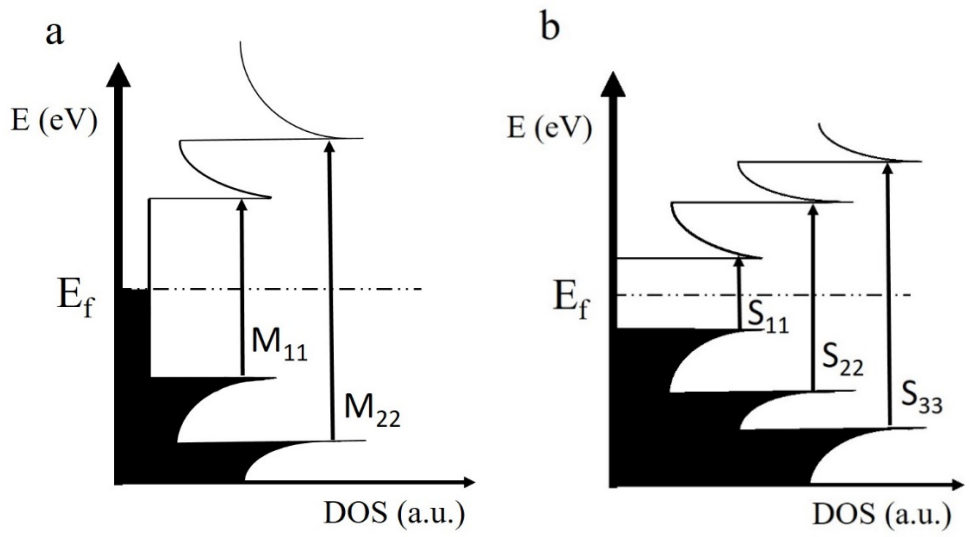

Figure 1-3. DOS diagrams for metallic and semiconducting CNTs show energy transitions near the Fermi energy level (E_f) from the lower valence band to the upper conduction band. Metallic transitions (M_{11} and M_{22}) are gapless. On the other hand, a bandgap occurs for semiconducting nanotubes allowing for photoluminescence emission from the S_{11} transition.

CNTs continue to amaze researchers as an exceptional nanomaterial with the capacity and potential to compete with today's bulk material. Metallic nanotubes have high conductivity with a maximum current density above 10^9 A/cm^2 or three orders of magnitude larger than Cu and other metals such as aluminum.[7] As nanowires, CNTs will shrink both the size and weight of current electronics, significantly advancing industries from personal electronics to aeronautics.[8-10] They have the capability to store energy as part of lithium ion batteries[11] and solar cells. Semiconducting nanotubes are highly sought after for near-infrared biomedical imaging applications[12,13] and traceable delivery systems of drugs or antibodies.[14]

Although exciting fundamental research continues to be discovered and novel devices are developed using CNTs there remain basic setbacks to utilizing

and understanding nanotubes. Mass production of CNTs for applications are severely hindered by impurities from catalytic production and the inability to have high structural purity material. Dispersing CNTs and maintaining stable solutions while retaining the important, useful electrical and optical properties remains an ongoing pursuit. Our work seeks to address the complications of dispersing and sorting carbon nanotubes.

1.2 Surfactant Dispersion of Carbon Nanotubes

The discovery of ultrasonicating CNTs in the presence of surfactants overcame important issues in sample preparation and discovered important optical properties.[15] Due to the strong van der Waals forces, nanotubes are tightly bundled together. In addition they are hydrophobic which created great difficulty for researchers wanting to prepare aqueous samples for experiments. Therefore dispersing CNTs is an energy intensive endeavor. Ultrasonication creates cavitation forces which exfoliates bundled nanotubes whereby aqueous surfactant molecules come between CNTs and adsorb to their outerwall, stabilizing and dispersing the tubes in water. To purify the solution, it is ultracentrifuged to remove impurities and bundled CNTs from the supernatant.

Surfactant dispersed CNTs were used to research the early work on optical properties of nanotubes. The debundling of CNTs limits radiative quenching especially between metallic and semiconducting species. Energy transitions as described above were measured by absorbance and photoluminescence spectroscopies leading to understanding the unique structure-dependent optical fingerprints of CNTs[16] and their excitonic nature (Figure 1-4).[17]

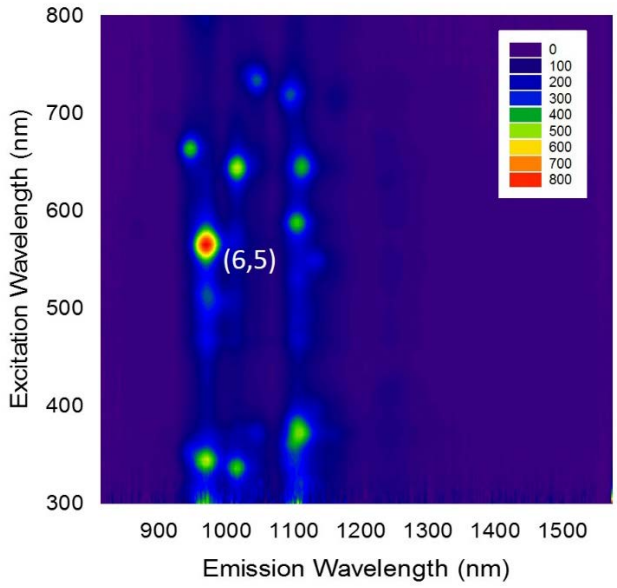

Figure 1-4. An excitation-emission map manifests the optical fingerprints of aqueous SDS surfactant dispersed HiPco SWCNTs, such as the labeled photoluminescent peak for chirality (6,5).

While many surfactants have been tested only a few provide long term solution stability. Sodium dodecylsulfate (SDS), sodium cholate (SC), and sodium dodecylsulfonate (SDBS) are typically used in sample preparation. While they are chosen for their adequate ability to disperse CNTs, the surfactants must be used at concentrations above their critical micelle concentration (CMC) and are difficult to remove from the surface of the nanotube when necessary.[18] As seen in Figure 1-5a, a SWCNT's structure is nearly completely masked by surfactant coverage. While these techniques have lead to important discoveries, they hinder the use of CNTs in applications where these impurities limit the advantages to this nanomaterial. Electronic devices require clean CNTs. Also surfactants can be biologically toxic and therefore will have harmful effects in bio-imaging or drug delivery systems.

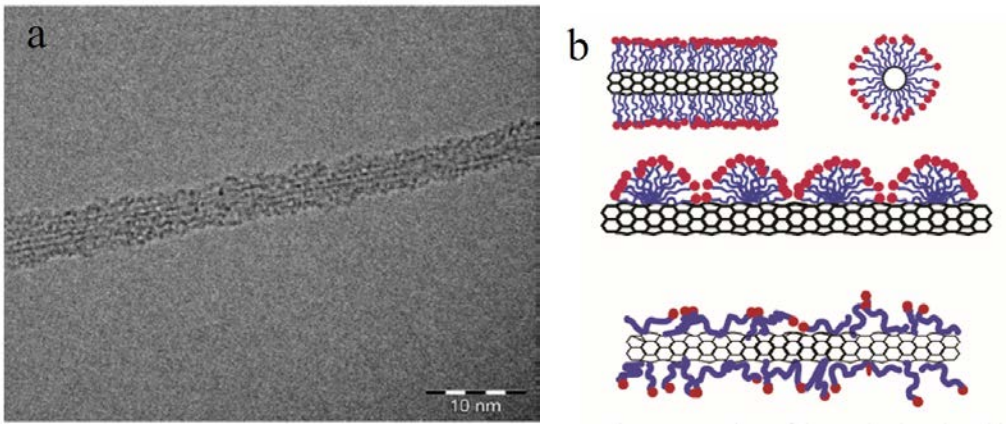

Figure 1-5. (a) A transmission electron microscope image of an approximate 0.7 nm diameter single-walled carbon nanotube with its surface covered by sodium deoxycholate surfactant from NIST Reference Material 8281.[19] (b) Three possible morphologies of surfactant adsorbed to the outerwall of a SWCNT with the polar head group exposed to the solvent.

1.3 Strategies for Sorting Single-Walled Carbon Nanotubes

Several methods of sorting single-walled carbon nanotubes have been developed in the last decade. These techniques vary in simplicity, sensitivity, scalability, and CNT sorting throughput. Each has its advantages and pitfalls.

Sorting SWCNTs with short single-stranded DNA sequences has garnered the attention of many researchers. Initial work used DNA to simply disperse SWCNTs, an important discovery as there are less contamination issues compared to surfactants, and DNA renders the nanotube with potential biological capabilities.[20] Nucleotide bases adsorb to the SWCNT outerwall through π-π stacking and the deoxyribose sugar-phosphate backbone disperses the complex in water (Figure 1-6). DNA soon showed promise as also being capable of sorting SWCNTs based on the DNA sequence.[21] Over time Ming Zheng and co-workers continued to refine their DNA sequences to recognize and purify 12

semiconducting SWCNTs from many structures in aqueous solution.[22] And the evolution in designing DNA sequences has progressed to distinguish racemic SWCNTs exhibiting circular dichroism and the metallic armchair SWCNTs (6,6) and (7,7).[23,24] While the selectivity towards a nanotube structure by a well-designed DNA sequence is sensitive this method is cost prohibitive by the availability of commercial oligomers and is not scalable for mass production.

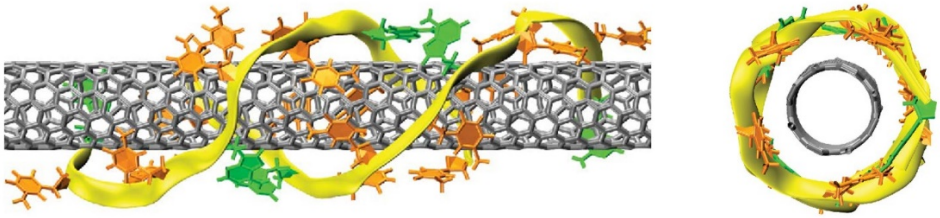

Figure 1-6. An (8,4)-SWCNT (grey) wrapped by DNA sequences of ATTTATTTATTT. The nucleotides adenine (green) and thymine (orange) adsorb along the nanotube axis leaving the polar DNA backbone (yellow) exposed to the solvent.[22]

A second approach to sorting SWCNTs is an instrument-heavy method using density gradient ultracentrifugation (DGU).[25] Here the buoyant densities of SWCNTs encased by structure-sensitive surfactants are exploited to sort by electronic type, semiconducting or metallic in addition to the purifying of (6,5) and (7,5) chiralities (Figure 1-7).[26] Nanotubes are first dispersed in surfactant with ultrasonication, then sorted by ultracentrifugation within a linear gradient of iodixanol, a non-ionic density gradient medium. After the DGU procedure, colorful layers of SWCNTs are fraction collected. This method has been further refined with the use of nonlinear gradients to enrich up to ten chiralities and the circular dichroic enantiomers of seven SWCNTs.[27]

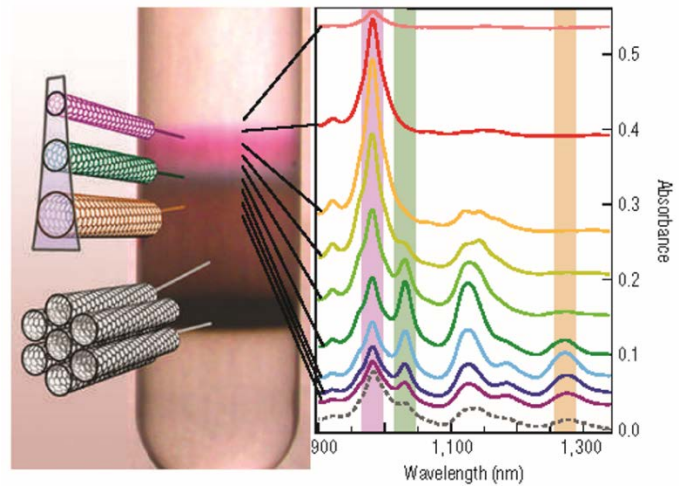

Figure 1-7. Physical sorting of SWCNTs by DGU with the upper purple band enriched in (6,5) chirality and the bottom layers containing more dense bundles and aggregates. Absorption spectra of fraction collected layers show structure sorting by diameters 7.6, 8.3, and 9.8-10.3 Å, respectively.[26]

However, DGU is time consuming and expensive to startup. The method is instrument-heavy requiring multiple ultracentrifuges to develop a scalable, reliable approach to sorting SWCNTs for continuous sample preparation. For the mass production of CNT devices and applications factories of ultracentrifuges would probably be a necessity to meet demand. Secondly, the gradient medium is also costly. Although this method is capable of separating semiconducting nanotubes from metallic, it has practical limitations, such as diffusive broadening and low mass throughput.

A novel, simple approach to sort SWCNTs is aqueous two-phase extraction (ATPE). Two aqueous polymers, polyethylene glycol (PEG) and dextran (DX), are chosen for their ability to spontaneously phase separate. During the process each phase retains specific SWCNT structures based on hydrophobicity and the species partition coefficients. After mixing, the phases separate with metallic nanotubes going to the hydrophilic, DX bottom phase and

semiconducting nanotubes remaining in the hydrophobic, PEG top phase (Figure 1-8).[28] This partition-based separation is likely ruled by the surfactant structure surrounding the nanotubes and the relative hydrophilicity and hydrophobicity of both the dispersed SWCNTs and the two phases. Either phase can be collected and further separated by iterative ATPE.[29] This technique has the potential to sort any chirality within a given sample and could be automated by the development of multistep extraction systems.

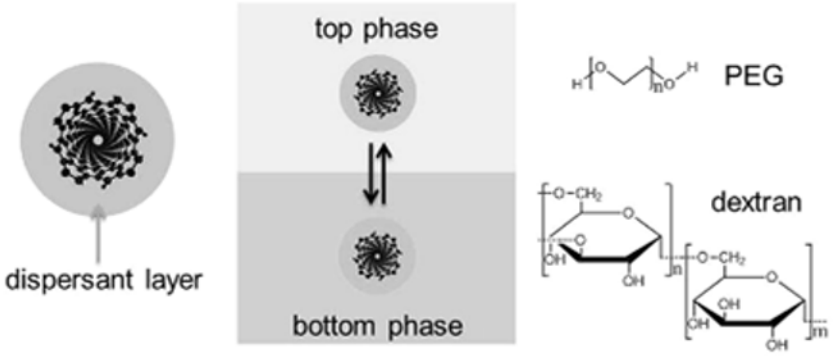

Figure 1-8. Aqueous two phase extraction (ATPE) places surfactant dispersed SWCNTs in immiscible aqueous polymers which spontaneously phase separate into a PEG top phase accepting semiconducting SWCNTs and a dextran bottom phase retaining metallic SWCNTs.[28]

ATPE while simple and inexpensive to perform can easily and quickly become an abundant chaos of samples by the power of two (2^n) due to the iterative process. Each successive sample can be split into two, mixed with the opposing immiscible aqueous polymer, phase separated, and split again. More importantly, the resolution of purity does not meet the standards for CNT applications, especially if a single or few chirality sample is desired.

Improvements to the ATPE method, most likely parameter adjustments, are needed to increase resolution, such as modifying the concentrations of

surfactants, researching alternative phase separating polymers and surfactants thereby changing the partition coefficients, and reducing or oxidizing the SWCNT samples to alter the surfactant morphology changing the hydrophilicity of nanotubes. Reducers and oxidizers could result in "pushing" a chirality to a specified phase.[30]

The most scalable method to date is gel chromatography. When first implemented, allyl dextran-based size-exclusion gel (Sephacryl S-200) sorted SDS dispersed SWCNTs by electronic structure, metallic separated from semiconducting.[31] Building upon this work, Liu *et al.* further developed gel chromatography sorting of SWCNTs in a multistep process requiring only a single surfactant and isolating 13 chiralities with purities ranging from 39-94% (Figure 1-9a).[32] By controlling the temperature of the gel column, they reduced the process to a single step to sort seven species, but with mixed results to the chirality purities obtained.[33] The gel column is overloaded with aqueous SDS-dispersed SWCNTs, and those chiralities with the strongest adsorption interactions occupy the column leaving weakly interacting species to flow through.[34] The SWCNTs adsorbed to the column are removed simply by eluting with a 2.5 times concentrated solution of aqueous SDS. In practice these columns can only be reused 4-5 times before irreversible binding of SWCNTs and impurities render the gel resin depleted of nanotube adsorption sites, despite claims that the columns are reusable.

There still remains a lack of understanding of the underlying mechanics behind SDS dispersed SWCNTs ability to sort by gel chromatography. Further

studies are needed to fully comprehend the differences in the rate in which SWCNTs bind to the column, even though the trend appears to start with small diameter nanotubes filling these sites first (Figure 1-9b). This work initially gained much excitement at the prospect of developing a scalable sorting system. However, the technique suffers from poor resolution of many chirality purities as low as 39% for (10,2).[32] (6,5) is the easiest species to purify up to 95%, but this is possibly due to a high population of the chirality in the starting material and its small diameter allowing many of the column binding sites to be taken up by (6,5).

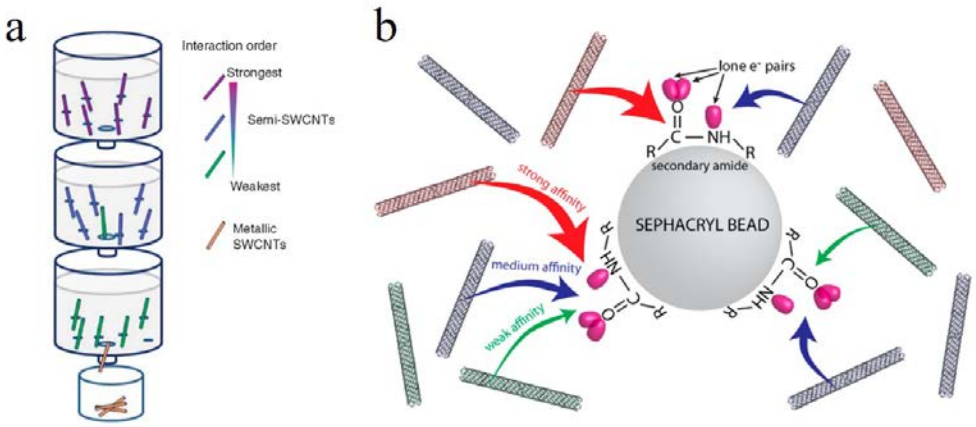

Figure 1-9. (a) Instead of a single column, single-surfactant multicolumn gel chromatography (SS-MUGEC) uses multiple small columns to sort up to 13 chiralities.[32] (b) Secondary amide groups on the gel resin surface present binding sites for SWCNTs with small diameter nanotubes having the strongest interactions.[34]

1.4 Conclusion

In the subsequent chapters, new chemical methods of dispersing and sorting SWCNTs are discussed. Methods are studied to control the dispersion of SWCNTs to provide sorted and clean nanotubes with and without the use of surfactants. We tune the gel chromatography process for obtaining chirality

purified nanotubes by using diazonium chemistry functionalization of SWCNTs to disrupt the adsorption of nanotubes to the column. Sample chirality populations are characterized by absorbance and photoluminescence spectroscopies to determine good dispersion and the extent of sorting. Transmission and scanning electron microscopies show clean substrate deposition of CNTs.

This work is motivated by an applications driven need for CNTs sorted by electronic and optical properties. The studies in sorting and dispersing CNTs offer new directions towards realizing the goals of uncontaminated, high purity CNTs for applications such as biological drug-delivery systems. We begin with a study of dispersing SWCNTs without surfactants.

Chapter 2: Acyclic Cucurbit[n]uril Molecular Containers Selectively Solubilize Single-Walled Carbon Nanotubes in Water

Adapted from Shen, C.; Ma, D.; Meany, B.; Isaacs, L.; Wang, Y. H. J. Am. Chem. Soc. 2012, 134.

C. Shen and B. Meany dispersed and complexd the single-walled carbon nanotubes with cucurbit[n]uril and characterized by absorption and fluorescence spectroscopies. C. Shen studied effects of either increasing the concentration of carbon nanotubes or cucurbit[n]uril and took SEM images at increasing concentrations of carbon nanotubes. B. Meany studied effect of salt concentraiton. D. Ma synthesized the cucurbit[n]uril both 1 and 2.

2.1 INTRODUCTION

Single-walled carbon nanotubes (SWCNTs) are insoluble in water and virtually all other conventional solvents, but the electronic and optical properties that make SWCNTs desirable electronic materials and biosensors are observed only in their individually dispersed states.[15] For this reason, enormous efforts have been devoted over the past decade to addressing this insolubility problem.[20,35-41] A successful common approach involves the use of a surfactant, such as sodium dodecyl sulfate (SDS), sodium dodecylbenzene sulfonate (SDBS), Triton X-100, and sodium cholate, to encapsulate the nanotube in micelles. Other approaches include wrapping the nanotube with synthetic polymers, DNA, or proteins to improve solubility and dispersion of the nanotubes.[36-39] However, the need for excess surfactants and the labile nature of the micelle structures often pose limitations to their applications.

Another major challenge in using SWCNTs is their broad structural distribution. Furthermore, each different structural type of SWCNT may exhibit significant differences in its chemical and physical properties. Accordingly, there has been great interest in the search for complexing agents that selectively solubilize SWCNTs based on their diameter and their chirality. Some successes have been achieved with specific DNA sequences that selectively wrap around SWCNTs according to diameter and chirality,[20] polyfluorenes that show the ability to discriminate between nanotube species in terms of either diameter or chiral angle,[42] chiral diporphyrin molecules that possess different binding affinities for left- and right-handed helical nanotube isomers,[43] and lastly, flavin mononucleotide that preferentially binds (8,6)-SWCNTs through concentric interactions between the two.[44] These molecular systems greatly deepen our understanding of the intermolecular interactions and properties of SWCNTs in solution, which can potentially lead to the design of molecules for structure-specific separation of SWCNTs at large scale. However, there is a great need for additional systems that display selective intermolecular interactions with specific classes of SWCNTs for use in the separation and solubilization of SWCNTs.

2.2 Materials and Methods

*2.2.1 Synthetic Procedures and Characterization Data for Acyclic cucurbit[n]uril **1** and **2***

Compounds **1** and **2** were prepared as described in the literature.[13]

*2.2.2 Preparation of Acyclic Cucurbit[n]uril **1** or **2** Container/SWCNTs solutions: **1**·SWCNT and **2**·SWCNT*

HiPco SWCNTs were purchased from Unidym Inc. (Lot no. R0513) and used as received. An aqueous suspension of SWCNTs was typically prepared by suspending 0.4 mg of the raw SWCNT material in 20 mL of D_2O (99.8%, Cambridge Isotope Laboratories, Inc.) with varying concentration of **1** or **2**. The mixture was sonicated in a bath sonicator (VWR, B2500A-DTH) for 30 min and then by a tip sonicator (Misonix S-4000 ultrasonicator, Farmingdale, NY) at 20% amplitude for 2 hrs. The dispersion was then centrifuged at 85,220 *g* for 2 hrs (Beckman Coulter Inc. Optima^{TM} LE-80 K Ultracentrifuge, type 70 Ti Rotor). The top ~50 vol.% supernatant was collected for measurements.

2.2.3 Spectroscopic Characterization

Optical absorption spectra were obtained with a Perkin-Elmer 1050 UV-vis-NIR spectrophotometer (Waltham, Massachusetts). Excitation-emission fluorescence maps were recorded with a Horiba JobinYvon Nanolog spectrofluorometer equipped with a liquid nitrogen cooled InGaAs array detector. All **1**·SWCNT and **2**·SWCNT samples do not show fluorescence until SDBS is added with shaking. A 4.5 mL solution of cucurbit[n]uril-container/SWCNTs is mixed with a 50 mg SDBS/0.5 mL of D_2O solution. The SDBS concentrations in the final solutions are 1.0%.

2.2.4 Scanning Electron Microscopy (SEM)

SEM images were taken in a Hitachi SU-70 SEM (Tokyo, Japan) at a beam energy of 1 kV or 3 kV. Samples for SEM were prepared by drop casting **1**•SWCNTs solutions on a silicon substrate and let dry in air.

2.2.5 Molecular Mechanics Simulations

Molecular mechanics simulations were performed to study the **1**•SWCNTs structure in water. SWCNTs of specific chirality were built with Nanotube Modeler (v1.4.0, JCrystalSoft). The length of each nanotube is 3 nm. Both nanotube ends are terminated with hydrogen atoms to avoid structural distortion due to dangling bonds. The structures of **1**•SWCNTs were optimized in vacuum within HyperChem 8.0 (Hypercube, Inc.) and then introduced into a 30Å x 30Å x 40Å periodic box consisting of ca. 1000 water molecules to account for the solvation energy. The water molecules inside the nanotube cavity are removed. All simulations were performed applying a MM+ force field. We used Polak-Ribiere conjugate gradient and the energy calculations were converged to RMS gradient < 0.05 kcal/(A mol).

2.3 Results and Discussion

2.3.1 Acyclic Cucurbit[n]uril

The cucurbit[n]uril family of molecular containers (CB[n], n = 5, 6, 7, 8, 10) is attracting significant interest because of their ability to bind to hydrophobic and cationic species in aqueous solution.[46-49] Recently, we reported the synthesis of two highly soluble acyclic cucurbituril congeners (**1** and **2**) with the ability to solubilize a variety of hydrophobic pharmaceutical agents.[45] In this paper, we

show that **1** and **2** solubilize individual SWCNTs in water even at a concentration 100-1000 times lower than typically required for surfactants or previous molecular systems. [42,43] The dispersion process is diameter dependent and exhibits selectivity towards low chiral angle structures, an important capability that is complementary to existing methods.[42,43] The structural selectivity is tunable based on the structure of the acyclic CB[n] receptor used and by the concentration of added salt.

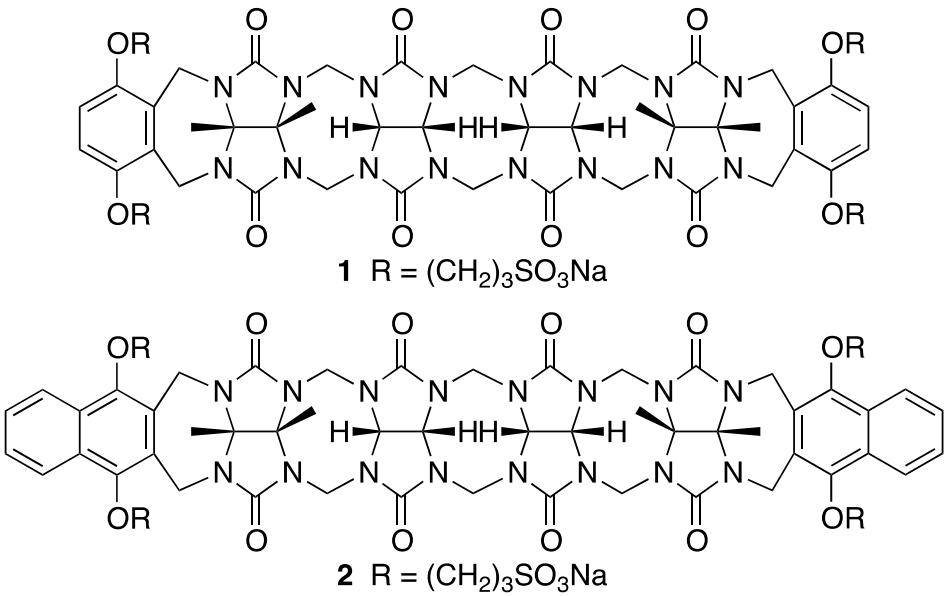

Figure 2-1. The molecular structure of acyclic CB[n] **1** (top) and acyclic CB[n] **2** (bottom).

Molecular containers **1** and **2** are composed of a central glycoluril tetramer unit that by virtue of the fused polycyclic ring system is preorganized into a C-shape, which is capped by two substituted aromatic rings that are terminated in sodium sulfonate groups (Figure 2-1).[45] We expected that the aromatic walls of **1** and **2** would allow them to form complexes with SWCNTs driven by π-π

interactions whereas the sulfonate groups would render **1**, **2** and their SWCNT complexes soluble in water. Furthermore, by virtue of their acyclic nature compounds **1** and **2** are able to expand the size of their cavities by conformational changes at the CH_2-bridges of their polycyclic backbone in much the same way as a hand flexes.[45,50] Such conformational flexibility allows **1** and **2** to adapt their shape to interact maximally with SWCNTs. Compounds **1** and **2** are acyclic members of the cucurbit[n]uril family of molecular containers and were therefore expected to retain the excellent recognition properties of this class of molecules toward cationic species in water.[45,46,48-50]

2.3.2 Cucurbit[n]uril CB[n]1 Disperses Single-Walled Carbon Nanotubes

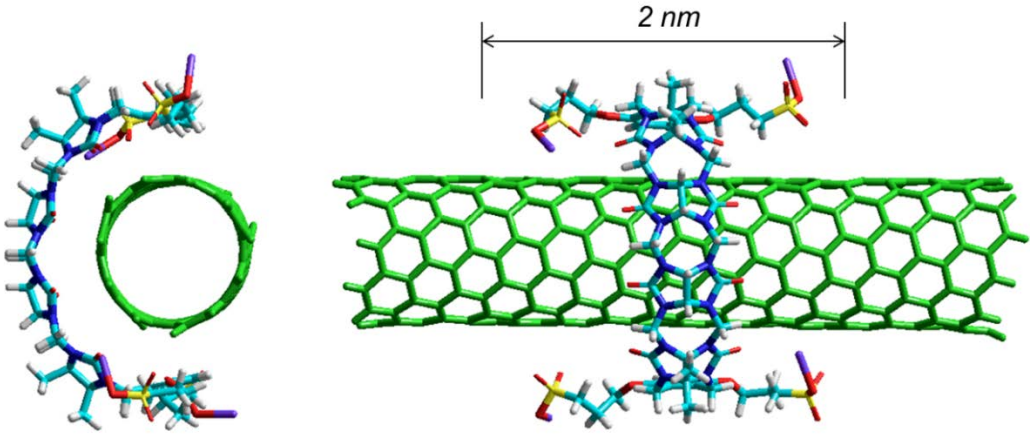

Figure 2-2. Molecular mechanics model of the complex between an (8,3**)** nanotube and container **1**. The geometry was optimized with HyperChem 8 applying the MM+ force field. The nanotube is 3.5 nm long and both ends are terminated by hydrogen atoms. Solvation is accounted for by applying a 3nm × 3nm × 4nm periodic box of water molecules. For clarity, the water molecules are not shown.

Figure 2-2 shows a molecular mechanics model of an (8,3)-SWCNT encapsulated by **1** in water. The optimized structure shows that the C-shaped molecule attaches to the nanotube like a clip, leaving portions of the nanotube exposed to the local environment. The model suggests a single molecule of **1** covers approximately a 2 nm length along the SWCNT. From molecular modeling, we know that a 2 nm length of an (8,3)-SWCNT contains 190 C-atoms weighing 2282 g mol^{-1}; which is comparable to the molecular weight of **1** (1541.4 g mol^{-1}). This simple calculation suggests that the amount of **1** required to fully cover the SWCNT occurs at a 0.7:1 wt:wt ratio. Owing to the high water solubility of **1** (~346 mM),[13] this molecular container readily renders small diameter SWCNTs soluble in water (Figure 2-3a and Figure 2-3b). Because these molecular containers are not traditional surfactants they do not exhibit a critical micelle concentration over the range of experimental conditions employed. There is, therefore, no need to use an excess amount of **1** to stabilize the SWCNT dispersion in aqueous solution. Even at 0.001 wt.%, a concentration 1000 times lower than that required of commonly used surfactants,[51,52] **1** can disperse SWCNTs to a concentration of 12.5 mg/L (Figure 2-3). To further understand this behavior, we performed titration experiments to quantify the amount of solubilized SWCNTs as a function of the initial SWCNT load and the starting concentrations of **1**. At a fixed concentration of **1** (0.001 wt.%), individually dispersed SWCNTs solutions of 4.8, 6.8, and 12.5 mg/L were obtained from starting suspensions of 20, 40, and 80 mg/L of HiPco SWNTs in D_2O, respectively. When the SWCNT load was increased to 120 mg/L, the absorption

of both **1** and carbon nanotubes surprisingly decreased (Figure 2-3b). This observation was very reproducible. Similarly, at a fixed SWCNT load of 20 mg/L, the final nanotube concentration decreases as the concentration of **1** increases from 0.001 wt.% to 0.4 wt.% Figure 2-3a. This titration experiment shows that **1** is capable of stabilizing the SWCNT even at a concentration that is well below the 0.7:1 ratio of a fully covered **1**•SWCNT structure. Because of the low concentration of **1**, **1**•SWCNT structures could be cleanly deposited on silicon substrates by direct drying of a droplet (Figure 2-4). However, due to drying induced aggregation, it is difficult to prevent nanotubes from bundling. More conclusive evidence regarding their dispersion states in solution was obtained from spectroscopic studies.

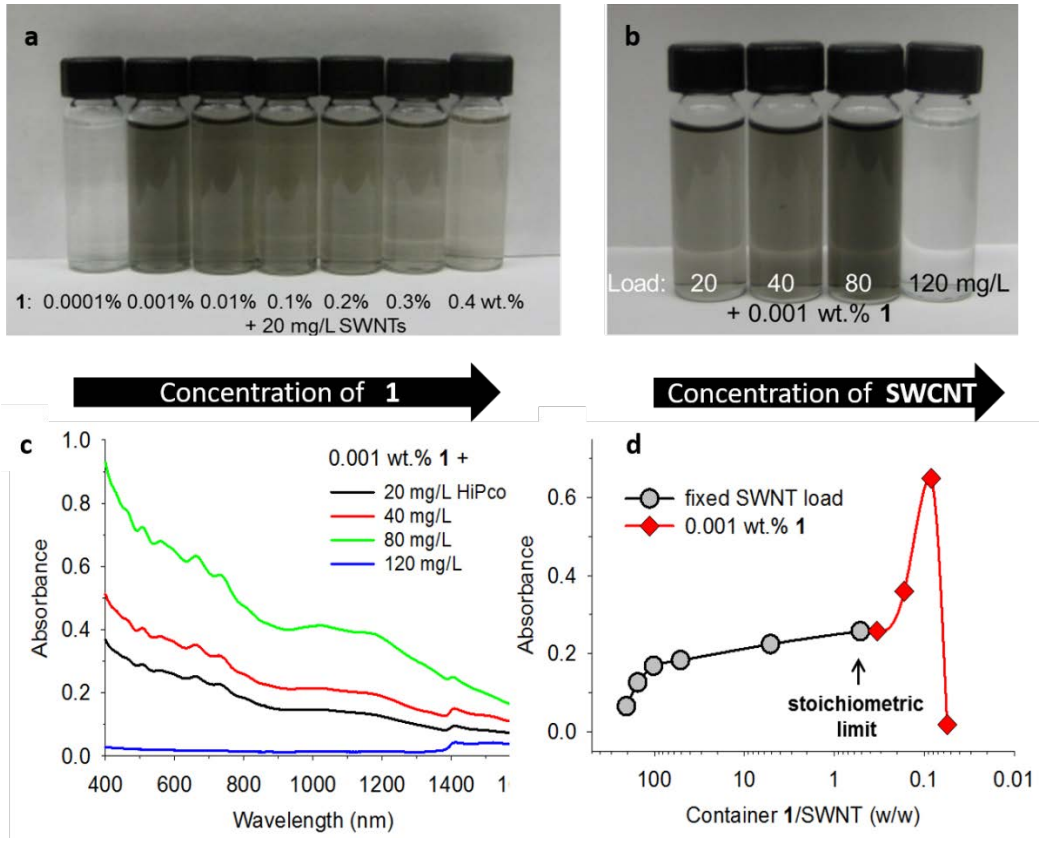

Figure 2-3. Compound **1** solubilizes SWCNTs below the stoichiometric limit. (a) Photograph of **1**•SWNTs solutions with starting concentrations of 20 mg/L SWNTs in increasing **1** concentrations (from left to right): 0.0001 wt.%, 0.001 wt.%, 0.01 wt.%, 0.1 wt.%, 0.2 wt.%, 0.3 wt.%, 0.4 wt.%. (b) Photograph of **1**•SWCNTs dispersions prepared from increasing initial nanotube load in 0.001 wt.% solutions of **1**. (c) Visible-NIR absorption spectra of the corresponding dispersions. (d) Optical absorbance of individually dispersed SWCNTs at 600 nm versus the weight ratio of **1** to SWCNT load. As the relative load of **1** decreases the concentration of individually dispersed SWCNTs steadily increases until the stoichiometric limit. At ratios well below the stoichiometric limit, a maximum is reached and then followed by a sharp decrease. The stoichiometric limit, as revealed by the molecular mechanics model, corresponds to one molecule of **1** approximately every 2 nm length of SWCNT.

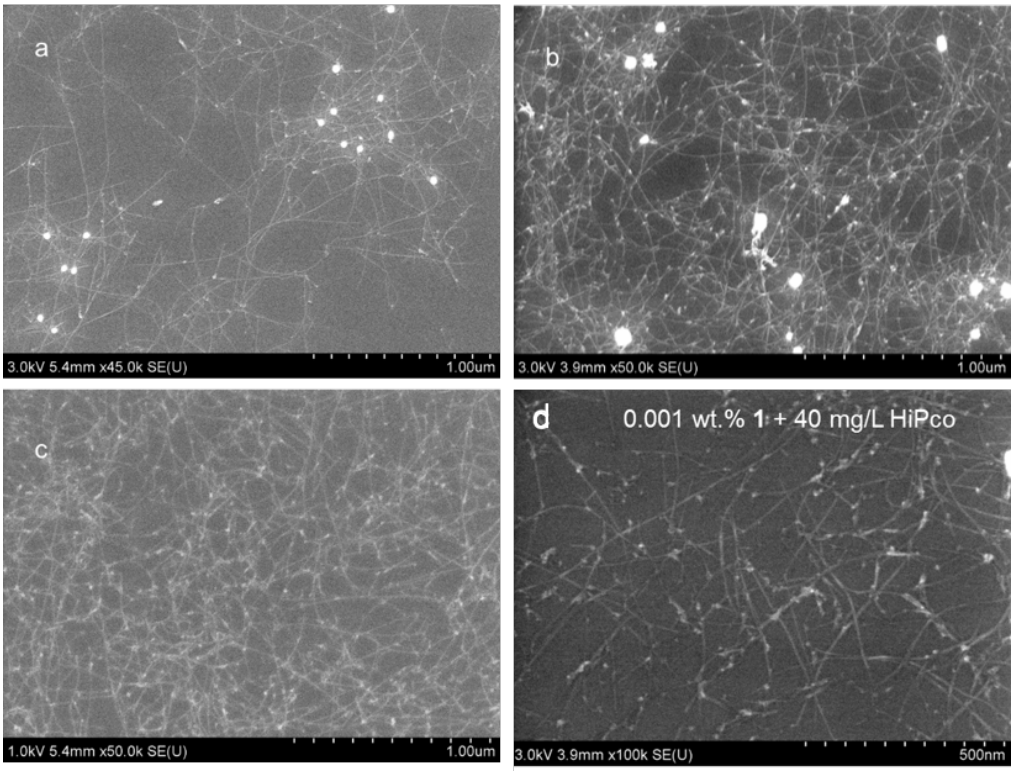

Figure 2-4. SEM images of **1**•SWCNTs structures on silicon substrates. The samples were prepared from 0.001 wt.% **1** with increasing initial concentration of HiPco SWNTs at 1.00 um scale (a) 20 mg/L, (b) 40 mg/L, (c) 80 mg/L, and (d) at 0.5 um scale for 40 mg/L.

2.3.3 Turn-on Effect: Optical Properties of 1•SWCNTs

UV-vis-NIR absorption spectra of the **1**•SWCNTs solutions are nearly featureless. However, upon adding SDBS and shaking the solution by hand, the

distinct van Hove absorption peaks that are characteristic of individually dispersed SWCNTs[53] were recovered (Figure 2-5). Consistently, SWCNTs solubilized with **1** initially did not fluoresce; however, strong fluorescence was observed upon the addition of SDBS with shaking (Figure 2-6b). Both fluorescence and van Hove absorption are characteristic of individually dispersed SWCNTs. Interestingly, the nanotubes must have already become debundled by **1** since no sonication was required to recover the optical features; rather, gentle shaking by hand was sufficient. This behavior suggests the **1**•SWCNTs were not strongly bundled but loosely associated individual nanotubes in water. We believe that the added SDBS molecules patch the exposed nanotube surface to recover the fluorescence and optical absorption by insulating the SWCNT from the environment and interactions with other nanotubes. This explanation is consistent with previous observation of enhanced fluorescence as the nanotube surface is more densely covered with an aliphatic analog of flavin mononucleotide.[54] The observed fluorescence turn-on effect may be useful in biomolecular sensing[55] and will be further explored in future studies.

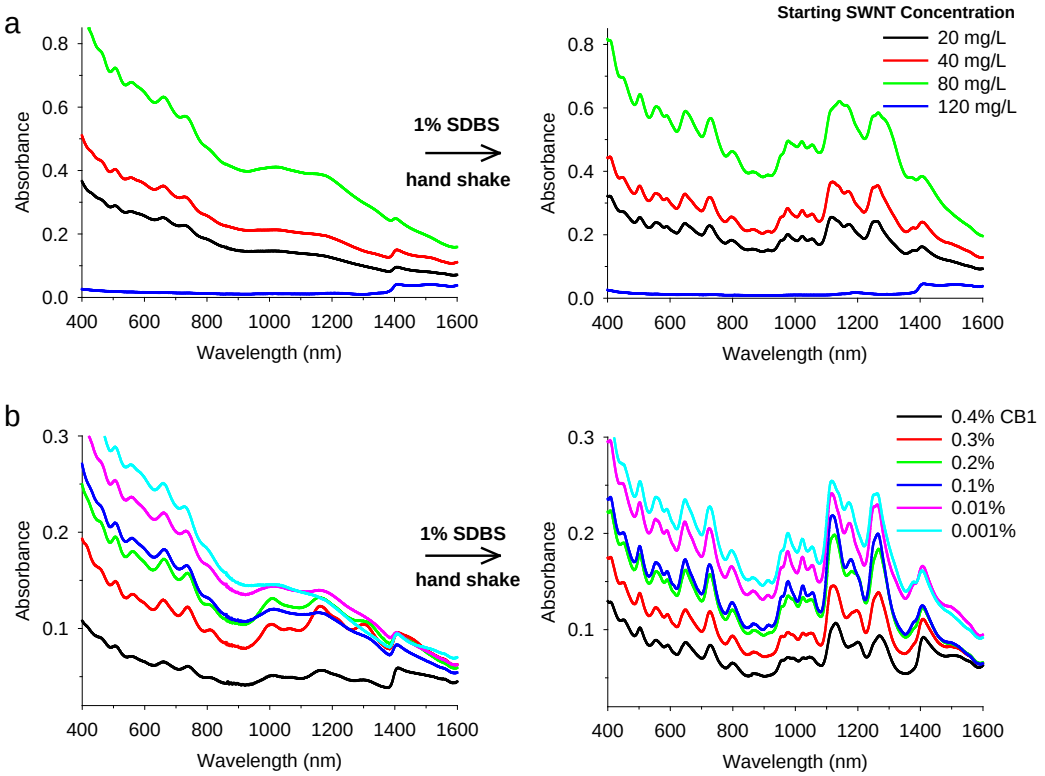

Figure 2-5. Optical turn-on effects: sharp optical absorption peaks were observed upon addition of 1 wt.% SDBS and hand shaking of the solutions. (a) Samples of 0.001 wt.% **1** with increasing loads of SWCNTs (20, 40, 80, and 120 mg/L of HiPco SWCNTs). (b) fixed SWCNT load (20 mg/L SWCNTs) in **1** of increasing concentrations: 0.0001 wt.%, 0.001 wt.%, 0.01 wt.%, 0.1 wt.%, 0.2 wt.%, 0.3 wt.%, 0.4 wt.%.

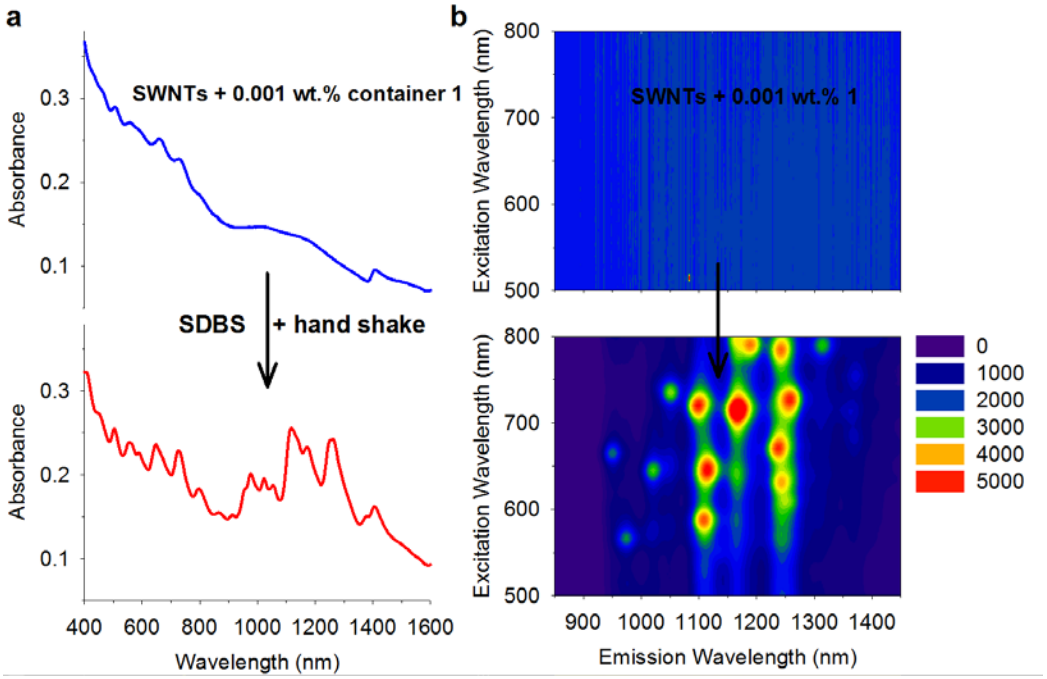

Figure 2-6. Turn-on optical properties upon addition of SDBS. The optical absorption (a) and fluorescence (b) that are characteristic of individually dispersed SWCNTs were turned on upon addition of SDBS (to a concentration of 1.0 wt.%). Shown is the case of 20 mg/L nanotube load in 0.001 wt.% **1**, but this phenomenon is general to all experimental conditions investigated in this work.

2.3.4 CB[n]1 and CB[n]2 Selectively Stabilizes Small Diameter Single-Walled Carbon Nanotubes

Intriguingly, excitation-emission fluorescence maps suggest that the container **1** selectively interacts with smaller diameter and low chiral angle SWCNTs (Figure 2-7). Compared to SDBS (Figure 2-7a), **1** and **2** (Figure 2-7b and 2-7c) show a clear tendency of much higher fluorescence intensities for smaller diameter nanotubes. Interestingly, the fluorescence intensity of SWCNTs systematically decreases as the concentration of **1** increases from 0.001 wt.% to 0.4 wt.% (Figure 2-8). For the 0.4 wt.% solution of **1**, strong emission peaks correspond to small diameter SWCNTs: (8,3), (8,4), and (9,4) with diameters of

7.8 Å, 8.4 Å, and 9.2 Å, respectively. The (8,3) accounts for 15.8% of the fluorescence intensity of the 0.4 wt.% **1**•SWCNTs solution, more than 3 times higher than that in the 0.001 wt.% **1** sample. On the other hand, the total amount of dispersed large diameter (d > 0.95 nm) SWCNTs (8,6), (8,7), (9,5), (10,5) decreases by 45% as the concentration of **1** increases (Figures 2-9a). Also there is a selectivity towards low chiral angle SWCNTs, demonstrated by a stronger emission signal for (9,4) compared with (7,6) even though their diameters are similar (Figure 2-9a). We also observed changes in the UV-Vis-NIR absorption spectra which are consistent with the selectivity patterns described above. However, the lower inherent sensitivity of the optical absorption spectra to differences in SWCNT structure and the significant background signal due to other carbonaceous by-products makes the fluorescence experiments described above more authoritative.

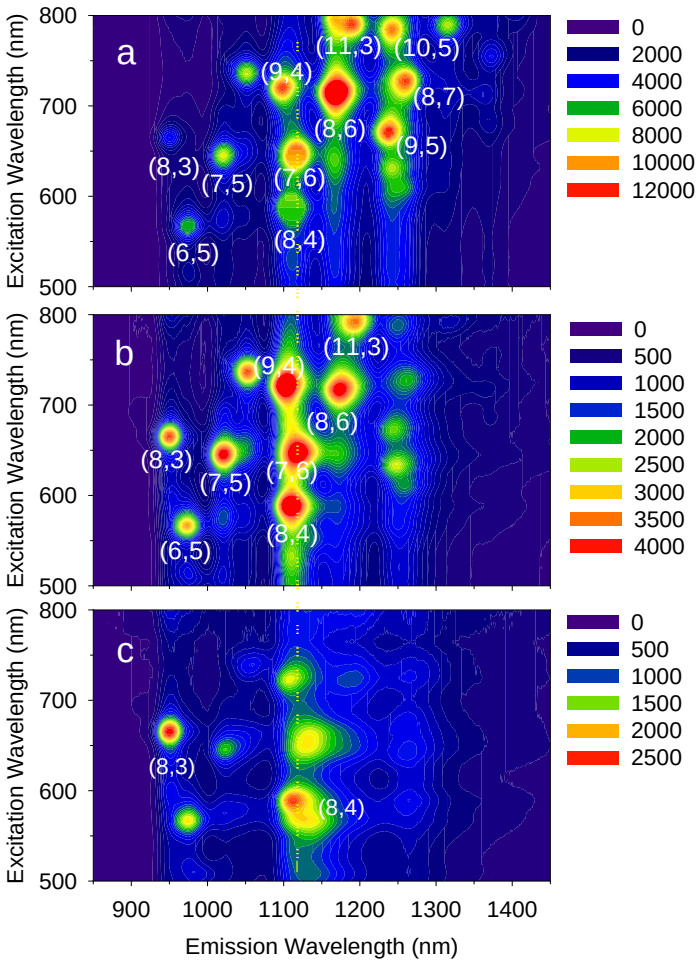

Figure 2-7. Excitation-emission fluorescence maps show evidence of selectively enrichment of smaller diameter SWCNTs in aqueous solutions by container molecules. Shown are solutions prepared from an initial load of 20 mg/L HiPco SWCNTs and (a) 1 wt.% SDBS, (b) 0.1 wt.% **1**, and (c) 0.1 wt.% **2**. Compared to SDBS control, **1** favors smaller diameter SWCNTs. The structural selectivity is further evidenced in **2**.

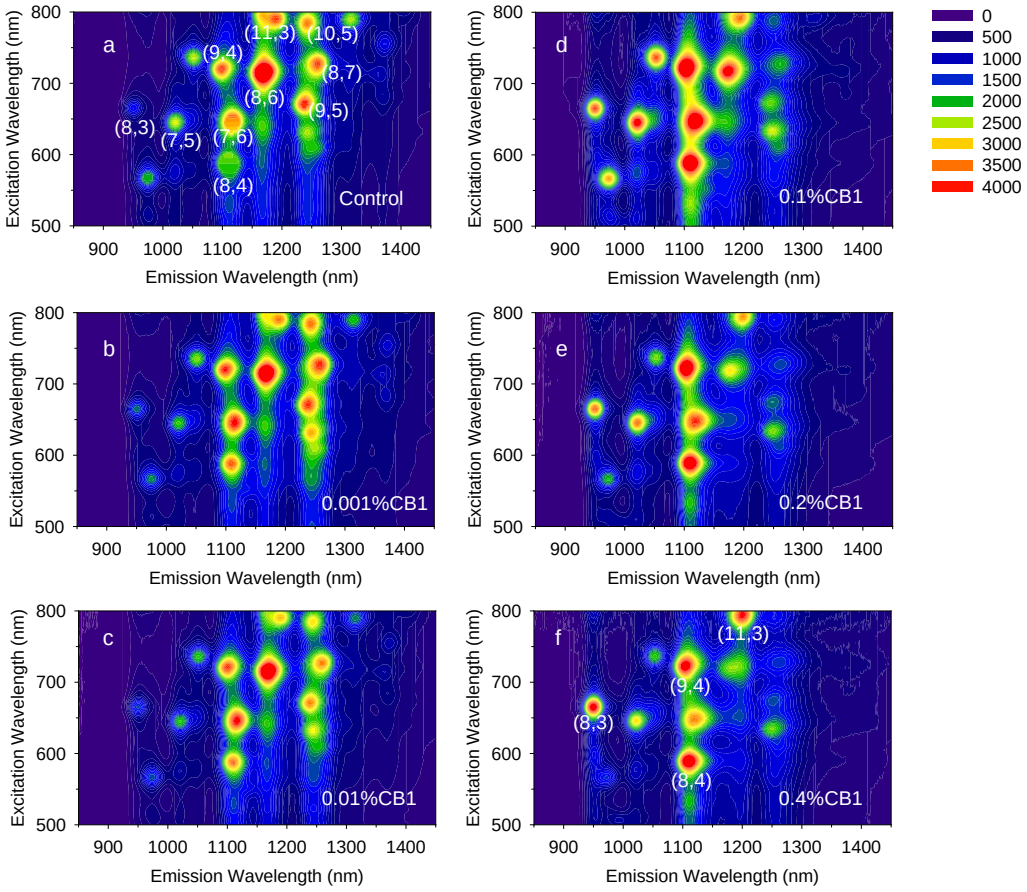

Figure 2-8. Excitation-emission fluorescence maps show enrichment of low chiral angle SWCNTs as the concentration of **1** increases. The control sample was prepared from 1 wt.% SDBS which is known to show little structural selectivity. From (b) to (f), the concentrations of **1** are 0.001 %, 0.01 %, 0.1 %, 0.2 %, and 0.4 % (wt./vol.), respectively. The starting SWCNT concentration was 20 mg/L.

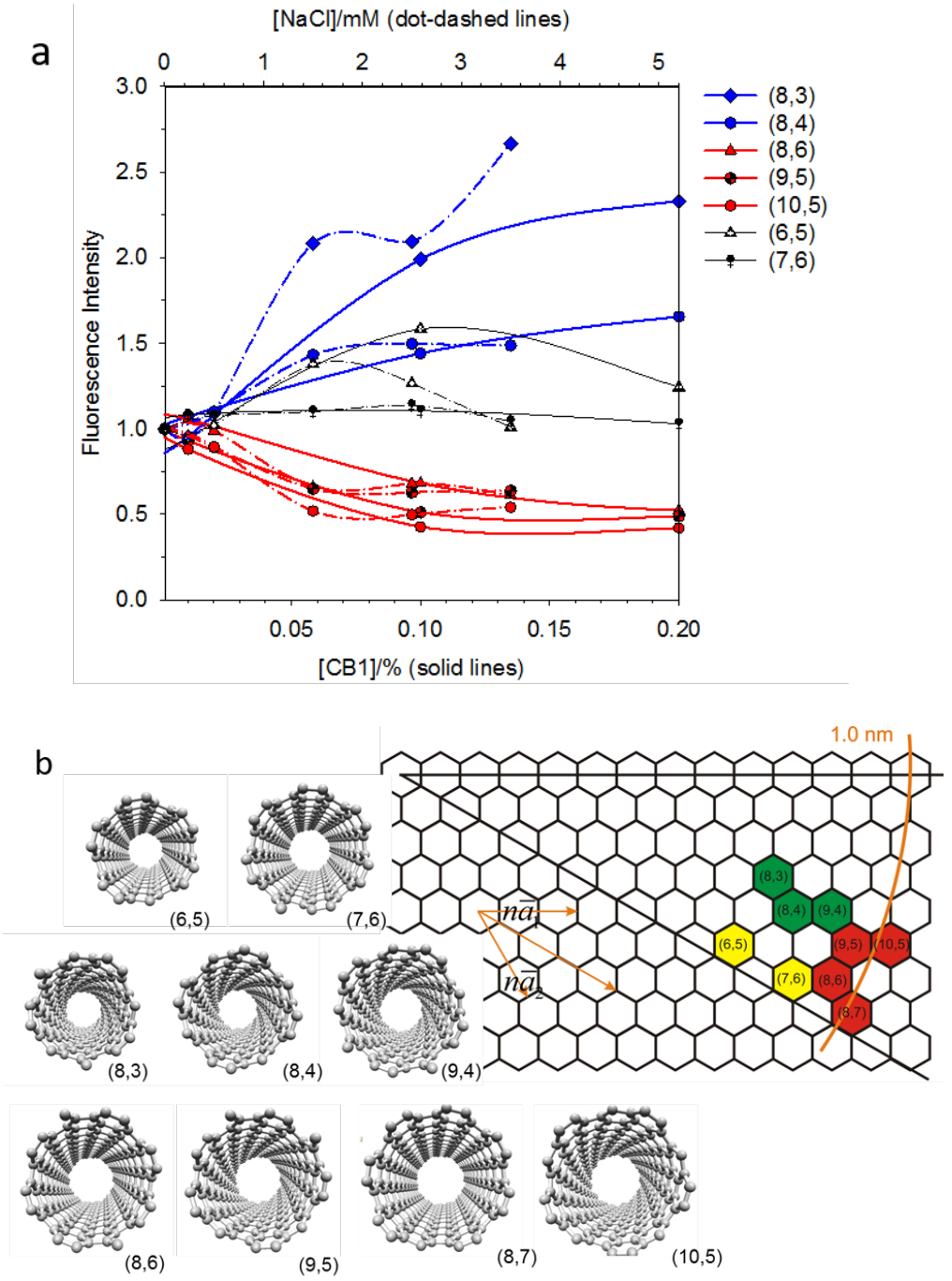

Figure 2-9. Structural selectivity of SWCNTs by increasing the concentration of **1** or NaCl. The populations of small diameter and low chiral angle species, e.g., (8,3), (8,4), and (9,4), are enriched by increasing the concentrations of **1** or salts. For larger diameter species, e.g., (8,6), (9,5), (8,7), and (9,6), the relative fluorescence intensities decrease by a factor of 2. While for small diameter, high chiral angle species, e.g., (6,5) and (7,6), the effects of increased concentrations of **1** or salts are negligible.

2.3.5 Salt Effects Enhance CB[n]1 and CB[n]2 Selectivity Towards Small Diameter Single-Walled Carbon Nanotubes

The observed concentration-dependent diameter selectivity can be explained by salt effects. We found that addition of 2.5 mM NaCl made the SWCNT fluorescence map of 0.001 wt.% **1** solution similar to that of the 0.1 wt.% **1** solution, which contains ~2.6 mM Na^+ (see Figure 2-10). As the NaCl concentration is increased from 0 to 3.5 mM, there is a systematic decrease of the SWCNT fluorescence intensity towards smaller diameter SWCNTs as shown in Figure 2-9a and Figure 2-11. For small diameter, low chiral angle species such as (8,3) and (8,4), the populations are similarly enhanced either by increasing the concentration of **1** or the salt. For large diameter species (8,6), (9,5), and (10,5), the populations are reduced. However, small diameter high chiral angle species (6,5) and (7,6) are not affected. These trends are corroborated by the corresponding visible-NIR absorption spectra (Figure 2-12). The salt effect was enhanced with a divalent salt solution. A concentration of 0.05 mM $CaCl_2$, compared to 2.5 mM NaCl, already shifts the selectivity towards small diameter SWCNTs.

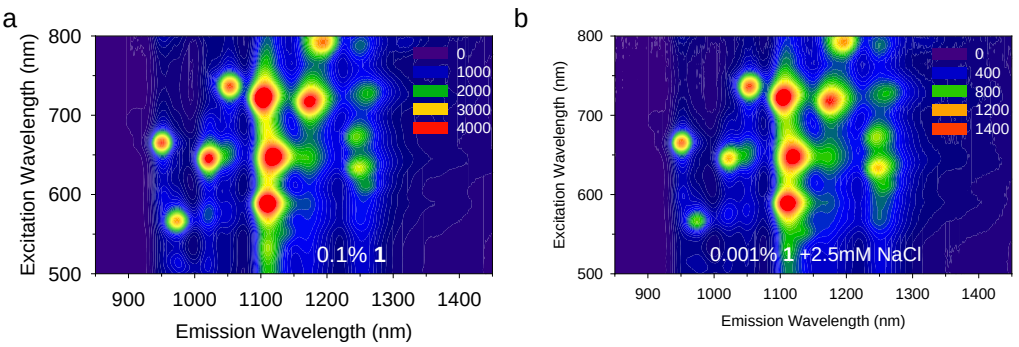

Figure 2-10. Excitation-emission fluorescence maps of **1**•SWCNT solutions prepared from 20 mg/L (initial load) of HiPco SWCNTs in 0.1 wt.% solution of **1** versus 0.001 wt.% **1** and 2.5 mM NaCl. The fluorescence maps were obtained after adding 1 wt.% SDBS and hand shaking the solutions. The added NaCl shows similar SWCNT selectivity as that high concentration **1**.

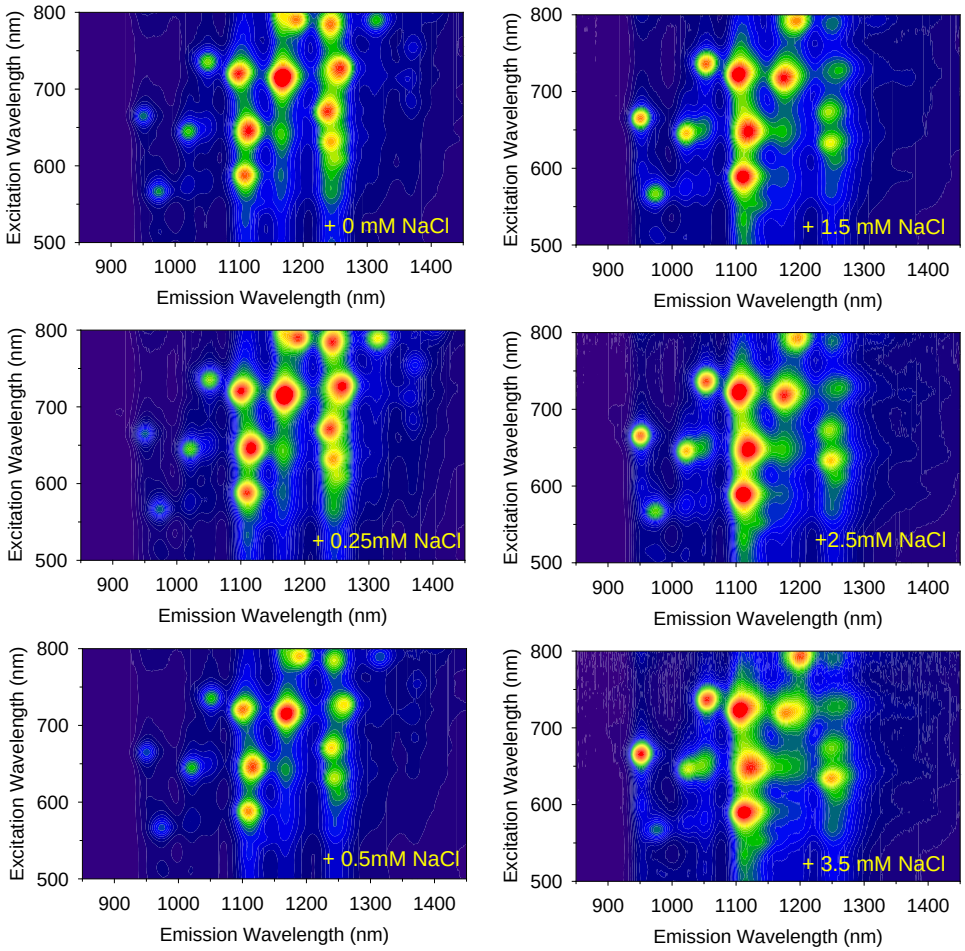

Figure 2-11. Salt effects on the structural selectivity of **1**•SWCNTs. Shown are **1**•SWCNTs prepared from 0.001 wt.% **1** + 20 mg/L HiPco SWCNTs at different NaCl concentrations (by adding 1.0 M NaCl/D2O solution to 20 mL **1**•SWCNTs dispersions). The fluorescence maps were obtained after adding 1 wt.% SDBS and shaking the solutions by hand.

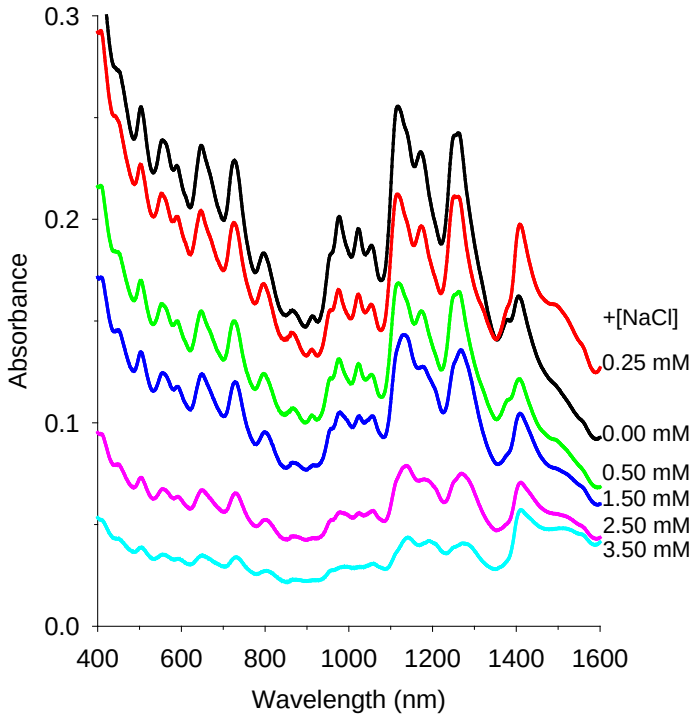

Figure 2-12. Salt effects on visible-NIR absorption spectra for **1**•SWCNTs that correspond to Figure 2-10 and 2-11. The spectra were collected after adding 1 wt.% SDBS and shaking the solutions by hand.

We rationalize the observed preference of **1** for smaller diameter SWCNTs at higher salt concentration based on the well-known metal ion binding properties of CB[n] compounds. The presence of metal cations rigidifies the C-shape of **1** by bridging adjacent C=O groups which results in higher curvature and a preference for smaller SWCNTs. Conversely, in the absence of metal cations, **1** is better able to expand its cavity to accommodate the larger diameter SWCNTs. This is consistent with previous observations by us and others that increasing the concentration of metal cations reduces the affinity of the acyclic cucurbit[n]uril congener toward guest molecules due to binding competition at the ureidyl C=O portals.[50,56,57] The preference for low chiral angle SWCNTs can be explained by the calculated geometry of the **1**•SWCNT complex (Figure 2-2). For low chiral

angle SWCNTs the π-π stacking interactions are stronger due to the matched orientation of the terminating aromatic motifs of **1** whereas for high chiral angle tubes the π-π interactions are weaker. As a test of the importance of π-π interactions toward the selective solubilization, we decided to investigate the interaction of **2** with SWCNTs. The strength of the π-π interactions between the SWCNTs and the acyclic CB[n] type receptor **2** would be expected to increase (relative to **1**) because of the larger π-surface area of the naphthalene walls of **2**. Satisfyingly, as shown in Figure 2-13, acyclic CB[n]-type container **2** shows similar optical turn-on effects and a clear selectivity towards low chiral angle, small diameter (8,3) and (8,4) SWCNTs at much lower (salt) concentrations.

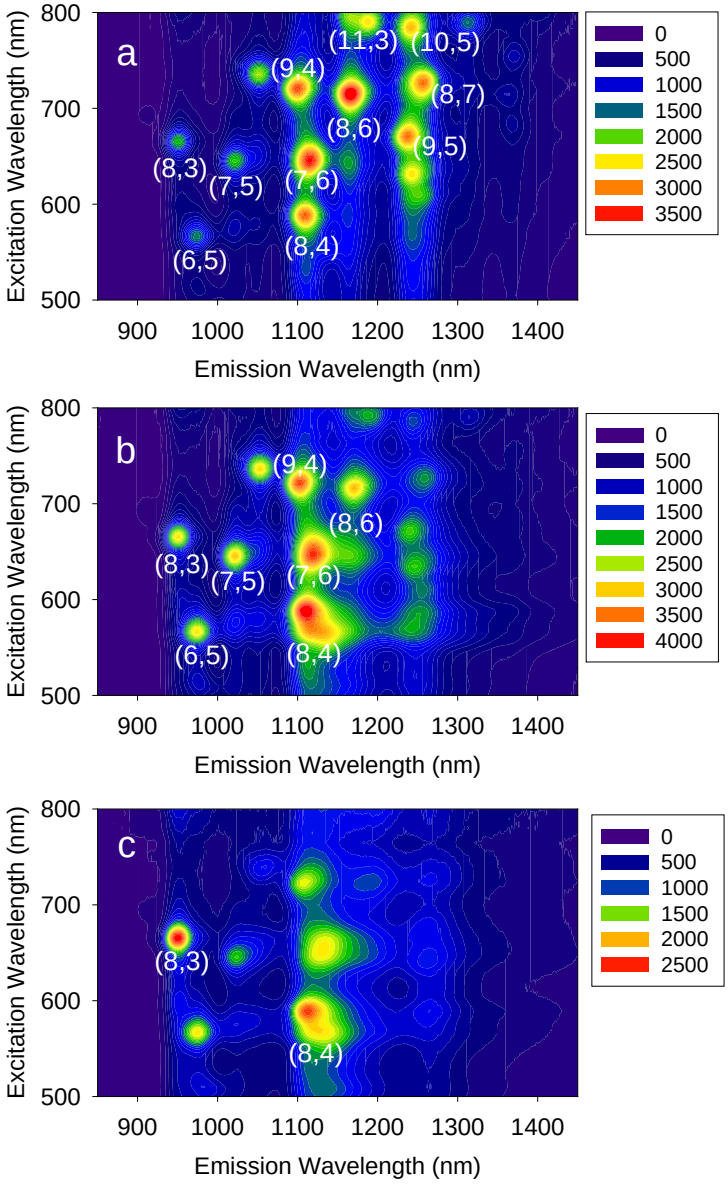

Figure 2-13. Concentration effects on the chirality selectivity of **2**. 20 mg/L SWCNT load with increasing **2** concentrations: (a) 0.001 wt.%, (b) 0.01 wt.%, (c) 0.1 wt.%. The fluorescence maps were collected after adding 1 wt.% SDBS and hand shaking of the solutions.

2.4 Conclusion

In summary, we have shown that acyclic cucurbit[n]uril type molecular containers **1** and **2** are able to solubilize SWCNTs at concentrations (0.001 wt%) that are 1000-fold lower than used in standard SDBS solubilization. The C-

shaped molecular containers clip on to SWCNTs by a combination of π-π interactions and the hydrophobic effect, and render nanotubes solubilized in water due to the presence of the sulfonate groups on **1** and **2**. Compounds **1** and **2** display a selectivity toward small diameter and low chirality SWCNTs due to the inherent curvature of **1** and **2** and the nature of the π-π interactions between the aromatic walls of the molecular containers and the SWCNTs. The presence of metal ions (e.g. Na^+ or Ca^{2+}) enhances the selectivity for small diameter, low chiral angle tubes by binding to the ureidyl C=O portals of **1** and **2**, thereby rigidifying their structures and making them less able to flex their methylene bridged glycoluril oligomer backbones to accommodate larger SWCNTs. The implications of the research presented are manifold. For example, by tailoring the nature of the aromatic walls of the acyclic CB[n]-type containers, it should be possible to tune the selectivity toward specific classes (e.g. diameter, chirality) of SWCNTs. The ability of **1** and **2** to solubilize SWCNTs at low concentrations while leaving the nanotube surface exposed enables the preparation of hybrids with biomolecular receptors, which are expected to combine the advantageous optical properties of the SWCNTs with the molecular recognition ability of the biomolecules.

Chapter 3: Ammonium Laurate Surfactant for Cleaner Deposition of Carbon Nanotubes

Adapted from Nilsson, H. M.; Meany, B.; Ticey, J.; Sun,C. F.; Wang, Y. H.; Cumings, J. Langmuir 2015, 31.

H.M. Nilsson prepared ammonium laurate solutions, conducted electrophoresis zeta potential measurements, and made AFM measurements. B. Meany prepared carbon nanotube solutions, and measured absorbance, photoluminescence, and Raman spectra. J. Ticey took TEM images.

3.1 Introduction

Carbon nanotubes (CNTs), closed cylinders of graphene, have exhibited promising properties for mechanical, optical, electrical, and thermal applications.[1, 16,58-60] However, an issue that commonly arises is that measurements of composites and bulk samples of CNTs do not show as promising properties as the individual nanotubes themselves.[61,62] In order to use CNTs in many applications, these bulk properties must be improved. Understanding and improving the bulk properties will inevitably require the ability to manipulate individual CNTs without altering the CNTs and without introducing property-changing contamination. It has been well-documented that the common procedures that are used to separate and measure individual CNTs introduce residues that change the effective properties of the CNTs.[63,64] There is currently a strong effort to develop cleaning procedures to

remove these residues from carbon nanomaterials,[65,66] but a better approach is to limit the sample's exposure to contaminants from the start.[67] One source of contamination residue is from resist used during lithography steps,[68,69] but another, less commonly addressed source, is surfactant residue from CNTs suspended in aqueous solutions. Electron micrograph images in publications sometimes even show the residue of reformed surfactant salt alongside the CNTs.[70,71] This residue is not only problematic for imaging, but also changes the properties of the deposited nanomaterial, including introducing higher electrical contact resistance.[63,72]

For almost two decades, research has shown that CNTs can be suspended in solutions and later deposited onto substrates for testing, but the approach remains notoriously difficult and unreliable to apply in practice. CNTs are hydrophobic and bundle together readily in most common solvents, and the solutions themselves—or the methods to produce them—often leave behind unwanted contamination. These studies have focused on both single-walled CNTs (SWCNTs)[15,73] and multi-walled CNTs (MWCNTs),[70] with numerous qualified successes. An appealing approach for the successful dispersion of individual CNTs is through covalent functionalization[74] or molecular wrapping.[20] While these methods can be ideal for certain applications, such as in some biological environments,[95] these semi-permanent chemical modifications often change the properties of the CNTs, for example the mechanical and emission properties,[76,77] and are therefore undesirable for many purposes. Efforts to remove the covalent species or wrapped molecules can have limited success, but complete removal without other alterations to the nanotubes is difficult to achieve, for example even extensive washing after nitric

acid treatment still leaves the nanotubes with measurable amounts of carboxylic acid groups.[78] Another option for improving the dispersability of CNTs in water is to oxidize their outer shells.[79] While this can be done gently to minimized damage to the CNTs, the nature of the process does still change CNT properties, for example, by reducing the burning temperature.[80] For some applications this may not be a critical flaw, but for others it may, and for cases where pristine CNTs are desired, this is not a suitable option. Other efforts have focused on dispersing CNTs in polar organic solvents such as dimethylformamide (DMF) and *N*-methylpyrrolidene (NMP).[81,82] Unfortunately, these solvents have low dispersion limits, less than ideal stability, and can be dangerous and expensive.[83] A small body of work has shown very high solubility for CNTs in superacids,[84] but strong acids are less compatible with typical processing environments. The covalent/non-covalent tradeoffs can be overcome through the development of covalently functionalized double-walled carbon nanotubes which feature tailored surface chemistry and protected inner tube properties.[85,40] However, the samples produced by this approach have covalently modified outer walls which prevent direct investigation of the starting materials. Since avoiding tube damage is so important, surfactants that non-covalently disperse CNTs have emerged as a common standard approach, especially when the goal is characterization of intrinsic properties.

Single surfactant molecules have hydrophilic and hydrophobic nature that allows them to form dispersions of hydrophobic CNTs in water. However, the contemporary understanding of how surfactant micelles form and interact with CNTs above the critical micelle concentration (CMC) is still quite limited.[86,87]

Nevertheless, it has been well documented that surfactants, especially coupled with sonication, can be used to create stable suspensions of individual CNTs.[70,88] In this category, there are also a wide variety of nonionic, anionic, cationic, and zwitterionic surfactants that have been investigated. Among the nonionic surfactants, octyl phenol ethoxylate (Triton X-100), alkylphenolethoxylate (IGP), and the TWEEN family (Polysorbate 20, TWEEN 60, etc.) are the most common and have shown high dispersion limits in some studies.[70,89] Cationic surfactants have shown less promise, but the ones most commonly cited are dodecyl trimethylammonium bromide (DTAB) and cetrimonium bromide (CTAB).[88,89] The most common category of surfactants used for individual CNT suspensions is anionic; these include sodium octanoate (SOCT), sodium dodecyl sulfate (SDS), and sodium dodecyl benzene-sulfate (SDBS).[88,90-92] After a series of promising leads in the area of surfactant development, there has been a stagnation of effort during the last ten years, with fewer studies proposing new or improved surfactant formulations for nanotube depositions. In this atmosphere, SDS has emerged as the *de facto* standard because, for many applications, it is better than the other alternatives, it is readily available and "good enough," or it at least serves as a point of reference for controlled studies.

We present a comparison between SDS and ammonium laurate (AL), the latter of which has not previously been used as a surfactant for CNT dispersion. As can be seen in Figure 1, AL and SDS both have a C_{12} alkane end group interacting with the CNTs and differ only in the ionic end group interacting with the solution. We find that AL shows promising results as compared to SDS, with a key advantage

being the elimination of surfactant residue after CNT deposition onto a substrate, among other benefits. In addition, we find that, compared to SDS, AL depositions show fewer unwanted carbon particles connected to the MWCNTs, such as fullerene onions. Despite having the same length and morphology of the hydrocarbon tail, the slight difference in head groups and the change from sodium to ammonia cation in AL unexpectedly improve the interaction with the MWCNTs for cleaner deposition of individual carbon nanotubes from surfactant-stabilized suspension. Electrophoresis measurements give insight into the reasons for the difference.

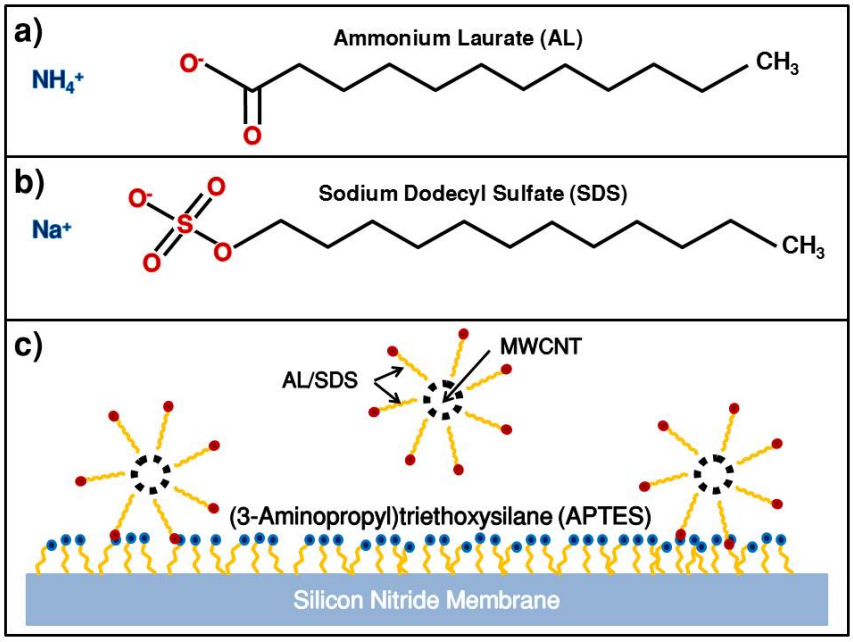

Figure 3-1. Molecular structure of surfactant system used to suspend and deposit MWCNTs. (a) AL surfactant, (b) SDS surfactant, and (c) MWCNTs encapsulated in surfactant micelles and their attraction to APTES treated silicon nitride membrane.

3.2 Materials and Methods

3.2.1 Silicon Nitride Substrate Treatment

The substrates used for nanotube deposition are 100 nm thick silicon nitride membranes purchased from Silson Ltd. They are treated with (3-Aminopropyl)triethoxysilane (APTES, Sigma Aldrich 99%) prior to the nanotube deposition, in order to form a self-assembled monolayer (SAM). Liquid APTES is evaporated into a vacuum chamber and diffusively re-deposited on to the membranes for 7 minutes. The membranes are then placed on a hot plate at 120 C for 30 minutes. The samples are dipped in 37% hydrochloric acid for 5 seconds and then transferred to DI water for 1 minute prior to being transferred into the nanotube solutions, where they are left for 48 hours. Upon being taken out of solution, the membranes are immediately dried with nitrogen gas.

3.2.2 Preparation of Carbon Nanotube Solutions

The nanotubes used are MWCNTs produced via arc-discharge[40] and purchased from Sigma-Aldrich in unprocessed boule form. Nanotube-dense regions of the boule are scraped out and crushed manually. Small amounts are added to 10 ml batches of aqueous solutions. After the MWCNTs are added to the solutions, they are bath sonicated for 20 minutes (70 W) then probe sonicated with a 13 mm circular tip for 2 minutes at 20% of 500 W with pulsing of 1 second on, 1 second off (Sonics Vibra Cell VC 505). Since the area of the bath sonicator is approximately 100 cm^2 the power density applied to the tubes during this process

is very gentle in comparison to the probe sonicator. Solutions are then centrifuged for 30 minutes at 1,000 g. The top portion of homogeneous solution is decanted (approximately 9 ml) by pipet after centrifugation so that the bottom portion of solution containing large amounts of graphitic particles could be discarded and solutions containing mostly suspended nanotubes and carbon nanoparticles are utilized for the following studies.

HiPco Single-Walled Carbon Nanotubes (SWCNTs) were purchased from Rice University and used as received. SWCNTs were dispersed in aqueous solutions of AL or SDS by 2 hours of ultrasonication at 10˚C (Misonex, S-4000, Farmingdale, NY). Following sonication the solutions were ultracentrifuged (170,499*g*) for 4 hours at 20˚C in order to remove bundled nanotubes and impurities. The upper 80% of the supernatant was removed for measurement.

3.2.3 Preparation of Surfactant Solutions

SDS solutions are prepared by weighing out appropriate amounts of SDS powder (Sigma Aldrich ReagentPlus, >98.5% (GC)) to glass vials and then adding 10 ml of DI water. The solutions are bath sonicated for 20 minutes until the SDS is dissolved.

AL solutions are prepared by first weighing out appropriate amounts of dodecanoic acid (>99% (GC/titration)) to glass vials and then adding 10 ml of DI water. Ammonium hydroxide is added dropwise to the solution to convert the lauric acid to AL, and the addition continues until the solution pH reaches 11 to ensure that the lauric acid is fully dissolved.

3.2.4 Transmission Electron Microscopy (TEM)

TEM images were obtained using a JEOL JEM-2100 LaB6 transmission electron microscope at 200 kV accelerating voltage. High resolution images were taken on a JEOL JEM 2100 FEG transmission electron microscope also at 200 kV.

3.2.5 Spectroscopic Characterization

Absorbance spectra were taken with a Perkin-Elmer 1050 UV-vis-NIR spectrophotometer (Waltham, Massachusetts). The Raman scattering spectra were obtained with a Horiba Jobin-Yvon LabRam HR-VIS microRaman system including a 633 nm helium neon laser excitation source. Excitation-emission maps fluorescence maps were measured with a Horiba JobinYvon Nanolog spectrofluorometer equipped with a liquid nitrogen cooled InGaAs array detector.

3.3 Results and Discussion

3.3.1 Surfactant Chemistry

Although AL is not commercially available as a compound, this surfactant can be conveniently prepared from the anionic acid, lauric acid, as a precursor by simple ionic exchange in aqueous solution. The lauric acid has a much higher pKa than the corresponding SDS anion; about 5 versus 1.9. By adding aqueous ammonia to a lauric acid/deionized water mixture, dissociation of the acid occurs and an AL solution is formed. The pH of the AL solutions is increased to 11 for shelf-stable solutions with very low anionic strength. Figure 3-1 shows the structure of the surfactants that were tested as well as the surface chemistry added to the substrates

prior to solution deposition. In order to gain a greater understanding for the effect of pH and addition of hydroxide, a series of tests were performed with different combinations of lauric acid, SDS, ammonium hydroxide, and sodium hydroxide. Through these experiments it was found that AL far outperforms the other ionic combinations and this work therefore only focuses on AL, in comparison with the numerous prior studies of SDS as a reference surfactant. The outcome of the other combinations can be found in the Table 3-1 and Figure 3-10. The substrate surface preparation was carried out by low-pressure silanization, as described above in the Experimental section, to improve adhesion of the surfactant anions.

The solutions tested ranged from 0.5 to 2.0 wt.% surfactant. For SDS, different studies have determined that the ideal concentrations of SDS for the dispersion of MWCNTs generally falls within the same range tested here.[91,94-96] These concentrations represent about 2 to 10 times the CMC for both surfactants. The CMC for AL is 9.25 mM,[97] which is just 11% higher than that of SDS. However, this difference may be the reason that AL does not start to perform well until 1.0 wt.% while SDS starts to suspend well even at 0.5 wt.%. A previous study using small-angle neutron scattering and time-averaged light scattering found that pure AL solutions form rod-like micelles above the CMC with a nearly constant radius of 15 angstrom.[97] The higher the concentration of AL, the longer the micelle rods become, which we speculate leads to AL forming stable cylindrical micelles around MWCNTs, in contrast to SDS, which is known to form isotropic spherical micelles in these concentration ranges.[98]

3.3.2 Solution Stability

The stability of the CNT dispersions is monitored for sedimentation and by recording absorption spectra over the course of 11 days. The procedure for creating these solutions is detailed in the Experimental section above and includes ultrasonic processing, centrifuging, and decanting the solutions. We note that compared to most CNT surfactant procedures,[92,99] which require sonication for many hours, ours requires only 20 minutes of gentle bath sonication and 2 minutes of probe sonication, which minimizes damage to the CNTs. An example of what happens to MWCNTs after a lengthy 2 hours of probe sonication in SDS and AL is shown in Figure 3-2, which confirms that the 2 minutes we use is indeed a gentle process.

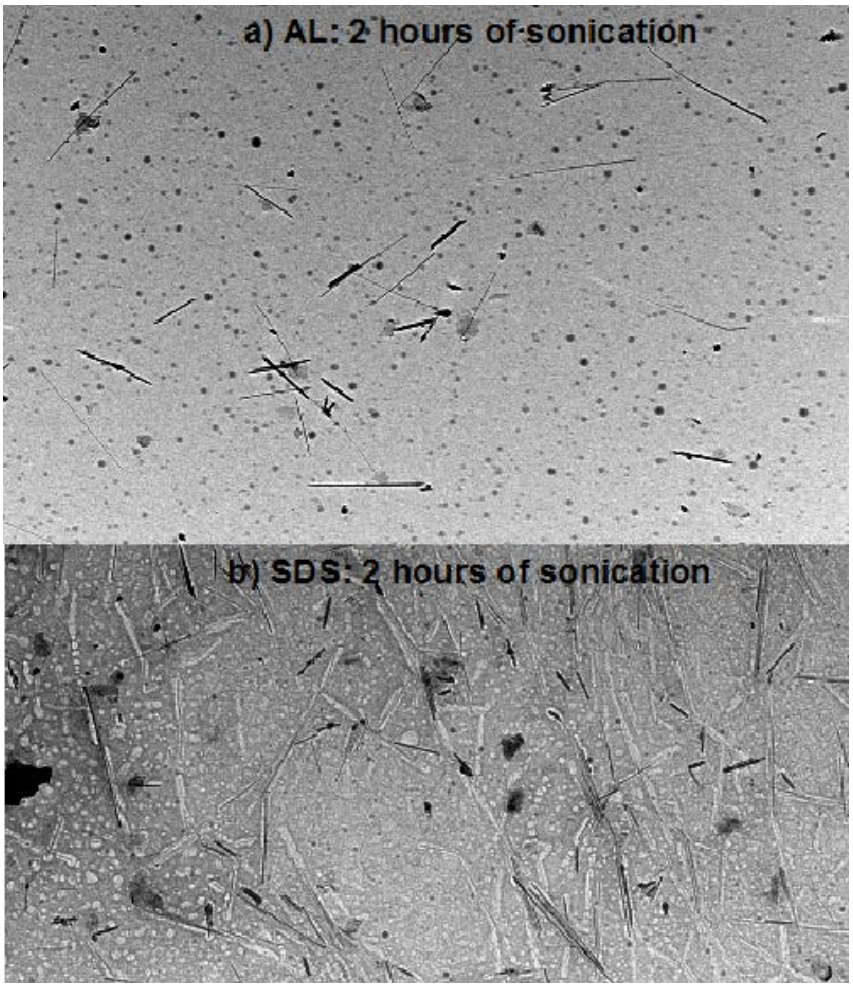

Figure 3-2. TEM images showing the result of extended (2 hours) probe sonication. a) is of an AL solution and b) is of an SDS solution. As compared to other images presented in this work which were all probe sonicated for 2 minutes, it is evident that the extended probe sonication does not improve the cleanliness of the SDS deposition and additionally it damaged/shortens the MWCNTs.

Absorption spectra are recorded for 1.0 wt. % surfactant solutions on days 1, 3, 8, and 11 after they are prepared. By looking at the average absorption from 300 nm to 800 nm we are able to obtain quantitative information of the MWCNT concentration retention over time. The raw absorption data is available in Figure 3-3.

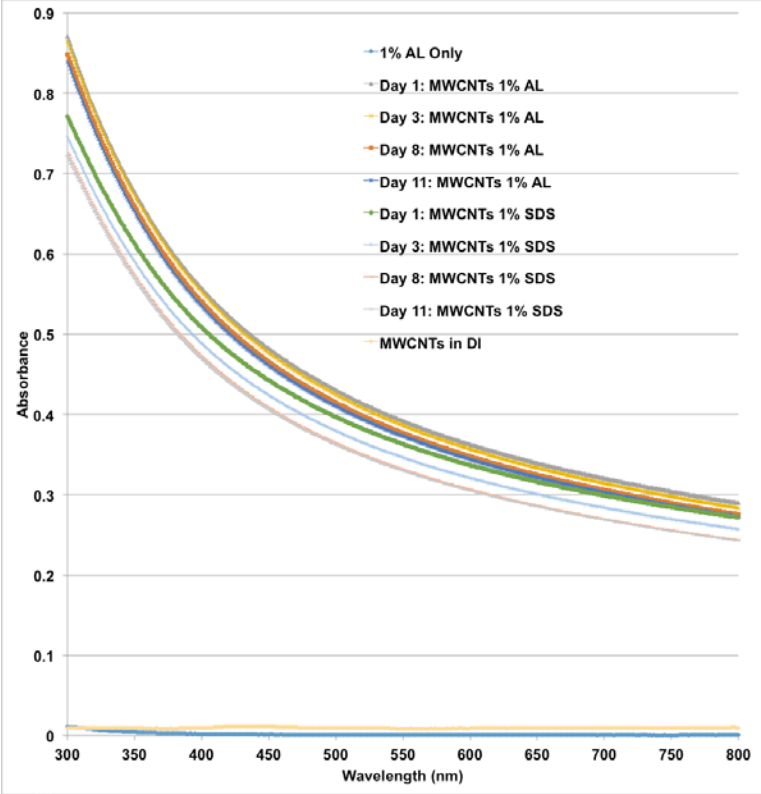

Figure 3-3. Raw absorbance data from 300 to 800 nm for the MWCNT surfactant solutions over time including the baseline absorbance of a solution without MWCNTs and a solution of MWCNTs in DI water.

A drop in absorption is lower for AL than for SDS as shown in Figure 3-4b, indicating that the MWCNT concentration decreases less over the course of the first 11 days for AL than for SDS. Figure 3-4b represents one set of solutions, but measurements on other batches show similar trends, with the lost MWCNTs becoming sediment at the bottom of the vials. In addition, the AL solution retains 95% of its optical absorption indicating high stability. By comparing photographs in Figure 3-4a for each solution, it is also possible to monitor the stability of the MWCNT suspensions. The variation in the MWCNT concentration seen in the different solutions is a function of the amount of material that is stable in solution

through the centrifuge process. This leads to the conclusion that the 1.0 and 2.0 wt. % AL solutions are most effective at keeping MWCNTs in suspension, with 1.0 and 2.0 wt. % SDS solutions showing successively and reproducibly lower MWCNT concentrations at the end of 11 days. The solution without any surfactant, labeled “DI” did not disperse visible amounts of nanomaterials, as expected. During the centrifuging process the DI-nanotube suspension could not be decanted, and instead was resonicated prior to the “Day 1” picture. The images of the “DI” solution also show that without surfactant, like most CNT specimens, our MWCNTs do not suspend well in deionized water—by day 10 the solution is nearly clear and the bottom of the vial contains the aggregated nanomaterials.

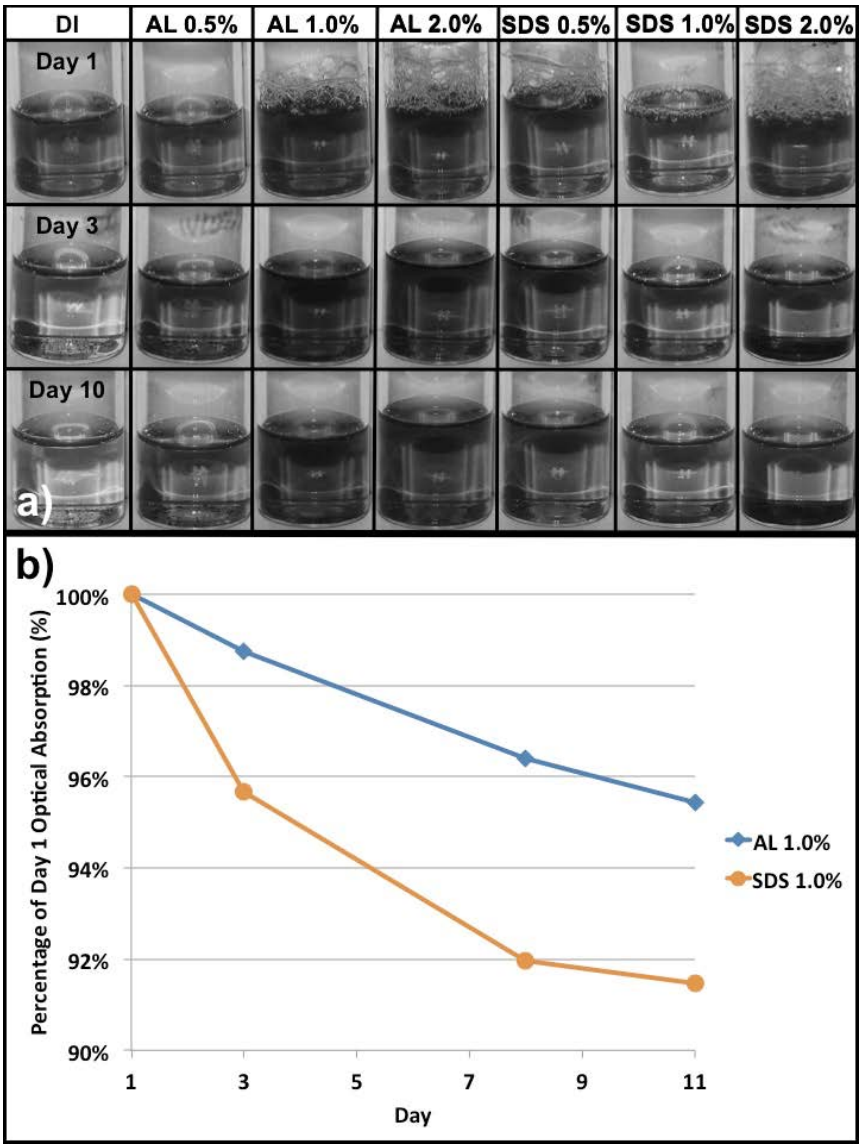

Figure 3-4. (a) Images of multiwalled carbon nanotubes (MWCNTs) in aqueous solutions. The first column shows MWCNTs in deionized water (DI) without any surfactant. The MWCNTs quickly drop out of solution without surfactant and can be seen at the bottom of the container. The second column shows a 0.5 wt.% solution of AL, at such a low concentration the MWCNTs are not stable and drop out of solution with time. The 1.0 and 2.0 wt.% AL are very stable over the course of 10 days and they are also dark showing that less MWCNTs dropped out of solution during the centrifugation process. The 0.5 and 1.0 wt.% SDS solutions are also stable over the course of 10 days. The 2.0 wt.% SDS solution shows less stability than the lower concentrations. (b) Chart showing the drop in optical absorption of a different set of 1.0 wt.% solutions over 11 days. The data points are the average absorption from wavelengths 300 nm to 800 nm as compared to the absorption on the day that the solutions were made. On day 1, the absorbance

for AL is 8% higher than SDS, but this chart shows the absorbance normalized to Day 1, for ease of comparison.

3.3.3 Electrophoresis zeta potential

Electrophoresis zeta potential measurements are also used to explore the stability of the solutions, even though the technique is generally only quantitative for charged spherical particulates. For cylindrically shaped species of unspecified length, measured zeta potential values cannot be compared with simple theories. However, trends can be compared to give information about relative stability. Solutions with MWCNTs were tested at the typical pH for the given surfactant; about 4 for SDS and 11 for AL. The average values of zeta potential for all AL and SDS MWCNT solutions tested are -50 mV or lower (higher in absolute value), showing that the solutions are indeed stable. These results are similar to those obtained for MWCNTs suspended in DTAB, where the strongest zeta potential value was about -40 mV at a pH of 12.[88] For comparison, we measure the zeta potential average without any surfactant as only -30 mV for MWCNTs in deionized water. For tests of 1.0 wt. % surfactant solutions without MWCNTs, the absolute value of the average zeta potential is consistently higher for AL than SDS, but the data frequently show multiple electrophoretic peaks for both solutions. In order to look at the effect of pH on these measurements and to explore the behavior of the ionic constituents of the surfactants with applied potential, a series of solutions were tested. The plots of these measurements can be found in Figures 3-5 and 3-6. It is found that the absolute value of the zeta potential for the solutions decreases with increasing pH for both, but most significantly for the AL, presumably due to the higher pKa. For AL, the absolute value of the zeta potential decreases by about 50%

from pH 9 to 11, showing that as the pH increases, the ionic dissociation becomes less pronounced. Nevertheless, even at pH 11, where the AL molecule would exist essentially as an un-dissociated polar salt molecule with little ionic character, the AL suspensions still show greater shelf-stability than their SDS counterparts, and, as we show below, produce far superior MWCNT depositions.

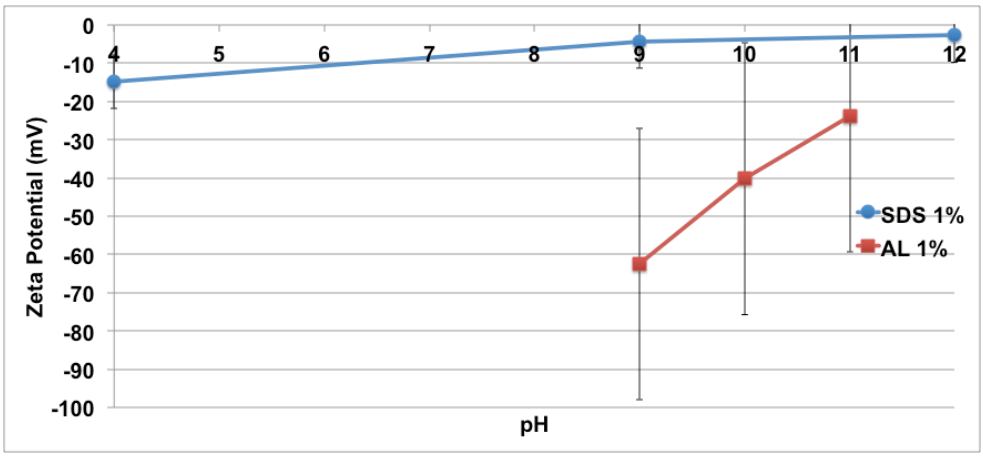

Figure 3-5. Results for measurements of zeta potential for surfactant solutions with different pH in order to look at the effect of pH on the measurements and to explore the behavior of the ionic constituents of the surfactants with applied potential. These solutions do not contain any MWCNTs. The values are the averages for 3 consecutive runs of the same solutions. The lauric acid requires a pH of 9 to dissolve so lower values are not shown. Typically SDS is used at a pH around 4; this is the condition when no additional acid is added.

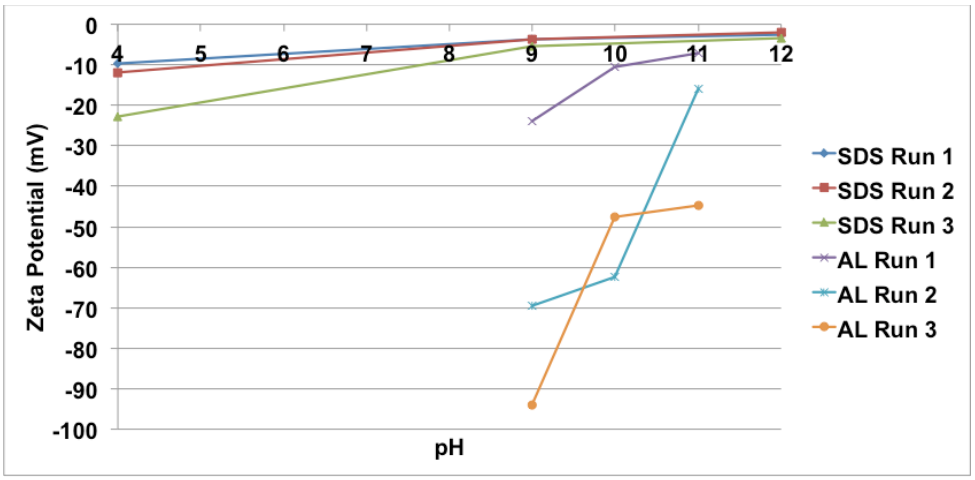

Figure 3-6. Results for measurements of zeta potential for surfactant solutions with different pHs for the 3 consecutive runs that were averaged in Figure 3-4.

3.3.4 TEM Observations of Deposited MWCNTs

MWCNTs are deposited from the surfactant solutions by overnight submersion of 100 nm thick silicon nitride membrane substrates that have been previously treated with (3-Aminopropyl) triethoxysilane (APTES, Sigma Aldrich 99%) to enhance anion adsorption. Membranes are removed from the vials the following day and immediately dried with nitrogen gas. Transmission electron microscopy (TEM) images show that the SDS salts reform on the membranes upon drying, while the AL salts do not. Figure 3-7 shows TEM images of MWCNTs deposited from AL and SDS at different resolutions. There is of course some variation in cleanliness and MWCNT dispersion across the area of the samples, but the images in Figure 3-7 have been chosen as typical representations of neither the worst nor the best areas of the samples. The SDS images show that the SDS reforms into salt residue on the membrane even where there are no MWCNTs. The AL

samples on the other hand, show no evidence of residue from the surfactant. For both samples, the dispersion includes mostly individual MWCNTs rather than bundles, as desired, but the SDS-deposited MWCNTs also show large amounts of unwanted carbon particles attached to their outer surfaces. In fact, when counting MWCNTs and carbon particles, over randomly-selected 72 um^2 areas, almost two times more unwanted carbon particles are found per MWCNT for SDS as compared to AL. While the AL deposition in Figure 3-7a shows some carbon particles, similar to those in the SDS deposition at higher magnification in Figure 3-7d, Figures 3-7a and 3-7b (which are the same magnification) show clear evidence that AL is better able to selectively separate individual MWCNTs within the solution.

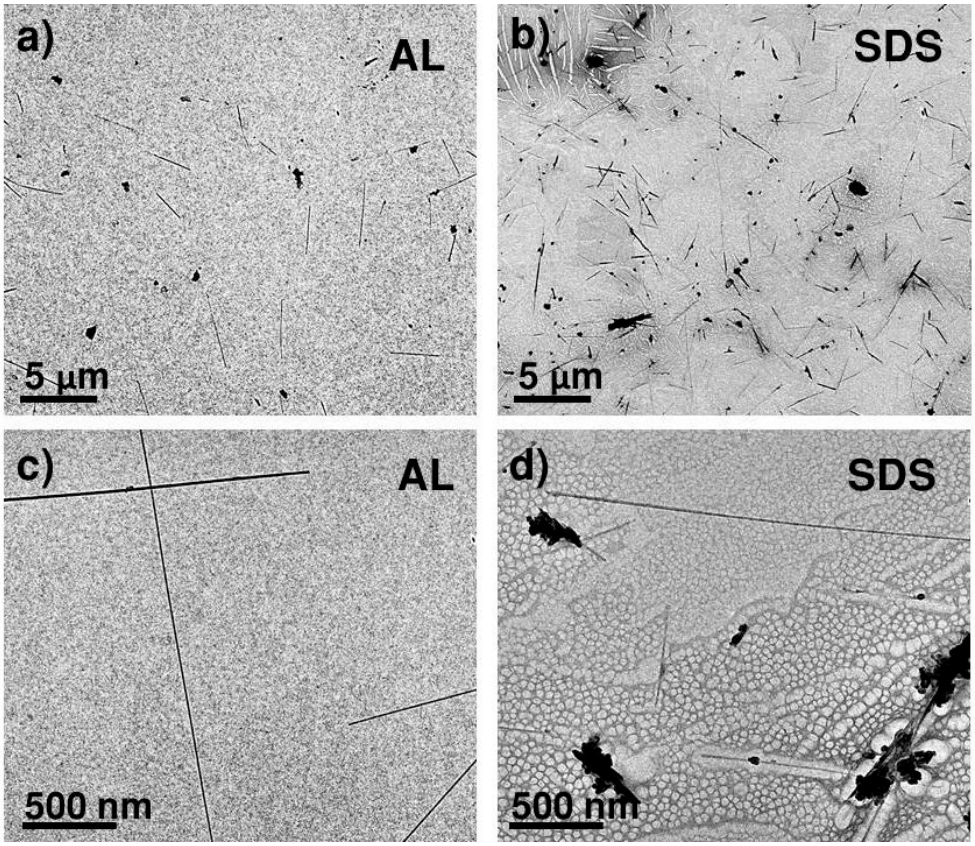

Figure 3-7. Typical TEM images at different magnifications of MWCNTs deposited on APTES treated SiN membranes. (a) and (c) are of MWCNTs that have been suspended in 1.0 wt. % AL prior to deposition. (b) and (d) are of MWCNTs that have been suspended in 1.0 wt. % SDS prior to deposition. The AL depositions do not show any surfactant residue and the MWCNTs are deposited individually without much bundling. The SDS depositions on the other hand show surfactant residue and there is notable presence of unwanted non-nanotube carbon deposits alongside the MWCNTs.

3.3.5 Raman Spectra Indicates AL Surfactant Deposits Cleaner MWCNTs

Further evidence of AL's ability to selectively suspend and deposit individual MWCNTs without unwanted particles was found through Raman spectroscopy. Typical spectra are shown in Figure 3-8, where the D-band to G-band intensity ratios show improved depositions of high-quality MWCNT with AL, in comparison with SDS. The average I_D/I_G was 0.65 without any surfactant, 0.27 for SDS, and 0.16 for AL. Higher intensity of the D-band signifies higher defect densities and the ratio of this intensity with the G-band is a generally accepted metric for the graphitic quality in the sample.[100] Our results show that depositions from AL solutions have fewer disordered graphitic particles than those from SDS. We can speculate that since spherical carbon particles contain more pentagon defects, to provide the curvature to close the structure,[101] SDS is either more effective at suspending spherical particles or is less effective overall at suspending the desired MWCNT nanomaterials.

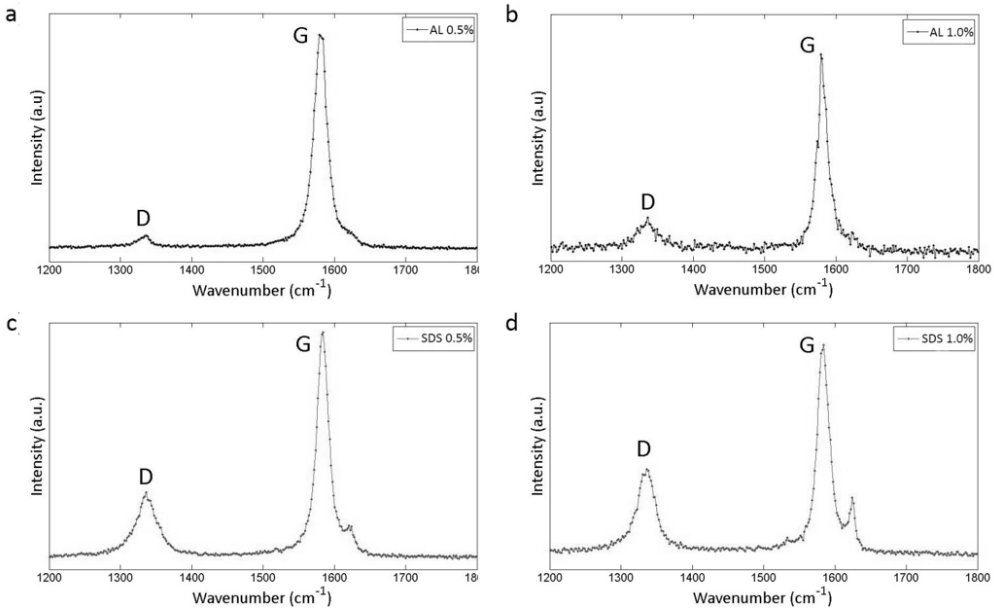

Figure 3-8. Raman spectra of MWCNTs prepared with (a) 0.5 % and (b) 1.0 % concentrations of ammonium laurate and (c) 0.5 % and (d) 1.0 % sodium dodecyl sulfate.

3.3.6 AFM Measurements of Surfactant Residues

In order to confirm that the residue shown on the SDS membranes is indeed layers of reformed salt, AFM measurements are performed. Anhydrous SDS has been found to have a double layer structure with a bilayer lamellar thickness of about 3.9 nm, which can decrease slightly with hydration.[102] AFM measurements of the step height of the SDS residue shown in Figure 3-9 are indeed in steps of approximately 4 nm. Both samples shown in Figure 3-9 are silicon chips treated with APTES then left in 1 wt. % surfactant solution without MWCNTs overnight and then dried with nitrogen upon removal from the solution. Figure 3-9 also shows that there is no noticeable AL reformation on the same surfaces.

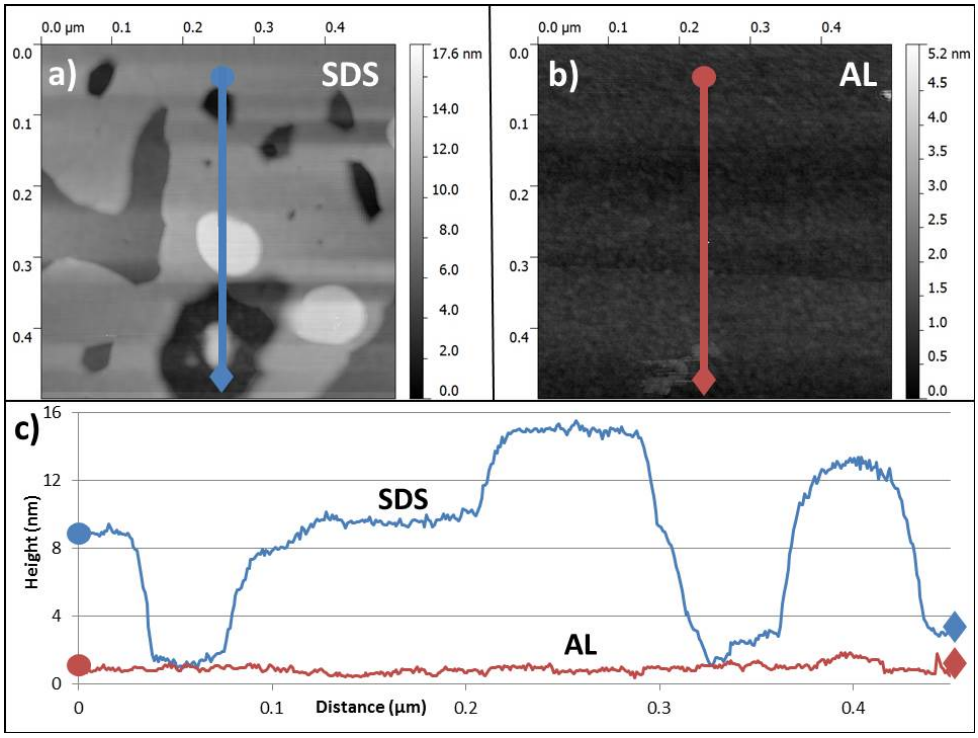

Figure 3-9. AFM images (a) SDS and (b) AL deposited on silicon chips after APTES treatment (without CNTs). SDS shows inhomogeneous layering of the micelles throughout the sample area. AL shows a comparatively smooth surface. (c) Line height profiles of the deposited surfactants show that the height difference between areas on the SDS sample differ in steps of about 4 nm. It is known that the bilayer thickness of SDS is approximately 4 nm, therefore a maximum height of 16 nm indicates up to 4 bilayers of SDS.

3.3.7 Salt Reformation

In order to further investigate the residue formation of the sodium-based surfactants, multiple combinations of bases are added to increase the pH of the solutions. The pH of these solutions is brought up to 11 to match that of the AL solutions investigated and to confirm that our results are not simply just a function of pH. These results can be seen in Table 3-1 and Figure 3-10. When sodium hydroxide is added to SDS, the residue shows very similar reformation patterns as

SDS without any added base. SDS, with ammonium hydroxide added, also shows residue formation, but the structure of the reformed salt appears thicker and more disordered in TEM images. Lauric acid reacted with sodium hydroxide produces a sodium-based version of AL, sodium laurate, which also readily produces residue formation, based on TEM observations of treated substrates. The process for reformation of the salt residue can be understood from the chemistry of the charged endgroup on the surfactant anion and its corresponding cation. The SDS solutions, regardless of increased pH, exhibit a strong tendency to reform the salt, likely because the sulfate group is a large ion, with weaker coulomb binding and corresponding higher ionic dissociation probability, in comparison to the smaller carboxylate group of the AL.[103] This means that the SDS is more likely to be freely charged in solution and thus more strongly attracted to the APTES functionalization on the membrane or any other charges which may be on a given surface. The lower pKa of ammonium hydroxide versus sodium hydroxide (9.25 versus 13.8) means that the NH_4 cation is also more likely to associate with the laurate anion, forming an aqueous solution that is more stable against unwanted charge-driven surface deposition.

Sample	*Base salt/lipid*	*Added base*	*pH*	*What happens?*	*How does it look?*
1	None	None	7	Solution is not stable, cannot centrifuge without NTs dropping out of the solution	Samples are clean, but there are mostly clumps of graphitic particles, not individual nanotubes
2	Sodium dodecyl sulfate	None	4.5	Stability and dispersion are good, but the samples are very dirty	Layers of SDS are easily seen all over the membranes even where there are no tubes or particles
3	Sodium dodecyl sulfate	Ammonium hydroxide	11	Stability similar to plain SDS, lower dispersion density	Lots of residue on the membrane, but it looks different from plain SDS, rather than forming layers evenly across the membrane there are clumps of thick residue
4	Sodium dodecyl sulfate	Sodium hydroxide	11	Very similar both in stability and dispersion to plain SDS	Residue almost identical to plain SDS
5	Lauric Acid	None		Doesn't dissolve in water	Don't have images because it doesn't dissolve so you can't get NTs dissolved in there
6	Lauric Acid	Ammonium hydroxide	11	Stability and dispersion very good, no visible residue	No visible residue, lots of individual NTs, not much junk particles
7	Lauric Acid	Sodium hydroxide	11	Very difficult to disperse, formed cloudy clumps until I probe sonicated	Very odd residue on the samples, pretty good single nanotube dispersion

Table 3-1. Description of the results of combining different ionic constituents to form surfactant suspended CNTs.

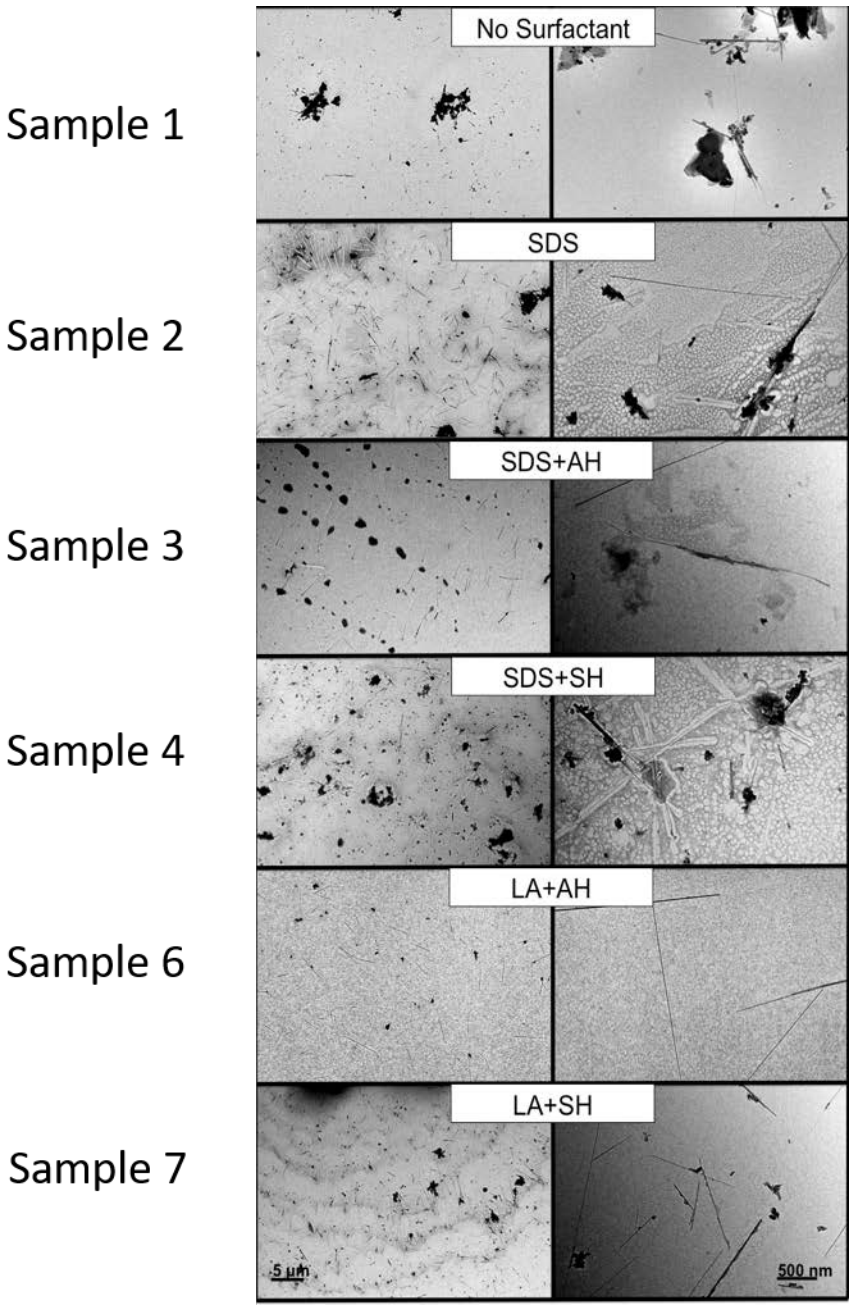

Figure 3-10. TEM images of CNTs deposited on SiN membranes after suspension in different combinations of surfactants. Images on the left are the same magnification (5 um) and those on the right are the same magnification (500 nm).

3.3.8 Residual Surfactant Salt Removal

With limited success, the excess SDS surfactant can be removed from the membranes with cleaning procedures.[72] Figure 3-11 shows the results after an APTES silicon nitride membrane is left in 1.0 wt.% SDS MWCNTs solution overnight and then rinsed thoroughly with deionized water for one minute and then left in clean deionized water for an additional minute prior to drying with nitrogen gas. Most, but not all of the SDS salt residue is removed through this cleaning procedure. However, it is clear that, after the cleaning, there is still a significant number of carbon onions on the MWCNTs that cannot be seen in the corresponding AL depositions. This again leads to the conclusion that AL does a better job of separating individual nanotubes, perhaps because AL naturally prefers to form cylindrical micelles, while SDS prefers spherical micelles.[97]

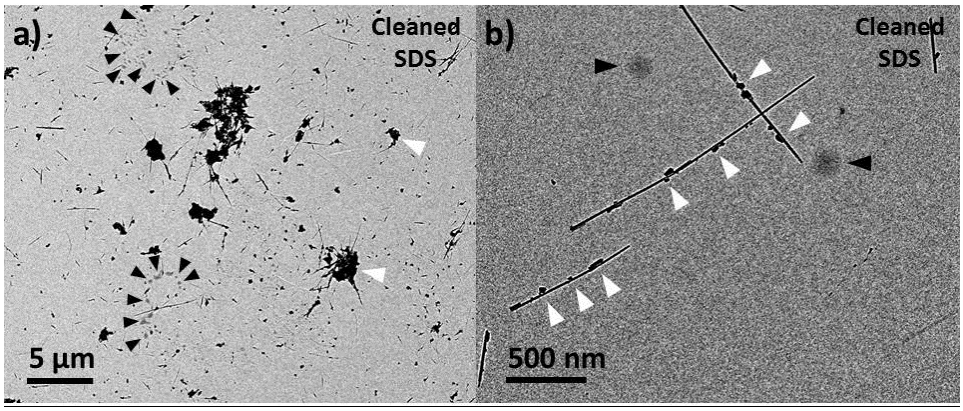

Figure 3-11. TEM images at different magnifications of MWCNTs deposited from 1.0 wt.% SDS solution onto APTES treated SiN membranes. After deposition, the membranes were cleaned by deionized water to remove the surfactant residue. Most, but not all of the SDS residue was removed through this process, and unwanted carbon onions (indicated by arrows) are still visible in the high resolution image (b). In both images, black arrows indicate examples of surfactant residue and white arrows indicate carbon contamination (mostly

fullerene onions). Compare with Figures 3-7a and 3-7c which show AL depositions without any residue.

In addition, lauric acid has a melting temperature of only 44 degrees Celsius and a vaporization temperature of about 298 degrees Celsius, compared to 206 and 380 degrees Celsius for SDS. These properties make it easy to remove CNTs from AL solutions by simple physical processing. Lauric acid can also be burned off of substrates at temperatures that do not damage carbon nanostructures.[104] Oxidation of SDS would leave sodium and sulfur containing residues, whereas AL would oxidize residue-free.

3.4 Conclusion

This study introduces ammonium laurate for use as a surfactant for the controlled suspension and clean deposition of CNTs. This is important for future applications of CNTs such as electronic devices and optical emitters where individual NTs are necessary. These stable solutions are simple to prepare and do not require excessive sonication, which is harmful to the CNTs. We show that a SAM on a substrate can be coupled with CNTs in ammonium laurate dispersions without build-up of the surfactant on the surface, as occurs with other common dispersants. The reason for this important improvement is that the low ionic strength of the AL solutions prevents it from interacting with the SAM and reforming salts at the interface. Another positive side effect of the approach is that,

compared to SDS, AL has a stronger tendency to selectively suspend individual CNTs without additional carbon particles attached. This is perhaps due to AL's tendency to form cylindrically shaped micelles, as opposed to the spherically shaped micelles formed by SDS. Through aqueous dispersion of CNTs with ammonium laurate, substrate deposited nanotubes show less debris than other common surfactants, providing cleaner samples for both future research and potential applications.

Chapter 4: Surface Chemistry Enhances Gel Chromatography Separation of Carbon Nanotubes

Adapted from Meany, B.; Kwon, H.; Kim, M.; Ramsdell, D.; Baker, E.; Wang, Y. H. to be submitted

B. Meany prepared SWCNT samples, developed chromatography instrument and sorted samples with chromatography instrument, and characterized final products with absorbance and photoluminescence spectroscopies. H. Kwon and M. Kim measured photoluminescence temperature effects. D. Ramsdell and E. Baker programmed the absorbance portion of the chromatography instrument with LabView.

4.1 INTRODUCTION

Single-walled carbon nanotubes (SWCNTs) have remarkable electrical and optical properties that are promising for many applications, including nanoelectronics, lightweight conductors, bio-imaging, and photovoltaics. However, SWCNTs are currently synthesized as a mixture of an assortment of chiralities. Each chirality is electronically unique and can be either semiconducting or metallic. Developing a simple, scalable process that is capable of sorting SWCNTs at the chirality level with high resolution is an essential step to fully realize their multifaceted potentials.

Over the last decade, significant advances have been made towards this goal; major techniques developed include DNA assisted sorting.[20,22] density gradient ultracentrifugation (DGU),[3] gel chromatography,[32,105] and aqueous two phase extraction (ATPE).[106] Particularly, work by Kataura and co-workers shows that allyl dextran based column chromatography can be used to separate up to 13 chiral structures at a purity of ~60 to 95%.[32] In this method, individual SWCNTs

stabilized in an aqueous solution of surfactant sodium dodecyl sulfate (SDS) are passed through a column filled with allyl dextran gel beads where semiconducting SWCNTs (s-SWCNTs) are selectively adsorbed to the gel and then eluted with SDS at 2.5x higher concentration. This chromatography technique has shown a significant amount of promise in both simplicity and scalability. Efforts to increase the purity by optimizing pH and temperature have also seen some success.[33,107] However, the selectivity of this method is significantly lower than other methods particularly DNA assisted sorting, and future work must further demonstrate its selectivity.

The gel chromatography method is based on varying interaction strengths between the SWCNTs/SDS aggregates and the allyl-dextran hydrogel. This phenomenon was examined by comparing various structural properties of the nanotubes to the order at which they elute from the column. From these results, Kataura *et al.* hypothesized that the physical structure of the SWCNTs effects the organization of the SDS layer in a manner which creates a varying affinity with the gel. Interestingly, the mechanism behind the adsorption process has also been the subject of a significant amount of debate. Originally, it was predicted that SDS encapsulated SWCNTs in large cylindrical micelles in a manner similar to how spherical micelles form in solution.[15] Simulation studies[108] and small-angle neutron scattering (SANS) experiments[86] later produced results widely different from this theory. Measurements using SANS did not detect the presence of cylindrical micelles. Molecular dynamics simulation suggests that SDS molecules have a tendency to lie flat on the nanotube with the charged head group

surprisingly close to the carbon lattice. A heterogeneous layer of surfactant molecules is formed with portions of the nanotube completely exposed to water. The morphology of the surfactant coating on SWCNTs is likely to be a controlling factor for their separation efficiency, as a recent study by Ziegler and co-workers suggests.[109] By introducing additives, such as gum arabic and electrolytes, the surfactant layer was disrupted to drastically decrease the separation yield of semiconducting SWCNTs using agarose in place of allyl dextran. This along with theoretical modeling, and experiments using functionalized agarose led to the conclusion that metallic SWCNTs have thick "brush like" surfactant layers which block their adsorption onto the agarose. Semiconducting SWCNTs, on the other hand, are likely to have thinner layers and adsorb onto the gel by ion-dipole interactions.

Here, we present a novel method for purification of semiconducting SWCNTs through surface enhancement thereby altering the well-researched separation of SWCNTs by allyl dextran-based size-exclusion gel chromatography. Through functionalizing the nanotube outerwall, the established interaction of SDS/nanotubes and gel is disrupted allowing for a single step flow-rate dependent separation method. In developing this method, a computer-controlled real-time *in situ* nanomaterial separation system is developed linking an HPLC instrument and UV-Vis absorption spectrometer.

4.2 Materials and Methods

4.2.1 Chirality-enriched SWCNT Samples Preparation

For experimental simplification, s-SWCNTs are isolated from HiPco SWCNTs (Rice University, batch # 194.3). 200 mg of nanotubes are dispersed in 100 mL 2 wt.% sodium dodecyl sulfate (SDS) (Sigma Aldrich, ≥98.5%) in nanopure water (BARNSTEAD ThermoFisher Scientific) by 2 hr ultrasonication with a 0.5 inch flat tip (Misonex, S-4000) at 20% amplitude (~33 W) and 10°C. To remove impurities and bundled tubes the sample is ultracentrifuged at 170,499*g* and 20°C for 4 hr (Optima LE-80K, Beckman-Coulter). From the centrifuge tubes the upper 85% of supernatant is removed for an initial modified gel chromatography purification on 1.5 mL bed volume columns of Sephacryl S-200 High-Resolution chromatography resin (GE Healthcare).[32,110] To obtain the s-SWCNT sample, 10 mL of HiPco SWCNT solution is loaded per column with the flow through being re-loaded 5 times. The columns are washed with aqueous 2 wt. % SDS followed by elution with aqueous 5 wt. % SDS. The final s-SWCNT solution is diluted with nanopure water to 1-2 wt. % SDS for functionalization and shelf-life stability.

4.2.2 Alkyl-functionalization of (6,5)-SWCNTs for Proof of Separation of Pristine and Functionalized SWCNTs by Column Chromatography

Aqueous HiPco SWCNTs prepared as described above, in 2 wt. % SDS are purified for pristine (6,5)-SWCNT samples (p-SWCNT) followed by a solvent exchange to 2 wt. % SDS/D_2O. Adsorbed to the column are (6,5)-SWCNTs at ~90% purity which are washed with 2 wt. % SDS/D_2O, eluted with 5 wt.%

SDS/D_2O, and diluted with D_2O to a final concentration of 2 wt.% SDS. A portion of p-SWCNT is then functionalized with the alkyl group -C_6H_{13} (a-SWCNT) by an alkylation chemistry developed by our group.[111]

For separation of pristine and functionalized nanotubes, an equal volume mixture of p-SWCNT and a-SWCNT is loaded on a 1.5 mL Sephacryl S-200 column. The column flow through (FT), wash, and elution (Elu) are collected and analyzed by absorption and fluorescence spectroscopies. a-SWCNTs pass through the column and are collected in the FT and wash, while p-SWCNTs adsorb to the gel column and are removed only through an elution step using a concentrated 5 wt. % SDS elution.

4.2.3 Surface Enhancement of s-SWCNTs by Diazonium Chemistry Creation of sp^3 Defects: For Gel Column Purification of Nanomaterials

Surface enhancement of s-SWCNTs was performed using dinitro-diazonium chemistry for controlled functionalization of the nanotube outerwall as previously described by our research group.[110] To determine the optimal degree of functionalization for separation purposes, surface enhancement is studied at several reaction concentrations by the ratio of dinitro-diazonium molecules to carbon atoms [Dz:C], namely [1:250], [1:500], [1:750], [1:1000], [1:1500], [1:2500], and [1:4000]. The best degree of functionalization for SWCNT chirality gel column separation is determined to be [1:2500].

4.2.4 Temperature and Degree of Functionalization Effects on SDS Morphology: van't Hoff Plots

To examine how the morphology of SDS micelle around (6,5)-SWCNT changes as a function of functionalization degree, a series of (6,5)-SWCNT-$C_6H_4NO_2$ samples were used for the temperature-dependent photoluminescence spectroscopy. At each 5 ^oC increment from 15 ^oC to 45 ^oC, a PL spectrum was collected. The temperature of the nanotube solution was controlled using a circulating water bath stage (FL-1027, Horiba Jobin Yvon). The temperature was measured with an immersion Surface Temperature Sensor and LabQuest 2 (Vernier). Van't Hoff plots were constructed from the integrated intensity ratios of E_{11} and E_{11}^- PL peaks plotted against temperature.

4.2.5 in situ-UV/VIS Absorption-HPLC Instrument for Selective Separation of Functionalized s-SWCNTs

The separation device is driven by an HPLC system (Dionex-ThermoFisher Scientific, Ultimate 3000) with a Sephacryl S-200 (GE Health) packed column. Sample is pumped through the column which is linked to a flow cell cuvette (Starna Cells, Inc.) placed in a UV/Vis absorption spectrometer (8453 photodiode array, Agilent Technologies) followed by fraction collection. We program the device with LabView (National Instruments) to develop a computer-controlled, real-time absorption *in situ* nanomaterial separation system. The operator is able to regulate and follow the separation and elution of nanomaterials by absorption spectroscopy in real time as sample comes off the column and determine approximate separation times for each different chiralities. The screen

interface displays both full absorption spectra from 200-1100 nm and absorption at selected wavelengths with respect to time.

4.2.6 Gel Chromatography for Selective Separation of Functionalized s-SWCNTs

After surface enhancement of s-SWCNTs, each sample is injected on top of a 2π cm^3 bed volume of cross-linked copolymer N,N-methylenebisacrylamide and allyl dextran resin pre-washed with aqueous 1 wt.% SDS in a glass column 8 cm long with an inner diameter of 1.0 cm. The sample is pumped through the column at a flow rate of 0.2 mL/min (upon which the pump is switched to a reserve aqueous 1 wt. % SDS solution for continuous flow and column washing). As separated chiralities elute from the column, their absorption are measured followed by fraction collection for further analysis by absorption, photoluminescence, and Raman spectroscopies. Based on the absorption measurements of the various SWCNTs' respective E_{11} and E_{22} transitions, separation times are determined and samples are collected. Functionalization of nanotubes weakens their interaction with the gel resin, therefore the concentration of SDS remains at 1 wt. % and is sufficient to elute the SWCNTs. Also this weakened adsorption of SWCNTs allows the column to be reused multiple times (at least 10 times) while maintaining good chirality separation.

4.2.7 Isolated Sample Characterization: Absorption, Photoluminescence, and Raman Spectroscopy

To further analyze separation and functionalization of the isolated s-SWCNTs, the absorption, photoluminescence (PL), and Raman spectra were measured. Absorbance spectra were taken from 200-1400 nm (Lambda-1050,

Perkin Elmer) to ensure purity and removal of those nanotubes which absorb beyond the limiting 1100 nm of the silicon diode array detector. In addition, excitation-emission maps were collected (Nanolog, HORIBA Jobin Yvon) to verify both purity and the existence of E_{11}^{-} fluorescence peaks, which are due to functionalizing the nanotube outerwall.[110] Last, Raman spectra were taken (HORIBA Jobin Yvon LabRAM HR-VIS microRaman system) to determine purity and degree of functionalization from the D/G ratio. All spectra and maps were plotted using SigmaPlot 11.0 (Systat Software, Inc.).

4.3 Results and Discussion

4.3.1 Separating Functionalized SWCNTs from Pristine SWCNTs

To demonstrate the surface enhanced SWCNT purification, we devised a reverse engineered experiment. Equal amounts of pristine (6,5)- SWCNT (p-SWCNT) and $-C_6H_{13}$ alkyl-functionalized (6,5)-SWCNT (a-SWCNT) are mixed creating a solution of both pristine and surface enhanced (6,5)-SWCNTs (mix-SWCNT). This purple mix-SWCNT sample is loaded on a 1.5 mL bed volume column and the flow through collected. Both the flow through and the initially white column are purple indicating that some (6,5)-SWCNTs are simply passing through (not interacting with) the column and that some (6,5)-SWCNTs are adsorbing to the gel resin. To identify those nanotubes on the column, the column is eluted with 3 mL of a 5 wt. % SDS/D_2O solution.

All samples are analyzed by absorption, photoluminescence (PL), and Raman spectroscopies. Excitation-emission maps show separation of a-SWCNTs

from p-SWCNTs (Figure 4-1). p-SWCNT should have a single PL peak at 977 nm while a-SWCNT should have two peaks, the original 977 nm and a second peak around 1200 nm due to functionalization. Initially when these samples are equally mixed, the mix-SWCNT sample displays both fluorescent peaks, the sharp peak at 977 nm due to the E_{11} transition and the broad fluorescent peak around 1200 nm due to the E_{11}^- transition. Following gel chromatography, mix-SWCNT is purified with the original a-SWCNTs passing through the column and the p-SWCNTs adsorbing to the column. To retrieve the p-SWCNTs they must be eluted with 5 wt. % SDS.

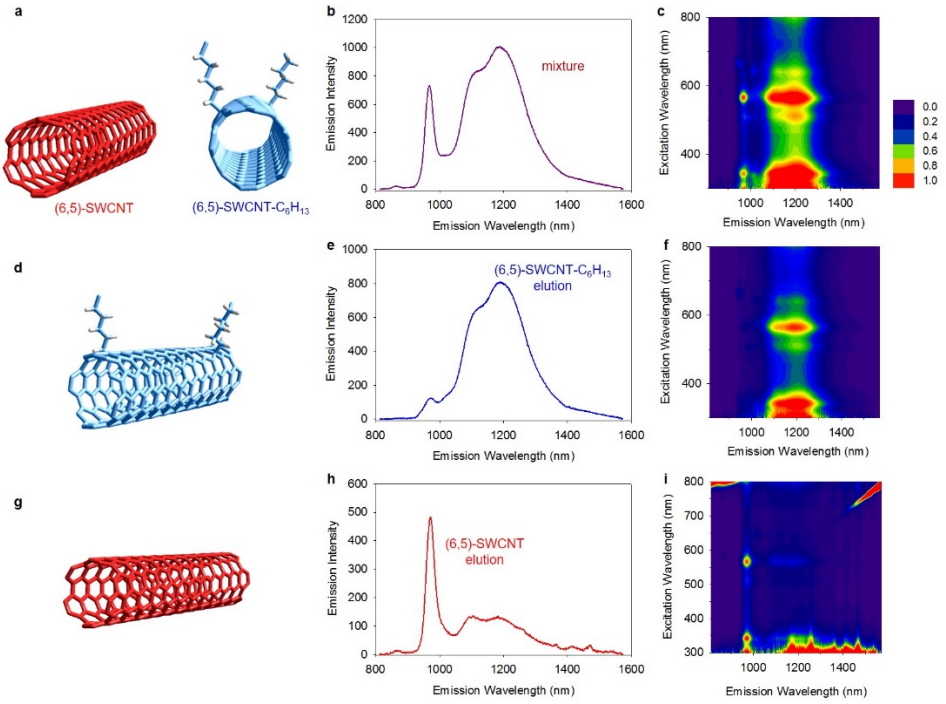

Figure 4-1. Covalent surface functionalization modifies the elution of SWCNTs and allows pristine SWCNTs to be isolated from functionalized SWCNTs. PL spectra and excitation-emission maps for a proof-of-principle gel chromatography separation. The sharp emission peak at 977 nm is the original E_{11} optical transition of (6,5)-SWCNTs, while the broad emission peak at 1200 nm is the E_{11}^- optical transition due to functionalizing the (6,5)-SWCNT outerwall. (a) mix-(6,5), an equal volume mixture of p-(6,5) and a-(6,5) before being loaded on gel column. (b) after loading mix-(6,5) on Sephacryl S-200 column, the resultant column flow

through and wash contains mostly functionalized SWCNTs, a-(6,5) as indicated by the E_{11}^- functionalization PL peak. (c) After eluting with 5 wt. % SDS/D_2O, the retained pristene SWCNTs, p-(6,5), desorb from the column as indicated by the single sharp 977 nm emission peak.

It is well established that under pristine (not functionalized) conditions (6,5)-SWCNT strongly adsorbs to the column.[32] Therefore, surface enhancement of the outer wall of (6,5)-SWCNT disrupts the adsorption of nanotubes to the resin allowing a-SWCNTs to simply pass through the column undisturbed while p-SWCNTs remain adsorbed to the gel resin.

This disruption of aqueous SWCNTs adsorbing to a gel column is likely due to a change in the packing of the surfactant surrounding the dispersed nanotubes. Strano *et al.* found that the morphology of SDS wrapping around a SWCNT strongly influences the strength at which a nanotube chirality will adsorb to the surface of the allyl dextran gel.[112] In general, small diameter nanotubes such as (7,3), (6,4) and (6,5) are surrounded by closer, densely packed SDS molecules allowing for shorter distances between the surfaces of nanotube and resin. Through alkyl-functionalization of the nanotube surface, there are multiple alkyl chains perpendicular to the SWCNT surface thereby decreasing the available surface area for surfactant adsorption. Reduced surface area and steric hindrance may induce a change in the SDS morphology surrounding functionalized nanotubes. This bulkier model suggests that when loaded on a column functionalized SWCNTs interact weaker than pristine nanotubes due to an increase in the distance between the surfaces of SWCNTs and the gel resin. The pristine nanotubes are surrounded by closer, densely packed surfactant while

surface enhancement loosens the packing density of surfactant, disrupting and decreasing the adsorption of tubes to the column.

4.3.2 Temperature Effects on SDS-dispersed SWCNTs

To study surfactant-nanotube interactions, we first look at the effects of temperature. By varying only solution temperature of pristine SDS-dispersed HiPco SWCNTs, the nanotube PL intensity varies (Figure 4-2). At 10°C, only pristine (6,5)-SWCNT displays measurable PL. Raising the solution temperature by 5°C brings about fluorescence from three other chiralities (8,3), (10,2) and (8,4). As the same sample is further heated (7,5)- and (9,4)-SWCNTs PL is detected and the overall intensity of each peak increases. Above 30°C the sample shows minimal changes in PL intensity or the appearance of other SWCNT chiralities. Therefore, below room temperature, nanotube PL manifests temperature dependence presumably due to changes in SDS-SWCNT interactions. Interestingly, this fluorescence quenching is reversible. A room temperature SWCNT solution can be cooled to 10°C followed by heating back to 30°C with recovery of PL intensity. Lowering the temperature would make SDS-SWCNT interactions more rigid and potentially induce changes in the surfactant packing surrounding the nanotubes, creating weak bundling between tubes. The effect is an inter-tube quenching of PL. As the temperature is raised van der Waals repulsions are enhanced altering the surfactant morphology and decoupling the weakly bundled nanotubes thereby decreasing the quenching and returning typical PL intensities.

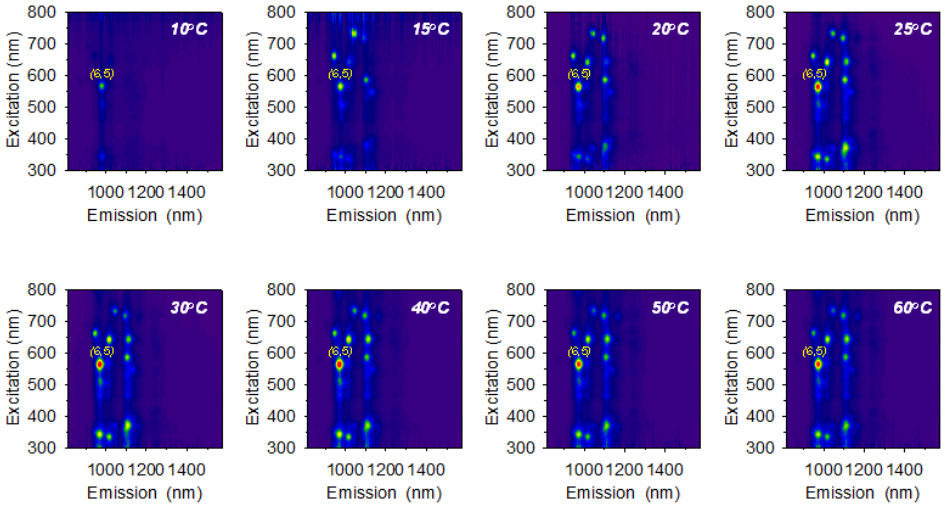

Figure 4-2. Temperature effects on the excitation-emission maps for pristine HiPco SWCNTs dispersed in aqueous 2 wt. % SDS. At low temperature (10˚C) only PL signal from (6,5)-SWCNT is seen. As the temperature is raised, the PL from other chiralities is detected.

4.3.3 van't Hoff Analysis of Temperature and Diazonium Chemistry Effects on SDS-dispersed SWCNTs

Further surfactant-SWCNT interactions are studied by a van't Hoff analysis of the effects of varying both temperature and degree of surface enhancement.[111] The van't Hoff plots describe a two-level system of E_{11} (free) and E_{11}^- (trapped) excitons at thermal equilibrium (Figure 4-3). E_{11} excitons are free to move along the nanotube axis, while E_{11}^- excitons are trapped at sp^3 introduced functionalization sites along the sidewall. These two distinct exciton populations recombine at different energies; the difference in measured PL being ΔE. Using the Boltzmann exponent, $e^{-\Delta E/kT}$, the van't Hoff analysis correlates temperature with the integrated intensities of free (I_{E11}) and trapped (I_{E11}^-) PL through the van't Hoff relation:

$\ln \frac{IE11}{IE11-} = -\frac{\Delta Ethermal}{k*T} + A'$, where A' is a correction factor and $\Delta E_{thermal}$ is the slope.

van't Hoff plots are constructed from PL maps for (6,5)-SWCNTs functionalized with $-C_6H_4NO_2$ by diazonium (Dz) chemistry (Figure 4-3). By altering the concentration of [Dz molecules:nanotube carbon atoms (C)] we study the following reactant ratios [Dz:C]; 1:4000, 1:2500, 1:1500, 1:1000, 1:750, 1:500 and 1:250, which correlates to the Dz adsorption density on the SWCNT outerwall. We find that functionalized SWCNTs transition from linear (at large enhancement) to V-shaped (at low enhancement) van't Hoff plots, resulting in a functional-degree dependent temperature-PL profile. Changes from linear to non-linear (V-shaped) as functionalization decreases indicates a temperature dependence with respect to the functionalized degree. Across the temperature regime, a linear plot is observed for the nanotubes with the highest functional defects ([Dz]:[C] = 1:250 and 1:750). When the defect density is low, the positive deviation at lower temperature gradually increases such that temperature dependent SDS/SWCNT interactions become more important. Hence, the V-shape of the van't Hoff plots may be affected by the defect density because a higher number of defects can result in enhanced van der Waals repulsion between nanotubes and effective nanotube suspension due to a reduction in impacts from surfactant-solution dynamics. By varying both temperature and degree of functionalization, van't Hoff plots correlate interactions between surfactant and surfaced enhanced SWCNTs. Similar to the temperature effects on pristine-SWCNTs, surface enhanced-SWCNTs with a lower functionalization degree

exhibit PL intensity maxima at 27.5ºC. Conversely, for SWCNTs with high defect densities of 1:500 and 1:250, the PL linearly decreases as temperature increases, retaining constant FWHM of both E_{11} and E_{11}^{-} (Figure 4-4).

This van't Hoff method is useful for studying surfactant effects. First, above 303 K the PL intensity is inversely proportional to temperature (Figure 4-4). This is consistent with measurements of SWCNT PL quantum yield in the solid state. Below 303 K, our aqueous SDS-stabilized SWCNTs show an increase in PL from 15-30˚C. This is in opposition to the temperature dependence of solid state SWCNT PL. The difference can be attributed to surfactant effects which become prominent at low temperature. Our previous work shows minimal surfactant effects above 303 K; however, at low temperatures surfactant reorganization surrounding the nanotube induces the V-shaped PL profile (Figure 4-3). The van't Hoff plot indicates the PL sensitivity to low temperature. Consistently the V-shape intersection of fitted data occurs at 27.5˚C among samples of differing defect densities. The fit at low temperature (15-27.5˚C) is a positive slope with strong dependence on defect density. Note the negative slope at high temperatures correlates to the trapping state depth of sp^3 functionalization defects which varies with defect density.

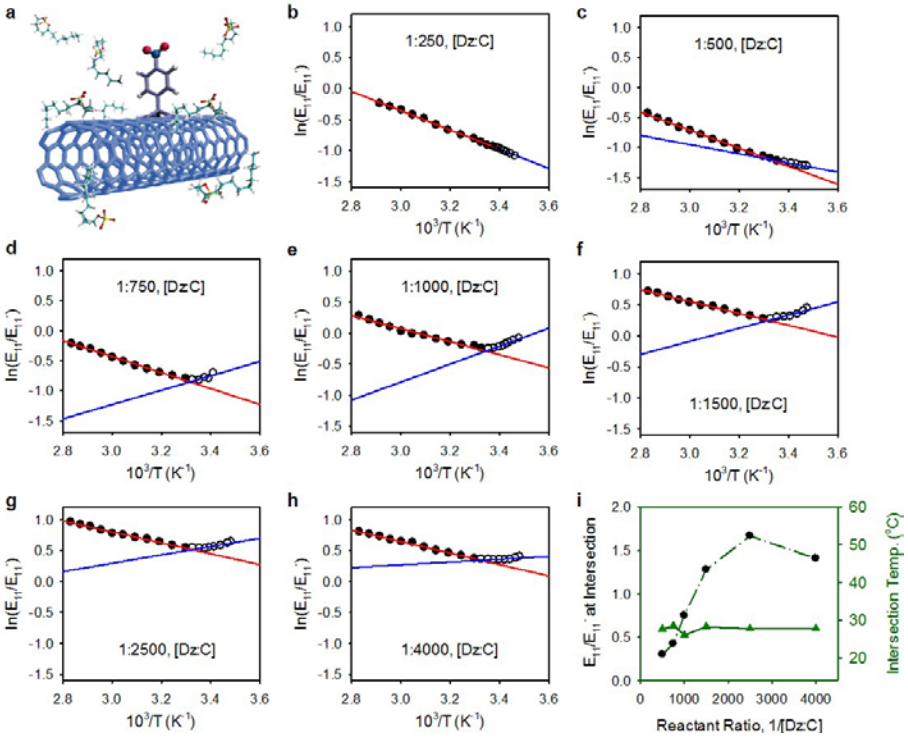

Figure 4-3. Temperature and functional group concentration dependence of SDS-SWCNT interactions determined by van 't Hoff plots for (6,5)-SWCNT-$C_6H_4NO_2$. High degree of functionalization, 1:250 – 1:750 (b,c,d) shows minimal temperature dependence and leads to prominent interactions between functional groups and well-dispersed nanotubes. Low degree of functionalization, 1:1000 – 1:4000 (e-h) at ambient temperatures disrupts and weakens the SDS-SWCNT interactions as indicated by positive slopes above 15°C. (i) A plots of the slop intersection with respect to E_{11}/E_{11}^- (y-axis) and to 1/T (x-axis).

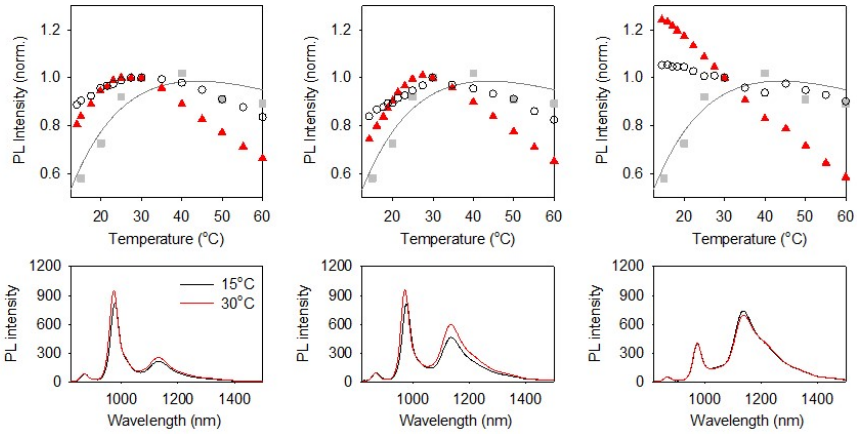

Figure 4-4. High defect density reduces the SDS reorganization effects at low temperature. The E_{11} (open circles) and E_{11}^- (red) PL of (6,5)-SWCNT-$C_6H_4NO_2$,varying the defect density, a, 1:2500, b, 1:1,000 and c, 1:500 of

[Dz]:[C] are temperature dependent. Gray rectangles are the E_{11} intensity profile of unfunctionalized (6,5)-SWCNTs. Each PL intensity is normalized to the PL intensity at 30°C. 565 nm single excitation PL spectra compare the PL intensity at 15°C (black) and 30°C (red) for (6,5)-SWCNT-$C_6H_4NO_2$,varying the defect density, e, 1:2500, f, 1:1,000 and g, 1:500 of [Dz]:[C]

4.3.4 Determining Optimal SWCNT Surface Enhancement for Gel Chromatography Sorting

With an understanding that adsorption of Dz on the SWCNT outerwall effects the surfactant packing and morphology, we turn to creating a novel separation technique for isolating (6,5)-SWCNT while regenerating the gel resin allowing for reuse and multiple separation cycles. First, adequate [Dz:C] conditions must be defined for suitable disruption of the surfactant packing along the nanotube allowing for column separations based on chirality.

The surface enhancement must be tuned for optimal column separation. If the nanotube interacts with an inadequate amount of Dz and is loaded on a column, it adsorbs to the resin similar to pristine-SWCNTs. On the other hand, if too much Dz adsorbs to the nanotube surface, the SWCNTs will simply pass through the column uninhibited. To determine optimal surface enhancement conditions we test a range of ratio concentrations of dinitro diazonium, [Dz:C]. A low concentration of Dz at [1:3000] maintains high nanotube-to-column adsorption. However, [1:300] leads to no adsorption; the SWCNTs freely flow through the column unhindered. Studying [1:1000], [1:1500], [1:2000], and [1:2500], a shift in the column adsorption ability of SWCNTs occurs and grows stronger from [1:100] towards [1:2500] (Figure 4-5). We find the chemical

condition [1:2500] maintains nanotube-column adsorptive properties that are exploitable for SWCNT chirality separation based on flow rate.

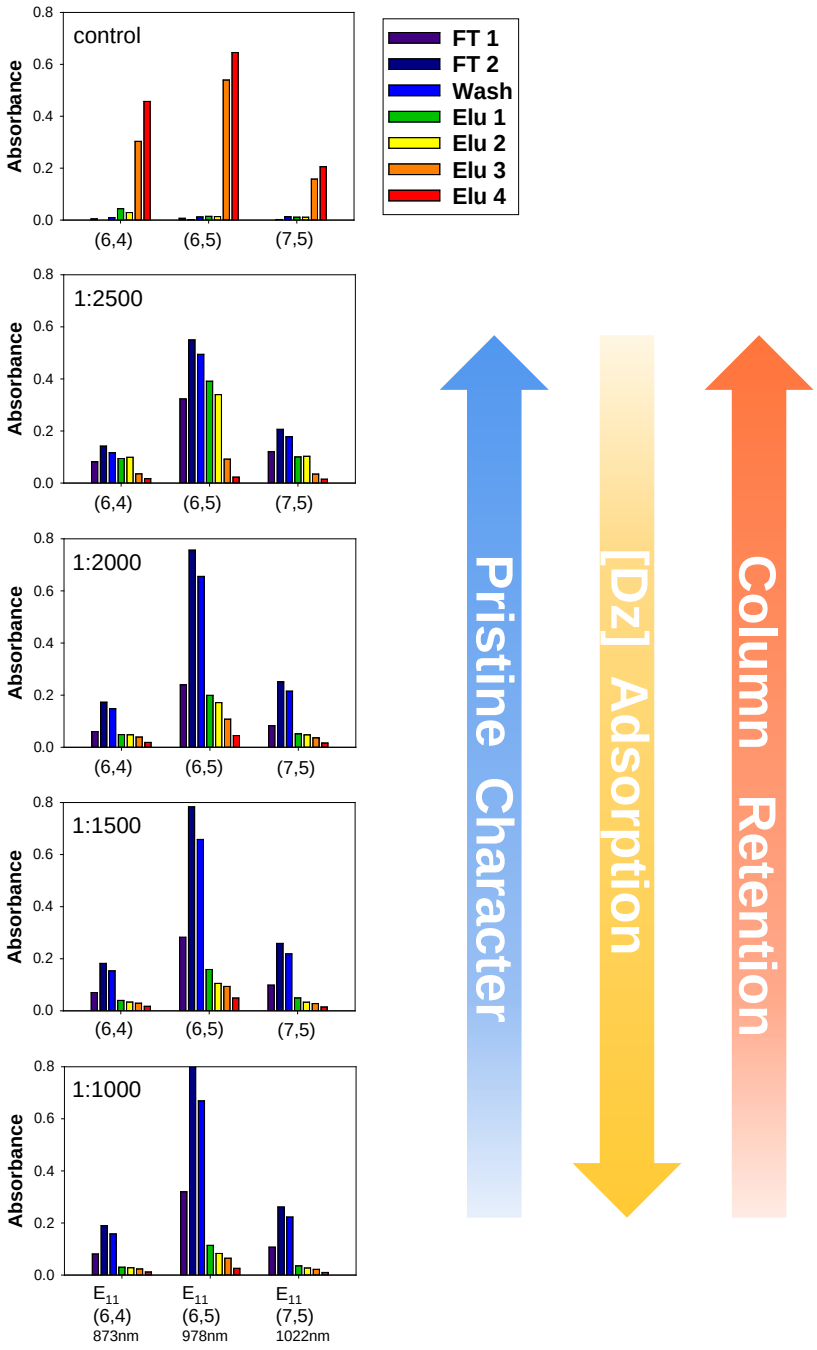

Figure 4-5. Bar graphs for the absorbance at E_{11} transitions for a (6,5)-, (6,4)-, and (7,5)-SWCNT solution (873 nm, 978 nm, and 1022 nm, respectively) at various sequential stages of the column separation process: flow through (FT), column wash (Wash), and column elution (Elu). At a [Dz:C] of [1:1000], most of the

SWCNTs are coming off the column immediately during the flow through, as indicated by the prominent purple to blue bar (FT 1, FT2, Wash). These samples are not adsorbing or strongly interacting with the gel resin. As the diazonium to carbon ratio decreases ([1:1000] to [1:2500]) the retention of SWCNTs shifts from the initial flow through stage of column separation to the elution stage. At [1:2500] SWCNTs are retained on the column as shown by the increasing absorbance values for Elu 1, Elu 2, Elu 3, and Elu 4 (green through red bars) and the significant decrease in the absorbance of the flow through and wash fractions (FT 1, FT2, Wash; blue through purple bars). The low concentration of Dz allows SWCNTs to interact with the gel resin, but still be easily eluted from the column. The control sample is pristine SWCNTs before functionalization which strongly adsorbs to the column and does not elute until the final two elutions (Elu 3 and 4).

4.3.5 Surface Enhanced Sorting of Semiconducting SWCNTs

With a [Dz:C] surface enhancement of [1:2500] we achieved high purification of (6,5)-SWCNT. This mixture of functionalized (6,5)-, (6,4)-, and (7,3)-SWCNTs differ in flow rates when injected onto a Sephacryl S-200 column (Figure 4-6). Enhanced (6,5)-SWCNTs flow the fastest eluting from the column first. This is possibly due to a higher concentration of outer wall adsorbed dinitro-diazonium by chiral selectivity.[113] Diazonium is shown to adsorb faster to (6,5) than to (6,4) and (7,3).[114] Without changing the surfactant concentration, the more free flowing surface enhanced-(6,5) elutes from the column 12 minutes before surfaced enhanced-(6,4) or -(7,3) allowing fraction collection of high purity (6,5)-SWCNTs (Figure 4-7).

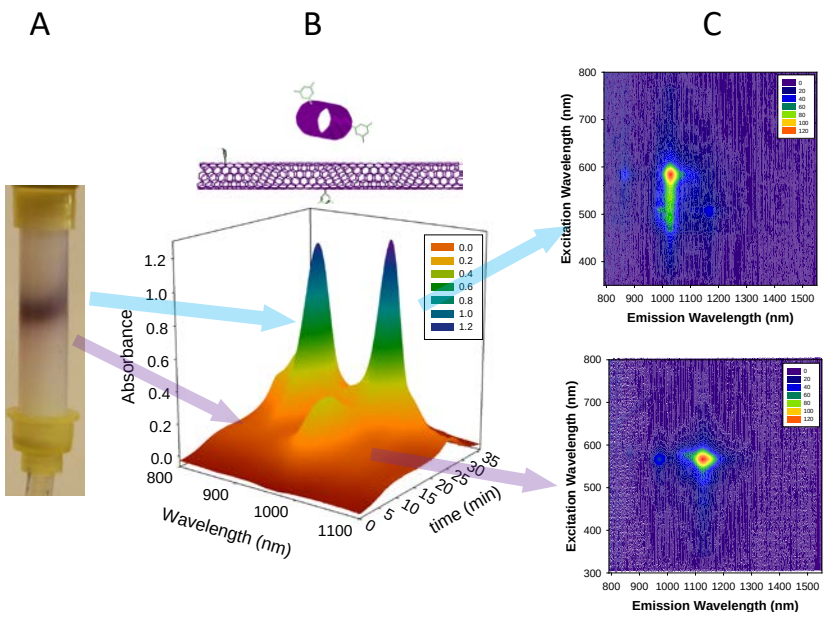

Figure 4-6. Surface chemistry enhanced gel chromatography for chirality purification of SWCNTs. (a) [1:2500] [Dz:C] surface enhanced SWCNT sample flowing through a gel chromatography column as a vertical purple-blue band. The bottom of the band contains (6,5)-SWCNTs while the top of the column band is (6,4)- and (7,3)-SWCNTs. (b) Absorption spectra with respect to time shows when different chiralities elute from the column. (6,5)-SWCNTs indicated by purple arrow elute first at 20 minutes followed by (6,4)- and (7,3)-SWCNTs 12 minutes later. (c) As the sample elutes from the column it is fraction collected. The lower excitation-emission map shows purified (6,5)-SWCNTs. The upper excitation-emission map shows (6,4)-SWCNTs without any (6,5)-SWCNTs.

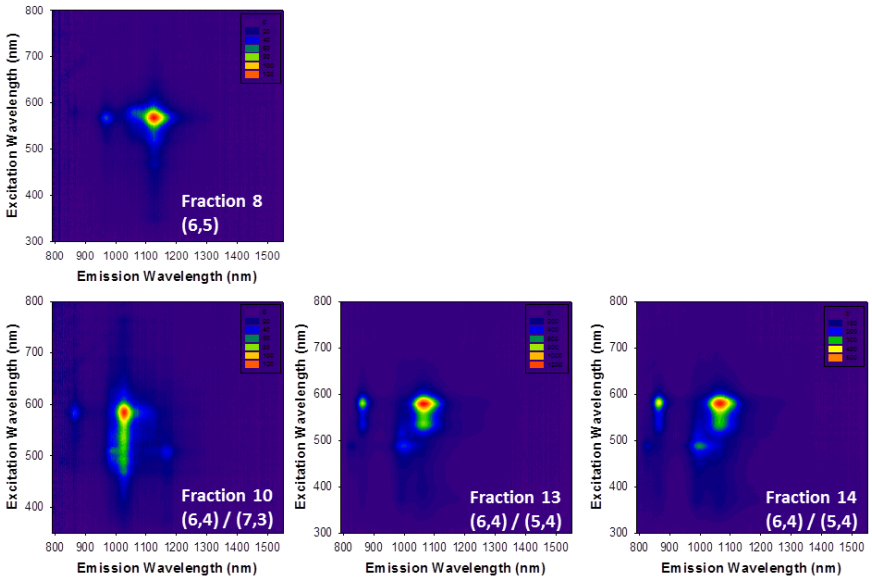

Figure 4-7. Excitation-emission maps of fractions collected by the surface enhanced SWCNT purification method. Fraction 8 shows a faint (6,5) E_{11} optical transition at 977 nm emission wavelength and a strong (6,5) E_{11}^{-} optical transition at 1139 nm emission wavelength.[110] The Fraction 10 map shows both the absence of (6,5) photoluminescence and the E_{11} and E_{11}^{-} PL peaks for (6,4).

As a control, pristine (6,5)-, (6,4)-, and (7,3)-SWCNTs are injected onto our column separation system. The nanotubes load at the top of the column and remain stuck as they adsorb stronger to the Sephacryl gel than surface enhanced nanotubes. As expected continuous pumping of aqueous 2 wt. % SDS does not *push* the pristine tubes further down the column. The pristine nanotubes can be eluted from the column only by increasing the SDS concentration to 5 wt. %.[32] This further indicates surface enhancement disrupts and weakens the surfactant/SWCNT/gel interaction.

Surface enhancement of SWCNTs decreases their adsorption potential to the gel resin. In addition this weakened interaction differs between nanotube chiralities potentially due to differences in functionization reaction rates from electrostatic effects of SDS dispersed nanotubes.[114] Our dinitro-diazonium surface

enhancement of semiconducting SWCNTs introduces chirality-dependent gel column flow rates. As the surfaced enhanced SWCNTs move through the column, the chiralities flow at differing rates allowing for separation.

4.4 Conclusion

In summary, we have developed a purification method for obtaining high purity (6,5)-SWCNTs based on gel chromatography and adsorption of diazonium chemistry at low concentration. This surface enhancement by adsorption of diazonium to the outerwall of the nanotube disrupts the arrangement of the aqueous, dispersing SDS surfactant. When these surface enhanced SCWNTs are purified by gel chromatography the chiralities flow through the column at different rates allowing for the isolation of (6,5)-SWCNT. In addition to diazonium chemistry, we find a similar effect when SWCNTs are surface enhanced by alkylization.

Chapter 5: Optically Triggered Melting of DNA on Single-Walled Carbon Nanotubes

Adapted from Wang, C.;† Meany, B.;† Wang, Y. H. Angew. Chem. Int. Ed. 2017, 56.
† These authors contributed equally to this work.

C. Wang prepared dsDNA wrapped SWCNTs from SDS surfactant sorted SWCNTs, made AFM measurements, measured dsDNA thermal melting, and contributed to laser irradiation experiments. B. Meany dispersed and sorted HiPco SWCNTs, characterized SWCNT and DNA-SWCNT samples by absorption and fluorescence spectroscopies, measured dsDNA-SWCNT optical melting, and setup and manipulated laser irradiation experiments.

5.1 Introduction

Optical nanoheaters convert incident photons to heat that may drive chemical reactions,[115-117] control drug release[118,119] and destroy cancer cells,[120-122] among a diverse array of potential applications.[123] The heating effect is intensively studied for metal nanoparticles (NPs) through recent advances, but remains largely unexplored for most other nanostructures. Metal NPs are attractive in part because electrons in noble metals such as Au feature strong, collective plasmon resonance that can be effectively harnessed to produce heat by optical excitation.[124] Richardson *et al.* measured the temperature change in a water droplet containing a colloidal suspension of 20 nm Au NPs under continuous-wave (CW) laser excitation and found that the solution temperature increases by 7 ºC due to collective heating of a large concentration of Au NPs.[125] Theoretical models suggest there is a 3°C increase in the surface temperature of optically excited NPs with intense excitation at the dilute limit (7.49×10^6 cm^{-3}). Notably, when exposed to sunlight, Au NPs can efficiently generate steam from

aqueous solutions.[126] These heating phenomena are also widely investigated for drug delivery and thermal therapy by combining biomaterials and light-absorbing nanoparticles.[127] Stehr *et al.* show that exciting an aggregate of Au NPs with a pulsed laser causes melting of double-stranded DNA (dsDNA).[128] Halas *et al.* found that irradiation of double-stranded DNA (dsDNA) coated Au nanomaterials with a CW laser releases molecular cargo from the particle surface.[129,130] It is suggested that a nonthermal mechanism may play a role in the light-triggered DNA release from Au NPs. Excitation with femtosecond laser may desorb thiolated DNA strands from the Au nanoparticle surface due to bond dissociation through coupling between photo-excited electrons of the nanoparticle and Au-S bond vibrations.[131] Hence, even for well-studied model systems such as Au NPs and DNA, the mechanisms for optically induced drug release from nanoparticles can be more complicated than initially thought. Furthermore, although optically induced heating of nanomaterials is a known phenomenon, most experiments require that a large concentration or aggregates of particles are excited to collectively induce the experimentally observable heating effect. This effect is typically too small to melt DNA.

Single-walled carbon nanotubes (SWCNTs) are tubular molecules of carbon that feature chemically stable, covalently bonded structures, with a typical diameter of 1 nm and lengths extending tens to thousands of nanometers. When stablized as individual nanoparticles by surfactants or polymers (such as DNA) in aqueous solution, nanotubes display structure dependent exciton absorption peaks that are remarkably sharp (Full Width Half Maxiumum ~25 meV) in both the

visible and the near-infrared (900-1400 nm) regions.[16,22] Their absorption cross section is on the order of 10^{-17} cm^2 per C-atom,[132-134] approximately two orders of magnitude higher than that of Au NPs on a per atom basis.[135] Contrary to Au NPs, semiconducting SWCNTs (s-SWCNTs) feature absorption and photoluminescence (PL) in the near-infrared region where tissue light scattering is minimized.[136] In addition there are over 30 unique nanotube structures, indexed as (*n*,*m*) chiralities, each with distinct optical fingerprints,[16,22] thereby providing a range of wavelength options for multimodality imaging and photothermal therapy. Pioneering work by Dai *et al.* has shown that SWCNTs can be optically excited to release DNA and other molecular cargo from nanotubes.[121] However, upon releasing the molecular cargo, the nanotubes aggregate irreversibly, indicative of an aggressive, non-selective release mechanism. While this heating occurs in highly concentrated carbon nanotube solutions, it is unclear whether the light-induced cargo release is due to localized heating in the vicinity of a nanotube, which is more selective and controllable for demanding applications such as drug release, or due to simply a temperature increase of the bulk solution.

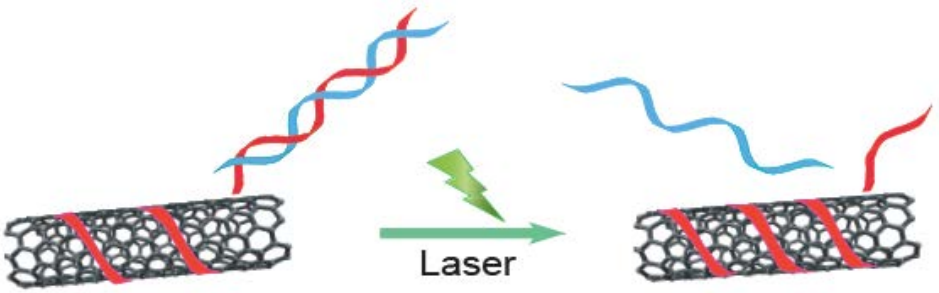

Scheme 5-1. Schematic illustration of optically triggered melting of a DNA duplex on a single-walled carbon nanotube. The DNA duplex has one longer strand (red), which comprises two segments: one wrapping the nanotube through pi-pi stacking while the other is still available for hybridization with a short, complementary DNA strand (blue). A laser beam with frequency tuned to

resonant with the nanotube heats the nanotube-DNA complex locally, leading to the melting of the DNA complex and release of the short DNA strand into the aqueous solution.

Here, we describe the synthesis of a novel SWCNT-DNA system that provides unambiguous experimental evidence of optical-induced heating and melting of dsDNA adsorbed to individual s-SWCNTs in the semidilute limit. Our experiments elucidate the important distinction between collective, bulk behaviors and individual particles by working in the semidilute regime,[137] where the particle-particle interactions are negligible such that the conclusions logically extend to single particles. Although the optically induced heating is a well-known phenonmenon for many different nanostructures, the localized heating of invidiual s-SWCNTs is unexpectedly large, making possible the melting of dsDNA that otherwise requires 22^{o}C higher solution temperature. Furthermore, unlike previous studies on metal NPs, our SWCNT-DNA system features well-defined surface chemistry and non-covalent bonding between DNA and nanotube, both of which are important for unambiguous experimental verification of the release mechanism.

5.2 Materials and Methods

5.2.1 SWCNTs Preparation and Purification

High pressure carbon monoxide (HiPco) SWCNTs (batch 194.3, Rice University) were dispersed in aqueous 1 wt.% sodium dodecyl sulfate (SDS, Sigma Aldrich) by tip sonication at 33 W and 10 ºC for 2 hr (Misonix, S-4000 ultrasonic liquid processor) followed by ultracentrifugation at 170,499 *g* (Beckman Coulter Optima LE-80K ultracentrifuge, 70 Ti fixed angle rotor) at 20 ºC for 4 hr. The top 80% of the resulting supernatant was isolated as the SWCNT-SDS sample.

The chirality purified (6,5)-SWCNT was isolated from the SWCNT-SDS sample by an adapted single-surfactant multicolumn gel chromatography procedure.[32] Using Sephacryl S-200 HR chromatography resin (GE Healthcare), columns were prepared and loaded with SWCNT-SDS. Small diameter SWCNTs such as (6,5), (7,5) and (8,4) adsorb to the resin while other semiconducting and metallic chiralities flow through the column. The columns are washed with aqueous 1 wt.% SDS followed by elution of the adsorbed SWCNTs with aqueous 5 wt.% SDS. Subsequent gel chromatography of the eluant further purified by chirality leading to the enriched (6,5)-SWCNT sample. For all SWCNT-DNA samples the concentration of nanotubes was 2.8 mg/L, unless otherwise specified, to maintain a concentration well within the semidilute regime.

5.2.2 SWCNT-DNA conjugates

SDS was replaced with ssDNA (5`-$(TAT)_4$ATGGTGGATAGGCGACTCACG-3`, Table 5-1; Integrated DNA Technologies, Inc.) by dialyzing the surfactant suspended SWCNT-SDS (20 ml) against a water bath (800 ml). The dialysis exchange was repeated 7 times over 36

hours. NaCl concentration was gradually increased from 0 mM (1^{st}-3^{rd} time) to 5 mM (4^{th}-5^{th}) and then 10 mM (6^{th} -7^{th}). The dialysis tube (Float-A-Lyzer G2, 10 kD, Spectrum Laboratories, Inc.) was selected because the pore size allowed SDS to freely diffuse into the dialysis bath while preventing ssDNA and SWCNTs from leaking out. Removal of SDS induced solvent exposure to the SWCNT surface allowing ssDNA to gradually replace the SDS and form SWCNT-ssDNA. It is known that ssDNA forms helical wrapping around nanotubes due to π-π interactions between the hydrophobic base pairs and carbon nanotube surface.[22] After the ssDNA wrapping, the solution was transferred to a 50 kD dialysis tube to remove residual free ssDNA by dialysis against 1 mM TB (Tris-Boric) buffer containing 10 mM NaCl for 24 hours at room temperature (Float-A-Lyzer G2, 50 kD, Spectrum Laboratories, Inc.). The complementary DNA (5`-CGTGAGTCGCCTATCCACCAT-3', Table 5-1) was then added to the solution. After annealing at 80 ºC for 10 min, the solution was slowly cooled down to the room temperature over a period of 2 hrs and then incubated at 4 ºC overnight followed by removal of free cDNA using a fresh 50 kD dialysis tube. This procedure produces the SWCNT-dsDNA; aqueous, individually suspended SWCNTs wrapped with ssDNA featuring a floating tethered duplex tail. All DNA oligos including modifications were produced by and purchased from IDT, Integrated DNA Technologies, Inc. All experiments were performed under the same buffer conditions of 1mM TB pH 7.4 and 10 mM NaCl.

5.2.3 UV-vis-NIR absorption spectra

The SWCNT samples were dispersed individual tubes (non-aggregated) and small bundles as revealed by absorption spectroscopy with a Perkin Elmer Lambda 1050 UV-visible-NIR spectrometer. The spectra were scanned from 200 nm to 1300 nm.

5.2.4 Photoluminescence spectroscopy

Excitation-emission photoluminescence maps were measured with a Horiba Jobin Yvon Nanolog spectrofluorometer using a liquid nitrogen cooled Symphony InGaAs CCD array detector. For the fluorescence spectra with the 6-FAM fluorophore, the excitation wavelength was fixed at 480 nm and the emission wavelength was measured from 490 nm to 650 nm using a PMT detector and a 1200 grooves/mm grating blazed at 500 nm.

5.2.5 Tail dsDNA thermal melting experiments

The melting curves were measured with a Perkin Elmer Lambda 35 UV-visible-NIR spectrometer equipped with a PTP-1 peltier temperature control system. The temperature of the solution was raised at a rate of 1 ºC/min. The absorbance at 260 nm was monitored as a function of temperature.

5.2.6 Laser irradiation

The SWCNT-DNA solutions, 2.4 ml in a 1-cm optical path quartz cuvette, were irradiated with a 561 nm laser (Cobalt Jive CW 561 DPSSL, Sweden) at a power density of ~1 W/cm^2 and an expanded beam diameter of ~8 mm. A 980 nm diode laser (Thorlabs, New Jersey), with an output of 100 mW and beam size of ~1 cm × 2 cm was used to excite (6,5)-SWCNT-dsDNA. The samples were maintained at set temperatures of 22 ºC and 40 ºC with a readout accuracy of ±0.5

ºC using a high capacity circulating water bath (Model 9105, Fisher Scientific). The sample temperature was confirmed with a thermal couple directly immersed in the solution.

5.2.7Atomic Force Microscopy (AFM)

The sample was deposited on a freshly peeled mica substrate (Ted Pella, Inc.) by adding a drop of solution on the substrate, allowing 10 minutes for binding, then gently rinsed with water and blown dry with nitrogen before the measurement. AFM images were acquired in tapping mode under ambient conditions using a Digital Instruments Multimode AFM equipped with a Nanoscope III controller 100 micron scanner (Veeco). Silicon nitride AFM probes with a radius of 15 nm were used for the measurements.

5.3 Results and Discussion

5.3.1 SWCNTs Complexed with DNA

In our experiments, s-SWCNTs are initially dispersed and purified in aqueous sodium dodecyl sulfate (SDS) followed by replacing the surfactant with single-stranded DNA (ssDNA) via dialysis exchange. The ssDNA sequence comprises two segments: a 5`-$(TAT)_4$- wrapping segment ending with a -ATGGTGGATAGGCGACTCACG-3` tail segment (Figure 5-1). The wrapping segment was designed following Zheng *et al.* to enable ssDNA wrapping on SWCNTs.[21] This segment selectively interacts with (6,5)-SWCNTs; however, the 21-base pair tail sequence lacks nanotube structure specificity (Table 5-1).[22] As a result, SWCNT-ssDNA are nanotubes stablized as individual particles in water by

the wrapping segment, while the tail sequence is left free-floating capable of forming a duplex with its complement strand, (cDNA).

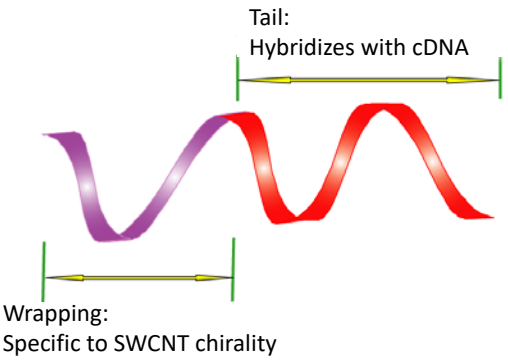

Figure 5-1. The wrapping ssDNA strand contains two segments: the wrapping segment (purple) designed to recognize (6,5)-SWCNTs, and the tail segment (red) available for hybridization with cDNA due to weaker interactions with the nanotube surface.

Sequence Name	**Single Strand Sequence**	**Nucleotide Length (base pairs)**
ssDNA	5`-$(TAT)_4$ATGGTGGATAGGCGACTCACG-3`	33
Wrapping segment	**5`-$(TAT)_4$**-3`	12
Tail segment	5`-**ATGGTGGATAGGCGACTCACG-3`**	21
cDNA	5`-CGTGAGTCGCCTATCCACCAT-3`	21
ssDNA-6FAM	5`-$(TAT)_4$ATGGTGGATAGGCGACTCACG-3`-6FAM	33
cDNA-IowaBlackFQ	IowaBlack-5`-CGTGAGTCGCCTATCCACCAT-3`	33

Table 5-1. ssDNA sequences used in the experiments.

The SWCNT-ssDNA was further incubated with cDNA, 5`-CGTGAGTCGCCTATCCACCAT-3`, which hybridizes with the tail segment to form an ssDNA-wrapped SWCNT featuring a DNA duplex tail (SWCNT-dsDNA) (Figure 5-2d). Although the tail segment can interact with the nanotube, this interaction is weaker than the competitive Watson-Crick base pairing formed during dsDNA hybridization. AFM images confirm that the SWCNT-dsDNA are individually dispersed, with a broad distribution of length centered around 160 nm (Figure 5-2c). Further improvement on selectivity of (6,5)-SWCNTs may be achieved with cDNA protection of the tail segment prior to wrapping the nanotube. Here, the studies uncover the basic features of this ssDNA cargo delivery system.

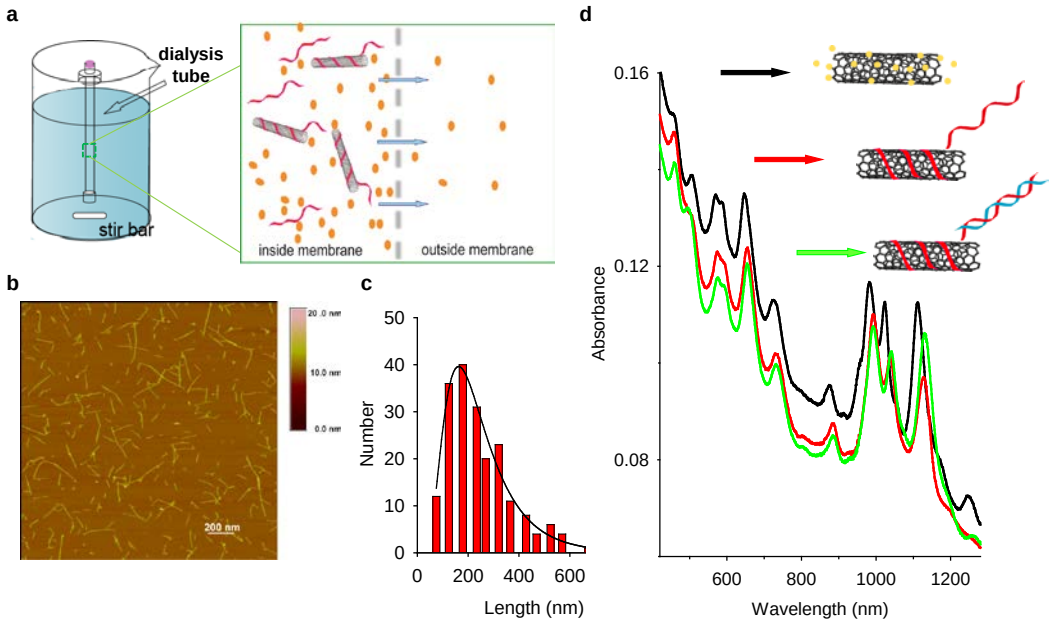

Figure 5-2. Preparation of SWCNT-dsDNA complexes by dialysis exchange. (a) Schematic illustration of replacing the surfactant of SDS-suspended SWCNTs with DNA in a 10 kD dialysis tube. As SDS leaves, the increasingly solvent exposed SWCNTs are wrapped by ssDNA. Free ssDNA are then removed using a

50 kD dialysis tube. Note that throughout this report we only show one single DNA strand for simplicity; multiple DNA strands are expected to wrap around a SWCNT since the average SWCNT length is much larger than the length of the wrapping DNA segment used in this study. (b) AFM topography image of individual well-dispersed SWCNT-dsDNA complexes on a mica substrate. (c) Histogram of the length distribution of the SWCNTs. (d) The absorption peaks of SWCNTs redshift upon formation of SWCNT-ssDNA complexes. The E_{11} absorption peaks of individually dispersed SWCNTs in 1% wt. SDS (black curve) redshifts 11 nm as SDS is replaced by ssDNA (red curve). Green curve represents the hybridized tail sample, SWCNT-dsDNA, with an additional 2 nm red shift.

Wrapping of nanotubes by ssDNA results in spectral redshifting of the E_{11} absorption peak characteristic of each nanotube chirality. The SDS suspended s-SWCNTs have E_{11} transition peaks at 982 nm, 1023 nm and 1112 nm, representing absorption by (6,5)-, (7,5)-, and (8,4)- chiral nanotubes, respectively (Figure 5-2d). Replacing SDS with ssDNA causes an 11-nm redshift for (6,5)-SWCNTs and 15-nm for (7,5) and (8,4). The redshift is due to a change in the nanotube dielectric constant as DNA replaces SDS.[138,139] Upon hybridization of the DNA-duplex tail, an additional 2 nm redshift occurs in the E_{11} peak for each SWCNT-dsDNA structure.

5.3.2 Optothermal Response of SWCNT-dsDNA

These synthesized SWCNT-dsDNA structures manifest interesting opto-thermal responsiveness, as revealed by comparative melting experiments of SDS-suspended SWCNTs (SWCNT-SDS), SWCNT-ssDNA, SWCNT-dsDNA and dsDNA alone. Thermal melting experiments monitor dehybridization of dsDNA by the absorbance change at 260 nm as the bulk sample temperature increases from 20 ºC to 80 ºC at a rate of 1 ºC/min. As expected, the SWCNT-SDS shows little response to temperature (black curve, Figure 5-3b and c). Similarly the

SWCNT-ssDNA (red curve) does not have a melting transition. The slight increase in absorbance at high temperature can be attributed to looser π-stacking of the ssDNA wrapped on the nanotube surface. Consistently, the E_{11} absorption peaks of the SWCNT-ssDNA maintained the same peak position (Figure 5-4a), suggesting that ssDNA wrapping on SWCNTs remains thermally stable up to 80ºC. In stark contrast, the SWCNT-dsDNA gives a well-defined melting transition at 52 ± 0.5ºC (Figure 5-3h). The control, free dsDNA duplex, shows a similar melting temperature of 49.0±0.2ºC. Since neither SWCNT-SDS nor SWCNT-ssDNA are thermally responsive, the observed absorbance jump at 52ºC must derive from melting the tail DNA duplex tethered to the nanotubes. Interestingly, the SWCNT-dsDNA features a melting transition with a FWHM of ~3.7ºC, almost three times sharper than that of free dsDNA duplex at a FWHM of ~9.8ºC (Figure 5-3i,l). The sharper transition may arise from a relatively high local concentration of DNA duplexes on the nanotubes, as previously observed by Mirkin *et al.* on gold nanoparticles.[140]

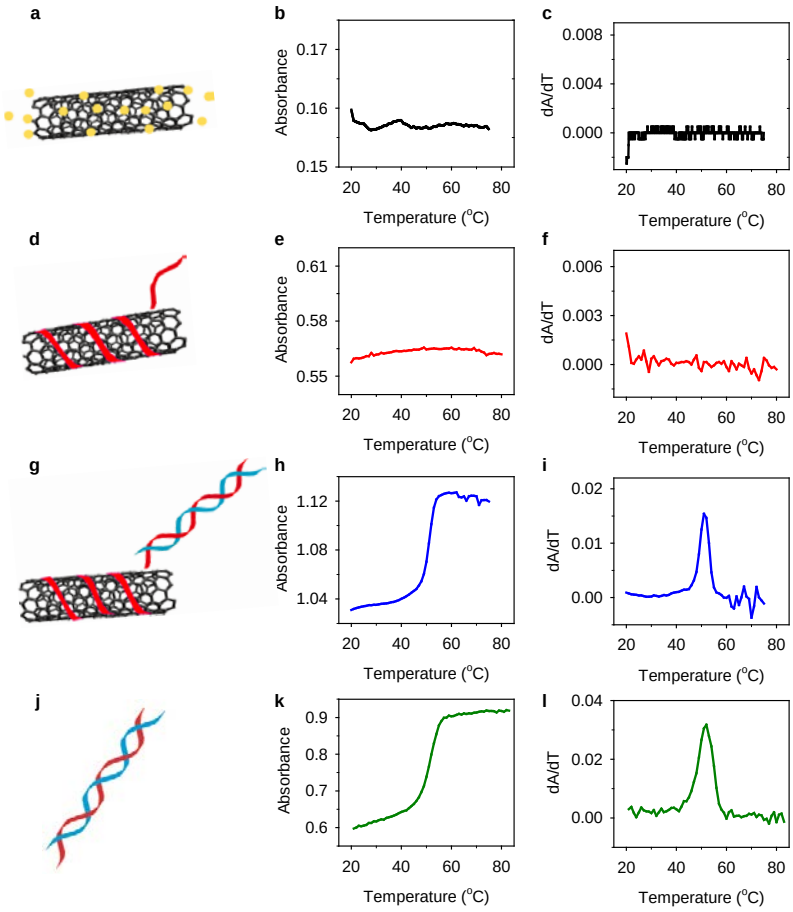

Figure 5-3. Thermal response of (**a,b,c**) SWCNT-1% SDS, (**d,e,f**) SWCNT-ssDNA, (**g,h,i**) SWCNT-dsDNA, and (**j,k,l**) dsDNA alone in solution. The dsDNA tail sequence is 21 base pairs in length. All DNA containing samples were in 1 mM TB at pH 7.4 and 10 mM NaCl. Only samples containing dsDNA (**g-l**) show DNA melting and therefore a thermal triggered response.

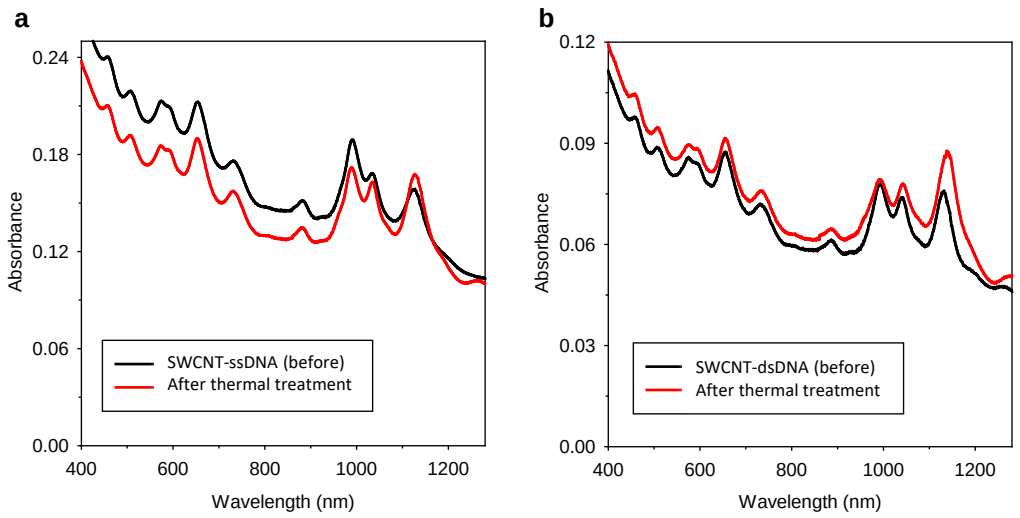

Figure 5-4. Comparision of UV-vis-NIR absorption spectra of SWCNT-DNA complexes before and after raising the samples from room temperature to 80 ºC at 1 ºC/min. (**a**) SWCNT-ssDNA before (black curve) and after (red curve) the thermal treatment show no discernible peak shifts. (**b**) SWCNT-dsDNA before (black curve) and after (red curve) thermal treatment show peak shifts for (6,5) and (8,4) chiralities. This absorption spectra peak shift is due to the melting of the dsDNA tail and release of the cDNA strand.

5.3.3 Optically Triggered Melting of dsDNA Complexed to SWCNT

In our optical trigger experiments, laser wavelengths of 561 nm and 980 nm were chosen to selectively excite (6,5)-SWCNTs through the E_{22} and E_{11} transition peaks, respectively. To avoid thermal crosstalk, the triggered melting experiments were performed in the semi-dilute regime (~2.8 mg/L) where nanotubes are largely prevented from being in contact with one another. At this concentration, the increase in bulk solution temperature due to laser heating is less than 0.6 ºC even after continuous irradiation for 60 minutes. By increasing the SWCNT concentration to 11.8 mg/L, we find the bulk solution temperature to rise 6.7 ºC after 20 minutes of 561 nm (500 mW ouput) irradiation, similar to Au NPs (Figure 5-5c).[125]

To demonstrate optically triggered melting of dsDNA complexed with s-SWCNTs, we devised a simple Forster Resonance Energy Transfer (FRET) experiment. 6-carboxyfluorescein (6-FAM), a fluorescent biomarker, is covalently attached to the 3` tail end of the ssDNA strand (sequence 1 in Table 5-1) while Iowa Black FQ, a complementary fluorescent quencher, is covalentrly attached to the 5` end of the cDNA. Upon hybridization the 6-FAM and Iowa Black are brought in close proximity leading to quenching of 6-FAM fluorescence. The fluorescence intensity of 6-FAM depends strongly on its distance from the quencher due to FRET; therefore melting of the dsDNA tail duplex separates fluorophore from quencher with recovery of the 6-FAM fluorescence (Figure 5-5).[141] This FRET-modulated fluorescence spectroscopy correlates with the previously discussed melting curves, verifying the hybridization of the labeled dsDNA tail and subsequent release of quencher-labeled cDNA upon optical heating of SWCNTs.

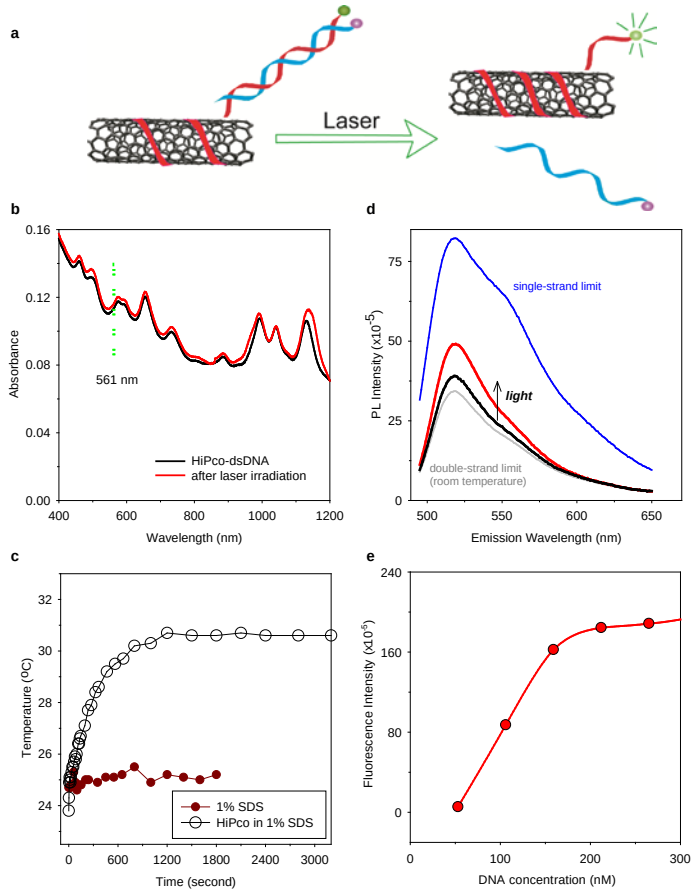

Figure 5-5. Laser-induced heating of SWCNTs melts adsorbed dsDNA. The release of the Iowa black FQ labled cDNA strand, which is a fluorescence quencher, leads to recovery of fluorescence from the 6-FAM labeled SWCNT-ssDNA. (**a**) Schematic illustration. (**b**) UV-vis-NIR absorption spectra of SWCNT-dsDNA complex before (black curve) and the resulting SWCNT-ssDNA complex after (red curve), 561 nm laser irradiation for 60 min. The samples were maintined at 40 ºC. (**c**) The optical exciting raises the bulk temperature of a SWCNT-SDS solution (here the SWCNT concentration is 11.8 mg/L) by 6.7 ºC, compared to an aqueous SDS control. (**d**) Fluorescence spectra of 6-FAM for the quenched SWCNT-dsDNA complex before (black curve) laser irradiation and the recovery of 6-FAM fluorescence from SWCNT-ssDNA complex after (red curve) DNA melting triggered by excitation of the SWCNT. This 6-FAM fluorescence recovery lies between the double-strand limit (fluorophore-quencher labeled dsDNA only) and the single-strand limit (complete separation into ssDNA-6FAM and cDNA-IowaBlack with complete recovery of 6-FAM fluorescence). (**e**) The fluorescence intensity of ssDNA tagged 6-FAM as a function of DNA concentration relates 6-FAM concentration to its intensity. 100 nmol 6-FAM modified ssDNA was chosen for our experiments. All of the fluorescence spectra were measured at 480 nm excitation in order to follow the emission of 6-FAM at 520 nm.

In addition to optical excitation alone, we simultaneously tested temperature effects of the bulk solution and optical excitation of the nanotubes. Exciting the nanotube dehybridizes the cDNA from the SWCNT-dsDNA at a bath temperature well below the dsDNA alone melting temperature (49 ºC). With the bulk solution at room temperature (22 ºC), the 6-FAM fluorescence intensity for SWCNT-dsDNA increases by 17% after optical excitation compared with the SWCNT-ssDNA control. The excited nanotube locally heats and melts the duplexed dsDNA tail releasing the Iowa Black labeled cDNA. Raising the bath temperature to 40 ºC followed by optical excitation results in a 58% increase in the FAM fluorescence intensity (Figure 5-5d). This elevated thermal bath is significantly lower than the melting temperature for dsDNA alone and is comparable to human body temperature. The fluorescence increase is accompanied by a 2-nm blueshift of the E_{11} peak for (6,5)-SWCNTs as expected due to the dehybridization of cDNA and a return to the SWCNT-ssDNA species. In addition, a redshift for the E_{11} peak of (8,4)-SWCNTs occurs from 1130 to 1137 nm (Figure 5-5b). These spectral changes are consistent with control samples that are melted thermally by increasing the bath temperature (Figure 5-6). Both 6-FAM fluorescence (494 nm) and DNA absorbance (260 nm) respectively increase with laser irradiation at 40 ºC indicating separation of 6-FAM from Iowa Black and therefore dehybridization of the DNA tail duplex.

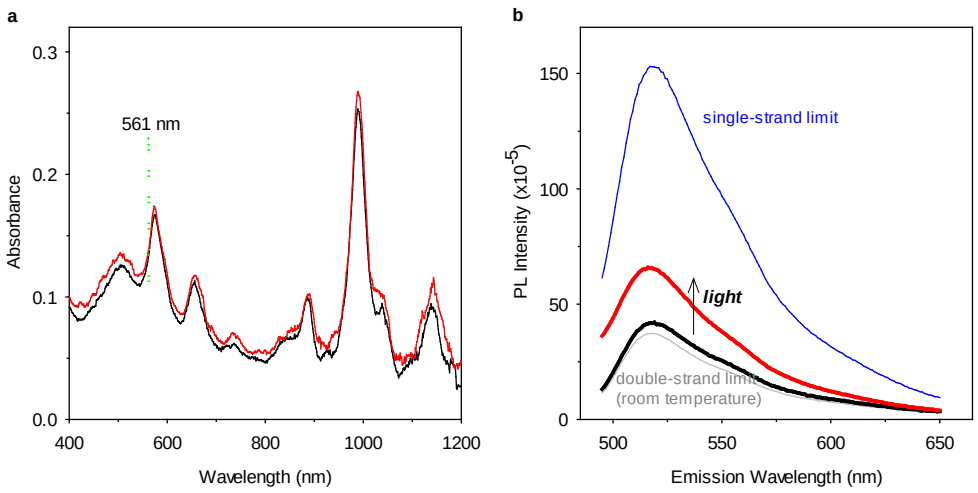

Figure 5-6. Laser-induced heating of (6,5)-enriched SWCNTs melts adsorbed dsDNA. (**a**) UV-vis-NIR absorption spectra of (6,5)-enriched SWCNT-dsDNA complex before (black curve) and the resulting SWCNT-ssDNA complex after (red curve), 561 nm laser irradiation for 60 min. The samples were maintined at 40 ^{o}C. (**b**) Fluorescence spectra of 6-FAM for the quenched SWCNT-dsDNA complex before (black curve) laser irradiation and the recovery of 6-FAM fluorescence from SWCNT-ssDNA complex after (red curve) DNA melting triggered by excitation of the SWCNT. The release of the Iowa black FQ labled cDNA strand, which is a fluorescence quencher, leads to recovery of fluorescence from the 6-FAM labeled SWCNT-ssDNA. This 6-FAM fluorescence recovery lies between the double-strand limit (fluorophore-quencher labeled dsDNA only) and the single-strand limit (complete separation into ssDNA-6FAM and cDNA-IowaBlack with complete recovery of 6-FAM fluorescence).

An important reason for the lack of complete recovery of 6-FAM fluorescence is structure-selective optical excitation of SWCNTs. Only (6,5)-SWCNTs significantly absorb at 561 nm (which is close to the second electronic transition of (6,5)-SWCNT at 568 nm) and 980 nm. Therefore to confirm our system is structure-selective, chirality-enriched (6,5)-SWCNTs were purified by gel chromatography and subsequently used to form the similar dsDNA complex, (6,5)-SWCNT-dsDNA. For the (6,5)-SWCNT-dsDNA sample, we found a 20% enhancement in dsDNA melting over the SWCNT-dsDNA sample based on FRET measurements (Fig. 5-6b). Since the SWCNT sample is a mixture of

multiple nanotube chiralities, it is less sensitive to a particular laser wavelength as compared with the (6,5) enriched sample.

5.3.4 Theoretical Modeling of Optically Triggered DNA Melting

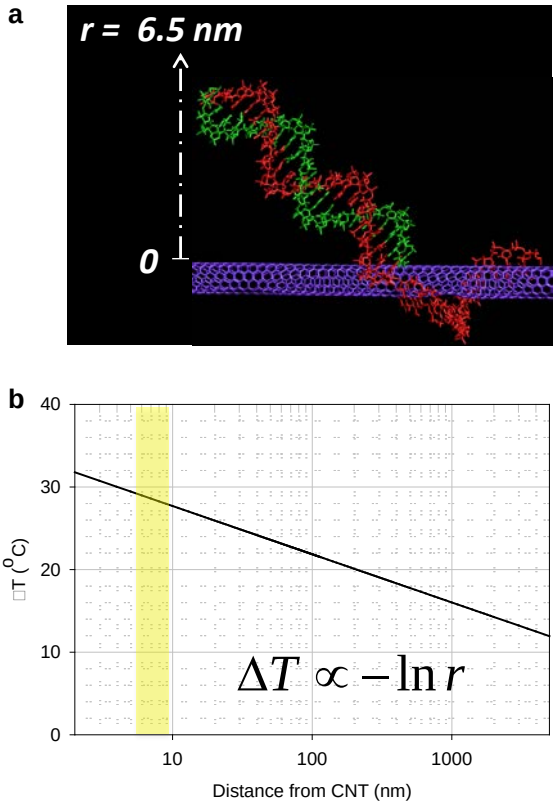

Figure 5-7. Heat transport model. (**a**) Molecular model of a (6,5)-SWCNT-dsDNA complex showing the close proximity (within 6.5 nm) of the dsDNA tail to the nanotube surface. (**b**) The change in solution temperature within the vicinity of an optically heated (6,5)-SWCNT excited at the E_{22} electronic transition with a CW laser at a power density of 1.0×10^3 W/cm^2.

Theoretical modeling suggests that the optical selectivity derives from the optoelectronically-induced local heating of individual SWCNTs. We note that the feasibility of optically induced heating of nanostructures has recently been demonstrated by others; including, for instance, Dai *et al.* with ensembles of

SWCNTs[121] and West *et al.* with collections of Au/Si core-shell nanoparticles.[120] Here we explore local heating at the single-molecule single-nanoparticle level. Since SWCNTs generally have a fluorescence quantum yield less than 1 %,[142,143] SWCNTs are extremely efficient radiation-to-thermal energy converters. Calculations show that thermal gradients can envelope carbon nanotubes depending on the amount of energy input per unit length, Q, from a laser:

$$Q = \frac{n_c}{l} \cdot w\sigma_{abs} \qquad \text{Equation 5-1}$$

where n_c is the number of carbon atoms contained in a SWCNT of length l, w is the laser power density, and σ_{abs} is the absorbance cross section per carbon atom. By treating the nanotube as a static linear heat source[144] and assume no convection, the temperature change of the solution (water or D_2O) surrounding the optically excited nanotube, $\Delta T(r,t)$, is found to drop exponentially as a function of the distance from the nanotube:

$$\Delta T(r,t) = \frac{Q}{4\pi K}\left(\ln\left(\frac{4Kt}{\rho c_v r^2}\right) - 0.5772\right), \qquad \text{Equation 5-2}$$

where ρ and c_v are the density and heat capacity respectively of the surrounding solvent, K is the thermal conductivity for water, and t is time. The localized temperature equalizes with that of the bulk solution at approximately 400 nm from the nanotube surface (Figure 5-7b). This tight spatial-temperature distribution illustrates strong localization of optically induced heating for our proposed nanotube system at the single molecular level. We expect that this localization effect will be even more pronounced by employing pulsed laser irradiation where the time variable enters the equation.

5.4 Conclusion

In conclusion, we show that optical excitation of individual semiconducting single-walled carbon nanotubes triggers strongly localized heating which efficiently melts non-covalently attached double-stranded oligonucleotides in solution. In contrast to conventional thermal dehybridization, this optically triggered DNA melting occurs at an ambient solution temperature 22˚C well below the double stranded DNA melting temperature, with a melting transition almost three times sharper (3.7˚C vs. 9.8˚C). To the best of our knowledge this is the first experimental confirmation of DNA melting due to localized optical heating of carbon nanotubes in the semidilute regime where the observation may be extended to single particle level given the negligible particle-particle interactions in this low concentration regime. Consistent with experiments, theoretical modeling suggests that under a modest photon flux, the local vicinity of an optically excited nanotube can reach a temperature 30˚C higher than that of the bulk solution. This strongly localized optical heating effect provides important new insights in the design of selective optical nanoheaters for a host of potential applications such as photothermal cancer therapy and on demand drug release.

Chapter 6: Conclusions and Outlook

The outlook for low-dimensional carbon materials continues to be bright. In particular, SWCNTs with their characteristic near-IR photoluminescence and exceptional electrical properties hold potential in the design of novel imaging and sensing devices, biological delivery applications, and quantum cryptography. However, the development of nanotube applications increases the demand for starting material of structure-purified SWCNTs. Therefore, separations science will continue to evolve along with applications research. New methods of sorting chiralities are being pursued such as ATPE[28] while older techniques: DGU and selective DNA sequence continue to be refined.[22,26]

To that end we entered the fray of the nanomaterial separations field in order to develop molecular routes to sorting SWCNTs with the intent of pushing the boundaries in carbon nanotube purification. First, CB-1 with an open ring molecular structure is shown to clip-on and disperse small diameter SWCNTs while larger nanotubes aggregate unable to fit within the slightly flexible CB-1. These C-shaped acyclic molecules complex with SWCNTs providing surfactant-free aqueous dispersed SWCNTs. If optical properties are desired simply adding a low concentration of SDBS induces a photoluminescent turn-on effect with minimal surfactant. Typically when dispersing SWCNTs the surfactant concentration is well above it's CMC. This leads to surfactant accumulating in a heterogeneous morphology surrounding the nanotube outer wall which also attracts impurities. The development of sensitive next-generation nanotube applications requires clean nanomaterials. Therefore, a previously unused

surfactant, ammonium laurate, is investigated and found to deposit clean MWCNTs on to silicon substrates. When incorporated in a device, nanotubes dispersed in surfactant typically are covered in residue after drying which is difficult to sufficiently remove. However, AL surfactant is surprisingly easier to remove than the similar structured SDS, and AL does not collect an abundance of impurities such as carbonaceous particles. Lastly, we refine the technique of gel chromatography to tune the adsorption of SWCNTs to the column. When introduced aryl-Dz moieties adsorb to nanotubes in solution disrupting the surfactant morphology. This change weakens the interaction between nanotube and gel column. Since the rate of adsorption of small molecules to the outer wall differs slightly by chiral structure, these nanotubes are purified by differences in flow rates when quickly loaded on a gel column. This technique has potential to sort several SWCNT chiralities.

While researching SWCNT purification, an application is developed to use the nanotube as a nanoheater heating only its immediate surroundings with minimal effect on the bulk solution temperature. Semiconducting (6,5)-SWCNTs are purified and wrapped with dsDNA. Upon resonant optical excitation of the nanotube, the SWCNT-dsDNA complex heats up melting the dsDNA, and complimentary ssDNA strands are released. This work has applications in biological drug delivery systems but could also be developed as a route to purifying SWCNTs.

By obtaining high purity samples of SWCNTs the research community comes closer to reaching a two decade old goal of growing single-crystal

nanotubes of a single chirality. While difficult the purified nanotubes would act as seeds for growing new SWCNTs of the same chirality.[145] With the ability to purify a variety of nanotube structures, one can grow a variety of SWCNT chiralities depending on the desired application. By vapor-phase epitaxy these single chirality SWCNT seeds with grow and extend.[146] This cloning procedure could ensure continuous growth of long, pristine nanotubes with applications in integrated circuits and other technological advancements. As previously described, our purification research takes a step closer towards obtaining highly enriched semiconducting SWCNTs for fundamental research, novel applications, and growing pristine, single chirality nanotubes.

Bibliography

(1) Iijima, S. Helical Microtubules of Graphitic Carbon. *Nature* **1991**, *354*, 56-58.

(2) Iijima, S.; Ajayan, P. M.; Ichihashi, T. Growth Model for Carbon Nanotubes. *Phys. Rev. Lett* **1992**, *69*, 3100-3103.

(3) Ajayan, P. M.; Ebbesen, T. W.; Ichihashi, T.; Iijima, S.; Tanigaki, K.; Hiura, H. Opening Carbon Nanotubes with Oxygen and Implications for Filling. *Nature* **1993**, *362*, 522-525.

(4) Saito, R.; Dresselhaus, G.; Dresselhaus, M. S. *Physical Properties of Carbon Nanotubes*; Imperial College Press: London, 1998.

(5) Saito, R.; Fujita, M.; Gresselhaus, G.; Dresselhaur, M. S. Electronic Structure of Chiral Graphene Tubules. *Appl. Phys. Lett.* **1992**, *60*, 2204-2206.

(6) Gavryushin, V. Graphene Brillouin Zone and Electronic Energy Dispersion. Project, W. D., Ed.; Wolfram Mathematica.

(7) Hong, S.; Myung, S. Nanotube Electronics: a Flexible Approach to Mobility. *Nat. Nanotechnol.* **2007**, *2*, 207-208.

(8) Ajayan, P. M.; Tour, J. M. Nanotube Composites. *Nature* **2007**, *447*, 1066-1068.

(9) Sandler, J.; Shaffer, M. S.; Prasse, T.; Bauhofer, W.; Schulte, K.; Windle, A. H. Development of a Dispersion Process for Carbon Nanotubes in an Epoxy Matrix and the Resulting Electrical Properties. *Polymer* **1999**, *40*, 5967-5971.

(10) Park, H.; Afzali, A.; Han, S. J.; Tulevski, G. S.; Franklin, A. D.; Tersoff, J.; Hannon, J. B.; Haensch, W. High-Density Integration of Carbon Nanotubes via Chemical Self-assembly. *Nat. Nanotechnol.* **2012**, *7*, 787-791.

(11) Sun, C.; Karki, K.; Jia, Z.; Liao, H.; Zhang, Y.; Li, T.; Qi, Y.; Cummings, J.; Rubloff, G. W.; Wang, Y. H. A Beaded-String Silicon Anode. *ACS Nano* **2013**, *7*, 2717-2724.

(12) Welsher, K.; Liu, Z.; Sherlock, S. P.; Robinson, J. T.; Chen, Z.; Daranciang, D.; Dai, H. A Route to Brightly Fluorescent Carbon Nanotubes for Near-Infrared Imaging in Mice. *Nat. Nanotechnol.* **2009**, *4*, 773-780.

(13) Hong, G.; Diao, S.; Chang, J.; Antaris, A. L.; Chen, C.; Zhang, B.; Zhao, S.; Atochin, D. N.; Huang, P. L.; Andreasson, K. I.; Kuo, C. J.; Dai, H. Through-Skull Fluorescence Imaging of the Brain in a New Near-Infrared Window. *Nat. Photon.* **2014**, *8*, 723-320.

(14) Mulvey, J. J.; Villa, C. H.; McDevitt, M. R.; Escorcia, F. E.; Case, E.; Scheinberg, D. A. Self-assembly of Carbon Nanotubes and Antibodies of Tumours for Targeted Amplified Delivery. *Nat. Nanotechnol.* **2013**, *8*, 763-771.

(15) O'Connell, M. J.; Bachilo, S. M.; Huffman, C. B.; Moore, V. C.; Strano, M. S.; Haroz, E. H.; Rialon, K. L.; Boul, P. J.; Noon, W. H.; Kittrell, C.; Ma, J.; Hauge, R. H.; Weisman, R. B.; Smalley, R. E. Band Gap Fluorescence from Individual Single-Walled Carbon Nanotubes. *Science* **2002**, *297*, 593-596.

(16) Bachilo, S. M.; Stano, M. S.; Kittrell, C.; Hauge, R. H.; Smalley, R. E.; Weisman, R. B. Structure-assigned Optical Spectra of Single-Walled Carbon Nanotubes. *Science* **2002**, *298*, 2361-2366.

(17) Wang, F.; Dukovic, G.; Brus, L. E.; Heinz, T. F. The Optical Resonances in Carbon Nanotubes Arise from Excitons. *Science* **2005**, *308*, 838-841.

(18) Leeds, J. D.; Fourkas, J. T.; Wang, Y. H. Achieving Ultrahigh Concentrations of Fluorescent Single-Walled Carbon Nanotubes Using Small-Molecule Viscosity Modifiers. *Small* **2013**, *9*, 241-247.

(19) NIST: Reference material 8281, Single-wall carbon nanotubes (dispersed, three length-resolved populations). National Institute of Standards and Technology: Gaithersburg, Maryland, 2013; pp 11.

(20) Zheng, M.; Jagota, A.; Semke, E. D.; Diner, B. A.; McLean, R. S.; Lustig, S. R.; Richardson, R. E.; Tassi, N. G. DNA-assisted Dispersion and Separation of Carbon Nanotubes. *Nat. Mater.* **2003**, *2*, 338-342.

(21) Zheng, M.; Jagota, A.; Strano, M.S.; Santos, A. P.; Barone, P.; Chou, S. G.; Diner, B. A.; Dresselhaus, M. S.; McLean, R. S.; Onoa, G. B.; Samsonidze, G. G.; Semke, E. D.; Usrey, M.; Walls, D. J. Structure-Based Carbon Nanotube Sorting by Sequence-Dependent DNA Assembly. *Science* **2003**, *302*, 1545-1548.

(22) Tu, X.; Manohar, S.; Jagota, A.; Zheng, M. DNA Sequence Motifs for Structure-Specific Recognition and Separation of Carbon Nanotubes. *Nature* **2009**, *460*, 250-253.

(23) Dukovic, G.; Balaz, M.; Doak, P.; Berova, N. D.; Zheng, M.; Mclean, R. S.; Brus, L. E. Racemic Single-Walled Carbon Nanotubes Exhibit Circular Dichroism When Wrapped with DNA. *J. Am. Chem. Soc* **2006**, *128*, 9004-9005.

(24) Tu, X.; Hight Walker, A. R.; Khripin, C. Y.; Zheng, M. Evolution of DNA Sequences Toward Recognition of Metallic Armchair Carbon Nanotubes. *J. Am. Chem. Soc* **2011**, 12998-13001.

(25) Arnold, M. S.; Stupp, S. I.; Hersam, M. C. Enrichment of Single-Walled Carbon Nanotubes by Diameter in Density Gradients. *Nano Lett.* **2005**, *5*, 713-718.

(26) Arnold, M. S.; Green, A. A.; Hulvat, J. F.; Stupp, S. I.; Hersam, M. C. Sorting Carbon Nanotubes by Electronic Structure Using Density Differentiation. **2006**, *1*, 60-65.

(27) Ghosh, S.; Bachilo, S. M.; Weisman, R. B. Advanced Sorting of Single-Walled Carbon Nanotubes by Nonlinear Density-Gradient Ultracentrifugation. *Nat. Nanotechnol.* **2010**, *5*, 443-450.

(28) Khripin, C. Y.; Fagan, J. A.; Zheng, M. Spontaneous Partition of Carbon Nanotubes in Polymer-Modified Aqueous Phases. *J. Am. Chem. Soc* **2013**, *135*, 6822-6825.

(29) Fagan, J. A.; Haroz, E. H.; Ihly, R.; Gui, H.; Blackburn, J. L.; Simpson, J. R.; Lam, S.; Hight Walker, A. R.; Doorn, S. K.; Zheng, M. Isolation of >1 nm Diameter Single-Wall Carbon Nanotube Species Using Aqueous Two-Phase Extraction. *ACS Nano* **2015**, *9*, 5377-5390.

(30) Gui, H.; Streit, J. K.; Fagan, J. A.; Hight Walker, A. R.; Zhou, C.; Zheng, M. Redox Sorting of Carbon Nanotubes. *Nano Lett.* **2015**, *15*, 1642-1646.

(31) Moshammer, K.; Hennrich, F.; Kappes, M. M. Selective Suspension in Aqueous Sodium Dodecyl Sulfate According to Electronic Structure Type Allow Simple Separation of Metallic from Semiconducting Single-Walled Carbon Nanotubes. *Nano Res* **2009**, *2*, 599-606.

(32) Liu, H.; Nishide, D.; Tanaka, T.; Kataura, H. Large-Scale Single-Chirality Separation of Single-Wall Carbon Nanotubes by Simple Gel Chromatography. *Nat. Commun.* **2011**, *2*, 309.

(33) Liu, H.; Tanaka, T.; Urabe, Y.; Kataura, H. High-Efficiency Single-Chirality Separation of Carbon Nanotubes Using Temperature-Controlled Gel Chromatography. *Nano Lett.* **2013**, *13*, 1996-2003.

(34) Tvrdy, K.; Jain, R. M.; Han, R.; Hilmer, A. J.; McNicolas, T. P.; Strano, M. S. A Kinetic Model for the Deterministic Prediction of Gel-Based Single-Chirality Single-Walled Carbon Nanotube Separation. *ACS Nano* **2013**, *7*, 1779-1789.

(35) O'Connell, M.; Boul, P.; Ericson, L. M.; Huffman, C.; Wang, Y. H.; Haroz, E.; Ausman, K. D.; Smalley, R. E. Reversible Water-Solubilization of Single-Walled Carbon Nanotubes by Polymer Wrapping. *Chem. Phys. Lett.* **2001**, *342*, 265.

(36) Backes, C.; Schmidt, C. D.; Rosenlehner, K.; Hauke, F.; Coleman, J. N.; Hirsch, A. Nanotube Surfactant Design: The Versatility of Water-Soluble Perylene Bisimides. *Adv. Mater.* **2010**, *22*, 788.

(37) Lin, S. C.; Blankschtein, D. Role of Bile Salt Surfactant Sodium Cholate in Enhancing the Aqueous Dispersion Stability of Single-Walled Carbon Nanotubes: A Molecular Dynamics Simulation Study. *J. Phys. Chem. B* **2010**, *114*, 15616.

(38) Komatsu, N. Separation of Nanocarbons by Molecular Recognition. *J. Incl. Phenom. Macrocycl. Chem.* **2008**, *61*, 195.

(39) Star, A.; Stoddart, J. F.; Steuerman, D.; Diehl, M.; Boukai, A.; Wong, E. W.; Yang, X.; Chung, S.-W.; Choi, H.; Heath, J. R. Preparation and Properties of Polymer-Wrapped Single-Walled Carbon Nanotubes. *Ange. Chem. Int. Ed.* **2001**, *40*, 1721.

(40) Brozena, A. H.; Moskowitz, J.; Shao, B.; Deng, S.; Liao, H.; Gaskell, K. J.; Wang, Y. H. Outer Wall Selectively Oxidized, Water-Soluble Double-Walled Carbon Nanotubes. *J. Am. Chem. Soc.* **2010**, *132*, 3932.

(41) Deng, S.; Zhang, Y.; Brozena, A. H.; Mayes, M. L.; Banerjee, P.; Chiou, W. A.; Rubloff, G. W.; Schatz, G. C.; Wang, Y. H. Confined Propagation of Covalent Chemical Reactions on Single-Walled Carbon Nanotubes. *Nat. Commun.* **2011**, *2*, 382.

(42) Nish, A.; Hwang, J.-Y.; Doig, J.; Nicholas, R. J. Highly Selective Dispersion of Single-Walled Carbon Nanotubes Using Aromatic Polymers. *Nat. Nanotechnol.* **2007**, *2*, 640.

(43) Peng, X.; Komatsu, N.; Bhattacharya, S.; Shimawaki, T.; Aonuma, S.; Kimura, T.; Osuka, A. Optically Active Single-Walled Carbon Nanotubes. *Nat. Nanotechnol.* **2007**, *2*, 361.

(44) Ju, S. Y.; Doll, J.; Sharma, I.; Papadimitrakopoulos, F. Selection of Carbon Nanotubes with Specific Chiralities Using Helical Assemblies of Flavin Mononucleotide. *Nat. Nanotechnol.* **2008**, *3*, 356.

(45) Ma, D.; Hettiarachchi, G.; Nguyen, D.; Zhang, B.; Wittenberg, J. B.; Zavalij, P. Y.; Briken, V.; Isaacs, L. Acyclc Cucurbit[*n*]uril Molecular Containers Enhance the Solubility and Bioactivity of Poorly Soluble Pharmaceuticals. *Nat. Chem.* **2012**, *4*, 503.

(46) Nau, W. M.; Florea, M.; Assaf, K. I. Deep Inside Cucurbiturils: Physical Properties and Volumes of Their Inner Cavity Determine the Hydrophobic Driving Force for Host-Guest Complexation. *Isr. J. Chem.* **2011**, *51*, 559.

(47) Isaacs, L. Cucurbit[*n*]urils: From Mechanism to Structure and Function. *Chem. Commun.* **2009**, 0, 619.

(48) Lee, J. W.; Samal, S.; Selvapalam, N.; Kim, H. J.; Kim, K. Cucurbituril Homologues and Derivatives: New Opportunities in Supramolecular Chemistry. *Acc. Chem. Res.* **2003**, *36*, 621.

(49) Ko, Y. H.; Kim, E.; Hwang, I.; Kim, K. Supramolecular Assemblies Built with Host-Stabilized Charge-Transfer Interactions. *Chem. Commun.* **2007**, 0, 1305.

(50) Ma, D.; Zavalij, P. Y.; Isaacs, L. Acyclic Cucurbit[*n*]uril Congeners Are High Affinity Hosts. *J. Org. Chem.* **2010**, *75*, 4786.

(51) Bales, B. L. A Definition of the Degree of Ionization of a Micelle Based on Its Aggregation Number. *J. Phys. Chem. B* **2001**, *105*, 6798.

(52) Niyogi, S.; Boukhalfa, S.; Chikkannanavar, S. B.; McDonald, T. J.; Heben, M. J.; Doorn, S. K. Selective Aggregation of Single-Walled Carbon Nanotubes via Salt Addition. *J. Am. Chem. Soc.* **2007**, *129*, 1898.

(53) Weisman, R. B.; Bachilo, S. M. Dependence of Optical Transition Energies on Structure for Single-Walled Carbon Nanotubes in Aqueous Suspension: An Empirical Kataura Plot. *Nano Lett.* **2003**, *3*, 1235.

(54) Ju, S.-Y.; Kopcha, W. P.; Papadimitrakopoulos, F. Brightly Fluorescent Single-Walled Carbon Nanotubes via an Oxygen-Excluding Surfactant Organization. *Science* **2009**, *323*, 1319.

(55) Satishkumar, B. C.; Brown, L. O.; Gao, Y.; Wang, C. C.; Wang, H. L.; Doorn, S. K. Reversible Fluorescence Quenching in Carbon Nanotubes for Biomolecular Sensing. *Nat. Nanotechnol.* **2007**, *2*, 560.

(56) Marquez, C.; Hudgins, R. R.; Nau, W. M. Mechanism of Host-Guest Complexation by Cuburbituril. *J. Am. Chem. Soc.* **2004**, *126*, 5806.

(57) Burnett, C. A.; Witt, D.; Fettinger, J. C.; Isaacs, L. Acyclic Congener of Cucurbituril: Synthesis and Recognition Properties. *J. Org. Chem.* **2003**, *68*, 6184.

(58) Treacy, M. M. J.; Ebbesen, T. W.; Gibson, J. M. Exceptionally High Young's Modulus Observed for Individual Carbon Nanotubes. *Nature* **1996**, *381*, 678-680.

(59) Fan, S. S.; Chapline, M. G.; Franklin, N. R.; Tombler, T. W.; Cassell, A. M.; Dai, H. J. Self-Oriented Regular Arrays of Carbon Nanotubes and Their Field Emission Properties. *Science* **1999**, *283*, 512-514.

(60) Biercuk, M. J.; Llaguno, M. C.; Radosavljevic, M.; Hyun, J. K.; Johnson, A. T.; Fischer, J. E. Carbon Nanotube Composites for Thermal Management. *Appl. Phys. Lett.* **2002**, *80*, 2767-2769.

(61) Kymakis, E.; Amaratunga, G. A. J. Electrical Properties of Single-Wall Carbon Nanotube-Polymer Composite Films. *J. Appl. Phys.* **2006**, *99*.

(62) Gonnet, P.; Liang, S. Y.; Choi, E. S.; Kadambala, R. S.; Zhang, C.; Brooks, J. S.; Wang, B.; Kramer, L. Thermal Conductivity of Magnetically Aligned Carbon Nanotube Buckypapers and Nanocomposites. *Curr. Appl. Phys.* **2006**, *6*, 119-122.

(63) Kim, Y. L.; Jung, H. Y.; Kar, S.; Jung, Y. J. Cleaning Organized Single-Walled Carbon Nanotube Interconnect Structures for Reduced Interfacial Contact Resistance. *Carbon* **2011**, *49*, 2450-2458.

(64) Shimauchi, H.; Ohno, Y.; Kishimoto, S.; Mizutani, T. Suppression of Hysteresis in Carbon Nanotube Field-Effect Transistors: Effect of Contamination Induced by Device Fabrication Process. *Japan. J. Appl. Phys.* **2006**, *45*, 5501-5503.

(65) Gahng, S.; Ra, C. H.; Cho, Y. J.; Kim, J. A.; Kim, T.; Yoo, W. J. Reduction of Metal Contact Resistance of Graphene Devices via CO2 Cluster Cleaning. *Appl. Phys. Lett.* **2014**, *104*, 223110.

(66) Joiner, C.; Roy, T.; Hesabi, Z.; Chakrabarti, B.; Vogel, E. Cleaning Graphene with a Titanium Sacrificial Layer. *Appl. Phys. Lett.* **2014**, *104*, 223109.

(67) Lee, S. W.; Muoth, M.; Helbling, T.; Mattmann, M.; Hierold, C. Suppression of Resist Contamination During Photolithography on Carbon Nanomaterials by a Sacrificial Layer. *Carbon* **2014**, *66*, 295-301.

(68) Nath, A.; Koehler, A.; Jernigan, G.; Wheeler, V.; Hite, J.; Hernández, S.; Robinson, Z.; Garces, N.; Myers-Ward, R.; Eddy Jr, C. Achieving Clean Epitaxial Graphene Surfaces Suitable for Device Applications by Improved Lithographic Process. *Appl. Phys. Lett.* **2014**, *104*, 224102.

(69) Macintyre, D. S.; Ignatova, O.; Thoms, S.; Thayne, I. G. Resist Residues and Transistor Gate Fabrication. *J. Vac. Sci. & Tech. B* **2009**, *27*, 2597-2601.

(70) Rastogi, R.; Kaushal, R.; Tripathi, S. K.; Sharma, A. L.; Kaur, I.; Bharadwaj, L. M. Comparative Study of Carbon Nanotube Dispersion Using Surfactants. *J. Coll. Inter. Sci.* **2008**, *328*, 421-428.

(71) Shin, J. Y.; Premkumar, T.; Geckeler, K. E. Dispersion of Single-Walled Carbon Nanotubes by Using Surfactants: Are the Type and Concentration Important? *Chem.-a Euro. J.* **2008**, *14*, 6044-6048.

(72) Geng, H. Z.; Kim, K. K.; So, K. P.; Lee, Y. S.; Chang, Y.; Lee, Y. H. Effect of Acid Treatment on Carbon Nanotube-Based Flexible Transparent Conducting Films. *J. Am. Chem. Soc.* **2007**, *129*, 7758-7759.

(73) Moore, V. C.; Strano, M. S.; Haroz, E. H.; Hauge, R. H.; Smalley, R. E.; Schmidt, J.; Talmon, Y. Individually Suspended Single-Walled Carbon Nanotubes in Various Surfactants. *Nano Lett.* **2003**, *3*, 1379-1382.

(74) Balasubramanian, K.; Burghard, M. Chemically Functionalized Carbon Nanotubes. *Small* **2005**, *1*, 180-192.

(75) Heister, E.; Lamprecht, C.; Neves, V.; Tilmaciu, C.; Datas, L.; Flahaut, E.; Soula, B.; Hinterdorfer, P.; Coley, H. M.; Silva, S. R. P.; McFadden, J. Higher Dispersion Efficacy of Functionalized Carbon Nanotubes in Chemical and Biological Environments. *ACS Nano* **2010**, *4*, 2615-2626.

(76) Barone, P. W.; Baik, S.; Heller, D. A.; Strano, M. S. Near-Infrared Optical Sensors Based on Single-Walled Carbon Nanotubes. *Nat. Mater.* **2005**, *4*, 86-U16.

(77) Garg, A.; Sinnott, S. B. Effect of Chemical Functionalization on the Mechanical Properties of Carbon Nanotubes. *Chem. Phys. Lett.* **1998**, *295*, 273-278.

(78) Worsley, K. A.; Kalinina, I.; Bekyarova, E.; Haddon, R. C. Functionalization and Dissolution of Nitric Acid Treated Single-Walled Carbon Nanotubes. *J. Am. Chem. Soc.* **2009**, *131*, 18153-18158.

(79) Rosca, I. D.; Watari, F.; Uo, M.; Akaska, T. Oxidation of Multiwalled Carbon Nanotubes by Nitric Acid. *Carbon* **2005**, *43*, 3124-3131.

(80) Martin, O.; Gutierrez, H. R.; Maroto-Valiente, A.; Terrones, M.; Blanco, T.; Baselga, J. An Efficient Method for the Carboxylation of Few-Wall Carbon Nanotubes with Little Damage to Their Sidewalls. *Mater. Chem. Phys.* **2013**, *140*, 499-507.

(81) Furtado, C. A.; Kim, U. J.; Gutierrez, H. R.; Pan, L.; Dickey, E. C.; Eklund, P. C. Debundling and Dissolution of Single-Walled Carbon Nanotubes in Amide Solvents. *J. Am. Chem. Soc.* **2004**, *126*, 6095-6105.

(82) Frolov, A. I.; Arif, R. N.; Kolar, M.; Romanova, A. O.; Fedorov, M. V.; Rozhin, A. G. Molecular Mechanisms of Salt Effects on Carbon Nanotube Dispersions in an Organic Solvent (N-methyl-2-pyrrolidone). *Chem. Sci.* **2012**, *3*, 541-548.

(83) Premkumar, T.; Mezzenga, R.; Geckeler, K. E. Carbon Nanotubes in the Liquid Phase: Addressing the Issue of Dispersion. *Small* **2012**, *8*, 1299-1313.

(84) Davis, V. A.; Parra-Vasquez, A. N. G.; Green, M. J.; Rai, P. K.; Behabtu, N.; Prieto, V.; Booker, R. D.; Schmidt, J.; Kesselman, E.; Zhou, W.; Fan, H.; Adams, W. W.; Hauge, R. H.; Fischer, J. E.; Cohen, Y.; Talmon, Y.; Smalley, R. E.; Pasquali, M. True Solutions of Single-Walled Carbon Nanotubes for Assembly into Macroscopic Materials. *Nat. Nanotechnol.* **2009**, *4*, 830-834.

(85) Huang, J.; Ng, A. L.; Piao, Y. M.; Chen, C. F.; Green, A. A.; Sun, C. F.; Hersam, M. C.; Lee, C. S.; Wang, Y. H. Covalently Functionalized Double-Walled Carbon Nanotubes Combine High Sensitivity and Selectivity in the Electrical Detection of Small Molecules. *J. Am. Chem. Soc.* **2013**, *135*, 2306-2312.

(86) Yurekli, K.; Mitchell, C. A.; Krishnamoorti, R. Small-Angle Neutron Scattering from Surfactant-Assisted Aqueous Dispersions of Carbon Nanotubes. *J. Am. Chem. Soc.* **2004**, *126*, 9902-9903.

(87) Richard, C.; Balavoine, F.; Schultz, P.; Ebbesen, T. W.; Mioskowski, C. Supramolecular Self-Assembly of Lipid Derivatives on Carbon Nanotubes. *Science* **2003**, *300*, 775-778.

(88) Madni, I.; Hwang, C. Y.; Park, S. D.; Choa, Y. H.; Kim, H. T. Mixed Surfactant System for Stable Suspension of Multiwalled Carbon Nanotubes. *Coll. Surf. a* **2010**, *358*, 101-107.

(89) Bai, Y.; Park, I. S.; Lee, S. J.; Bae, T. S.; Watari, F.; Uo, M.; Lee, M. H. Aqueous Dispersion of Surfactant-Modified Multiwalled Carbon Nanotubes and Their Application as an Antibacterial Agent. *Carbon* **2011**, *49*, 3663-3671.

(90) Yu, J. R.; Grossiord, N.; Koning, C. E.; Loos, J. Controlling the Dispersion of Multi-Wall Carbon Nanotubes in Aqueous Surfactant Solution. *Carbon* **2007**, *45*, 618-623.

(91) Jiang, L.; Gao, L.; Sun, J. Production of Aqueous Colloidal Dispersions of Carbon Nanotubes. *J. Coll. Interf. Sci.* **2003**, *260*, 89-94.

(92) Bystrzejewski, M.; Huczko, A.; Lange, H.; Gemming, T.; Buchner, B.; Rummeli, M. H. Dispersion and Diameter Separation of Multi-Wall Carbon Nanotubes in Aqueous Solutions. *J. Coll. Interf. Sci.* **2010**, *345*, 138-142.

(93) Ebbesen, T. W.; Ajayan, P. M. Large-Scale Synthesis of Carbon Nanotubes. *Nature* **1992**, *358*, 220-222.

(94) Choi, K.; Bourgoin, J.; Auvray, S.; Esteve, D.; Duesberg, G.; Roth, S.; Burghard, M. Controlled Deposition of Carbon Nanotubes on a Patterned Substrate. *Surf. Sci.* **2000**, *462*, 195-202.

(95) Duesberg, G.; Muster, J.; Krstic, V.; Burghard, M.; Roth, S. Chromatographic Size Separation of Single-Wall Carbon Nanotubes. *Appl. Phys. A* **1998**, *67*, 117-119.

(96) Wang, B. M.; Ma, H. N.; Zhang, T. T.; Zhang, Y.; Chuan, L. F. Effects of Sodium Dodecyl Sulfate Concentrations on the Dispersion of Carbon Nanofibers in Water. *Nanosci. Nanotech. Lett.* **2013**, *5*, 377-383.

(97) Clapperton, R.; Ottewill, R.; Rennie, A.; Ingram, B. Comparison of the Size and Shape of Ammonium Decanoate and Ammonium Dodecanoate Micelles. *Coll. Poly. Sci.* **1999**, *277*, 15-24.

(98) Hayter, J.; Penfold, J. Determination of Micelle Structure and Charge by Neutron Small-Angle Scattering. *Coll. Poly. Sci.* **1983**, *261*, 1022-1030.

(99) Flavel, B. S.; Moore, K. E.; Pfohl, M.; Kappes, M. M.; Hennrich, F. Separation of Single-Walled Carbon Nanotubes with a Gel Permeation Chromatography System. *ACS Nano* **2014**, *8*, 1817-1826.

(100) Heise, H. M.; Kuckuk, R.; Ojha, A. K.; Srivastava, A.; Srivastava, V.; Asthana, B. P. Characterisation of Carbonaceous Materials Using Raman Spectroscopy: A Comparison of Carbon Nanotube Filters, Single- and Multi-Walled Nanotubes, Graphitised Porous Carbon and Graphite. *J. Ram. Spec.* **2009**, *40*, 344-353.

(101) Kroto, H. W.; Heath, J. R.; Obrien, S. C.; Curl, R. F.; Smalley, R. E. C-60 - BUCKMINSTERFULLERENE. *Nature* **1985**, *318*, 162-163.

(102) Smith, L. A.; Hammond, R. B.; Roberts, K. J.; Machin, D.; McLeod, G. Determination of the Crystal Structure of Anhydrous Sodium Dodecyl Sulphate Using a Combination of Synchrotron Radiation Powder Diffraction and Molecular Modelling Techniques. *J. Mol. Struc.* **2000**, *554*, 173-182.

(103) Bongiovanni, R.; Ottewill, R. H.; Rennie, A. R.; Laughlin, R. G. Interaction of Small Ions with the Micellar Surface of an Ultralong Chain Zwitterionic Surfactant. *Langmuir* **1996**, *12*, 4681-4690.

(104) Savvatimskiy, A. Measurements of the Melting Point of Graphite and the Properties of Liquid Carbon (A Review for 1963–2003). *Carbon* **2005**, *43*, 1115-1142.

(105) Liu, H.,; Feng, Y.; Tanaka, T.; Urabe, Y.; Kataura, H. Diameter-Selective Metal/Semiconductor Separation of Single-Wall Carbon Nanotubes by Agarose Gel. *J. Phys. Chem. C* **2010**, *114*, 9270.

(106) Khripin, C. Y.; Fagan, J. A.; Zheng, M. Spontaneous Partition of Carbon Nanotubes in Polymer-Modified Aqueous Phases. *J. Am. Chem. Soc.* **2013**, *135*, 6822.

(107) Flavel, B. S.; Kappes, M. M.; Krupke, R.; Hennrich, F. Separation of Single-Walled Carbon Nanotubes by 1-Dodecanol-Mediated Size-Exclusion Chromatography. *ACS Nano* **2013**, *7*, 3557.

(108) Xu, Z.; Yang, X.; Yang, Z. A Molecular Simulation Probing of Structure and Interaction for Supramolecular Sodium Dodecyl Sulfate/Single-Wall Carbon Nanotube Assemblies. *Nano Lett* **2010**, *10*, 985.

(109) Silvera-Batista, C. A.; Scott, D. C.; McLeod, S. M.; Ziegler, K. J. A Mechanistic Study of the Selective Retention of SDS-Suspended Single-

Wall Carbon Nanotubes on Agarose Gels. *J. Phys. Chem. C* **2011**, *115*, 9361.

(110) Piao, Y.; Meany, B.; Powell, L. R.; Valley, N.; Kwon, H.; Schatz, G. C.; Wang, Y. H. Brightening of Carbon Nanotube Photoluminescence Through the Incorporation of sp^3 Defects. *Nat. Chem.* **2013**, *5*, 840.

(111) Kwon, H.; Furmanchuck, A.; Kim, M.; Meany, B.; Guo, Y.; Schatz, C.; Wang, Y. H. Molecularly Tunable Fluorescent Quantum Defects. *J. Am. Chem. Soc.* **2016**, *138*, 6878.

(112) Jain, R. M.; Tvrdy, K.; Han, R.; Ulissi, Z.; Strano, M. S. Quantitative Theory of Adsorptive Separation for the Electronic Sorting of Single-Walled Carbon Nanotubes. *ACS Nano* **2014**, *8*, 3367.

(113) O'Connell, M. J.; Eibergen, E. E.; Doorn, S. K. Chiral Selectivity in the Charge-Transfer Bleaching of Single-Walled Carbon-Nanotube Spectra. *Nat. Mater.* **2005**, *4*, 412.

(114) Hilmer, A. J.; McNicolas, T. P.; Lin, S.; Zhang, J.; Wang, Q. H.; Mendenhall, J. D.; Song, C.; Heller, D. A.; Barone, P. W.; Blankschtein, D.; Strano, M. S. Role of Adsorbed Surfactant in the Reaction of Aryl Diazonium Salts with Single-Walled Carbon Nanotubes. *Langmuir* **2012**, *28*, 1309.

(115) Pastine, S. J.; Okawa, D.; Zettl, A.; Frechet, J. M. J. Chemicals On Demand with Phototriggerable Microcapsules. *J. Am. Chem. Soc.* **2009**, *131*, 13586.

(116) Blankschien, M. D.; Pretzer, L. A.; Huschka, R.; Halas, N. J.; Gonzalez, R.; Wong, M. S. Light-Triggered Biocatalysis Using Thermophilic Enzyme-Gold Nanoparticle Complexes. *ACS Nano* **2013**, *7*, 654.

(117) Powell, L. R.; Piao, Y.; Wang, Y. Optical Excitation of Carbon Nanotubes Drives Localized Diazonium Reactions. *J. Phys. Chem. Lett.* **2016**, 3690.

(118) Wu, G.; Milkhailovsky, A.; Khant, H. A.; Fu, C.; Chiu, W.; Zasadzinski, J. A. Remotely Triggered Liposome Release by Near-Infrared Light Absorption via Hollow Gold Nanoshells. *J. Am. Chem. Soc.* **2008**, *130*, 8175.

(119) Timko, B. P.; Dvir, T.; Kohane, D. S. Remotely Triggerable Drug Delivery Systems. *Adv. Mater.* **2010**, *22*, 4925.

(120) Hirsch, L. R.; Stafford, R. J.; Bankson, J. A.; Sershen, S. R.; Rivera, B.; Price, R. E.; Hazle, J. D.; Halas, N. J.; West, J. L. Nanoshell-Mediated

Near-Infrared Thermal Therapy of Tumors Under Magnetic Resonance Guidance. *Proc. Nat. Acad. Sci. U.S.A.* **2003**, *100*, 13549.

(121) Kam, N. W. S.; O'Connell, M. J.; Wisdom, J. A.; Dai, H. Carbon Nanotubes as Multifunctional Biological Transporters and Near-Infrared Agents for Selective Cancer Cell Destruction. *Proc. Nat. Acad. Sci. U.S.A.* **2005**, *102*, 11600.

(122) Huang, X. H.; El-Sayed, I. H.; Qian, W.; El-Sayed, M. A. Cancer Cell Imaging and Photothermal Therapy in the Near-Infrared Region by Using Gold Nanorods. *J. Am. Chem. Soc.* **2006**, *128*, 2115.

(123) Bardhan, R.; Lal, S.; Joshi, A.; Halas, N. J. Theranostic Nanoshells: From Probe Design to Imaging and Treatment of Cancer. *Acc. Chem. Res.* **2011**, *44*, 936.

(124) Qin, Z. P.; Bischof, J. C. Thermophysical and Biological Responses of Gold Nanoparticle Laser Heating. *Chem. Soc. Rev.* **2012**, *41*, 1191.

(125) Richardson, H. H.; Carlson, M. T.; Tandler, P. J.; Hernandez, P.; Govorov, A. O. Experimental and Theoretical Studies of Light-to-Heat Conversion and Collective Heating Effects in Metal Nanoparticle Solutions. *Nano Lett.* **2009**, *9*, 1139.

(126) Hogan, N. J.; Urban, A. S.; Ayala-Orozco, C.; Pimpinelli, A.; Nordander, P.; Halas, N. J. Nanoparticles Heat Through Light Localization. *Nano Lett.* **2014**, *14*, 4640.

(127) Doane, T. L.; Burda, C. The Unique Role of Nanoparticles in Nanomedicine Imaging, Drug Delivery and Therapy. *Chem. Soc. Rev.* **2012**, *41*, 2885.

(128) Stehr, J.; Hrelescu, C.; Sperling, R. A.; Raschke, G.; Wunderlich, M.; Nichtl, A.; Heindl, D.; Kürzinger, K.; Parak, W. J.; Klar, T. A.; Feldmann, J. Gold NanoStoves for Microsecond DNA Melting Analysis. *Nano Lett.* **2008**, *8*, 619.

(129) Barhoumi, A.; Huschka, R.; Bardhan, R.; Knight, M. W.; Halas, N. J. Light-Induced Release of DNA from Plasmon-Resonant Nanoparticles: Towards Light-Controlled Gene Therapy. *Chem. Phys. Lett.* **2009**, *482*, 171.

(130) Huschka, R.; Zuloaga, J.; Knight, M. W.; Brown, L. V.; Nordlander, P.; Halas, N. J. Light-Induced Release of DNA from Gold Nanoparticles: Nanoshells and Nanorods. *J. Am. Chem. Soc.* **2011**, *133*, 12247.

(131) Jain, P. K.; Qian, W.; El-Sayed, M. A. Ultrafast Cooling of Photoexcited Electrons in Gold Nanoparticle-Thiolated DNA Conjugates Involves the Dissociation of the Gold-Thiol Bond. *J. Am. Chem. Soc.* **2006**, *128*, 2426.

(132) Koyama, T.; Miyata, Y.; Kishida, H.; Shinohara, H.; Nakamura, A. Photophysics in Single-Walled Carbon Nanotubes with (6,4) Chirality at High Excitation Densities: Bimolecular Auger Recombination and Phase-Space Filling Excitons. *J. Phys. Chem. C* **2013**, *117*, 1974.

(133) Schöppler, F.; Mann, C.; Hain, T. C.; Neubauer, F. M.; Privitera, G.; Bonaccorso, F.; Chu, D.; Ferrari, A. C.; Hertel, T. Molar Extinction Coefficient of Single-Wall Carbon Nanotube. *J. Phys. Chem. C* **2011**, *115*, 14682.

(134) Streit, J. K.; Bachilo, S. M.; Ghosh, S.; Lin, C. W.; Weisman, R. B. Directly Measured Optical Absorption Cross Section for Structure-Selected Single-Walled Carbon Nanotubes. *Nano Lett.* **2014**, *14*, 1530.

(135) Jain, P. K.; Lee, K. S.; El-Sayed, I. H.; El-Sayed, M. A. Calculated Absorption and Scattering Properties of Gold Nanoparticles of Different Size, Shape, and Composition: Applications in Biological Imaging and Biomedicine. *J. Phys. Chem. B* **2006**, *110*, 7238.

(136) Hong, G.; Lee, J. C.; Robinson, J. T.; Raaz, U.; Xie, L.; Huang, N. F.; Cooke, J. P.; Dai, H. Multifunctional *in vivo* Vascular Imaging Using Near-Infrared II Fluorescence. *Nat. Med.* **2012**, *18*, 1841.

(137) Duggal, R.; Pasquali, M. Dynamics of Individual Single-Walled Carbon Nanotubes in Water by Real-Time Visualization. *Phys. Rev. Lett.* **2006**, *96*, 246104.

(138) Strano, M. S.; Moore, V. C.; Miller, M. K.; Allen, M. J.; Haroz, E. H.; Kittrell, C.; Hauge, R. H.; Smalley, R. E. The Role of Surfactant Adsorption During Ultrasonication in the Dispersion of Single-Walled Carbon Nanotubes. *J. Nanosci. Nanotechnol.* **2003**, *3*, 81.

(139) Strano, M. S.; Zheng, M.; Jagota, A.; Onoa, G. B.; Heller, D. A.; Barone, P. W.; Usrey, M. L. Understanding the Nature of the DNA-Assisted Separation of Single-Walled Carbon Nanotubes Using Fluorescence and Raman Spectroscopy. *Nano Lett.* **2004**, *4*, 543.

(140) Demers, L. M.; Ostblom, M.; Zhang, H.; Jang, N. H.; Liedberg, B.; Mirkin, C. A. Thermal Desorption Behavior and Binding Properties of DNA Bases and Nucleosides on Gold. *J. Am. Chem. Soc.* **2002**, *124*, 11248.

(141) Lakowicz, J. R. *Principles of Fluorescence Spectroscopy*; 3 ed.; Springer, 2006.

(142) Carlson, L. J.; Maccagnano, S. E.; Zheng, M.; Silcox, J.; Krauss, T. D. Fluorescence Efficiency of Individual Carbon Nanotubes. *Nano Lett.* **2007**, *7*, 3698.

(143) Crochet, J.; Clemens, M.; Hertel, T. Quantum Yield Heterogeneities of Aqueous Single-Wall Carbon Nanotube Suspensions. *J. Am. Chem. Soc.* **2007**, *129*, 8058.

(144) Carslaw, H. S.; Jaeger, J. C. *Conduction of Heat in Solids*; 2nd ed.; Oxford University Press, 1986.

(145) Wang, Y. H.; Kim, M. K.; Shan, H.; Kittrell, C.; Fan, H.; Ericson, L. M.; Hwang, W. F.; Arepalli, S.; Hauge, R. H.; Smalley, R. E. Continuted Growth of Single-Walled Carbon Nanotubes. *Nano Lett.* 2005, *5*, 997.

(146) Liu, J.; Wang, C.; Tu, X.; Liu, B.; Chen, L.; Zheng, M.; Zhou, C. Chirality-Controlled Synthesis of Single-Wall Carbon Nanotubes Using Vapor-Phase Epitaxy. *Nat. Commun.* 2012, *3*.